August 2015

Fabric and Soft Materials Composites for Bio-Inspired Adhesives and Prosthetics

Daniel R. King
University of Massachusetts - Amherst

FABRIC AND SOFT MATERIALS COMPOSITES FOR BIO-INSPIRED ADHESIVES AND PROSTHETICS

A Dissertation Presented
by
DANIEL RUDOLF KING

Submitted to the Graduate School of the
University of Massachusetts Amherst in partial fulfillment
of the requirements for the degree of

DOCTOR OF PHILOSOPHY

May 2015

Polymer Science and Engineering

FABRIC AND SOFT MATERIALS COMPOSITES FOR BIO-INSPIRED ADHESIVES AND PROSTHETICS

A Dissertation Presented

by

DANIEL RUDOLF KING

Approved as to style and content by:

_____
Alfred J. Crosby, Co-Chair

_____
E. Bryan Coughlin, Co-Chair

_____
Duncan J. Irschick, Member

_____
David A. Hoagland, Department Head
Polymer Science and Engineering

To my family, for always supporting me

ACKNOWLEDGEMENTS

First and foremost, I would like to thank my advisor, Al Crosby, for taking a chance on me, and supporting me over the last four and a half years. Entering my PhD, my knowledge of mechanics was minimal, but I will never forget Al telling me that I have a "particular set of skills" that would make a valuable member to the Crosby Group. Al has managed to create a research group which does cutting edge research, while maintaining a collaborative and enjoyable environment. I never once dreaded heading to work. Without Al's constant positive attitude and support, completing this dissertation would not have been possible.

Additionally, I would like to thank the rest of my committee, including co-chair Bryan Coughlin and Duncan Irschick. Professor Coughlin has been a fantastic committee member, providing me an outlet to talk about chemistry, but also reminding me that there is so much about chemistry I still have to learn. Additionally, he has played an important role helping me decide the course of my future plans. Before starting my thesis work, my knowledge of Biology consisted only of what I learned in 10^{th} grade, but by collaborating with Duncan, I was able to learn an incredible amount about the world around us. He additionally taught me about the importance of rigorous statistics, and I can no longer view data without thinking, "but is this result significant?" I would like to thank both of you for taking the time to be a part of my committee.

While not an official member of my committee, I would like to thank Jian Ping Gong for her support and friendship over the last two years. Her willingness to accept and help fund my trip to Hokkaido University in the summer of 2013 was one of the greatest and most important experiences of my life. I look forward to us collaborating and working

together more in the future. To all my friends and colleagues at Hokkaido University, thanks for making my time in Japan feel like home. I would like to specifically thank Nonoyama-san, Kuriyama-san, Yashima-san, Haiyan, Min, Taolin, Chuanxi, and Saika for their friendship, as well as the entire Chinese and Bangladeshi communities at LSW for their acceptance and inclusion in social events.

My experience with undergraduate research guided me towards graduate school, and I am forever grateful to Ralph Colby for giving me an opportunity, starting in my freshman year, to work in his lab. Despite that it took years for my research to become valuable, this experience quickly put me on a path towards graduate school. He also allowed me to network with other people in the field of polymer physics, and helped me attain a summer internship with Karen Winey. Karen importantly was the first person to tell me that UMass Amherst would be a great place for me to go to graduate school, which was ultimately an extremely important decision in my life. I would like to thank both of you for all your support over the years.

As I previously mentioned, the Crosby Group has been a great home for the last four years. To all the previous and current members of the group, Derek, Chelsea, Hyun Suk, Dong Yun, Jun, Mike, Yuri, Sam, Cheol, Shelby, Sami, Jon, Yujie, Marcos, Yu-Cheng, Minchao, Mike, Satyan, Shruti, Kasey, Yongjin, and David, thanks for all your friendship, support, great times, and putting up with my messes. I would like to thank Jun for giving me someone to talk about chemistry with, in my early years in the group. Mike and I spent many hours together over the years, from learning how to make Geckskin, to one of the many videos we recorded, to traveling to conferences. Thanks for being a fantastic mentor and friend. Shelby was an invaluable resource to our group, giving me

hope that a career in academics is possible, and taught me so much about science in general. I would like to thank Jon for being available to hang out and talk about anything, be it science, sports, or life. I truly believe after spending four years here that Big Ten schools really do develop a different breed of students. Additionally, I would like to thank Jon for playing the role of referee during all of the fights that occurred between Yujie and me. Yujie, thanks for being my best friend. To the rest of Crosby group, thanks for all the fantastic times we spent together, and good luck finishing your PhD's.

Outside of Crosby group, I would like acknowledge the Class of 2010. We were a great class, and the times we spent together in class and studying for the cumulative exams will always be a great memory for me. Furthermore, I would like to specifically acknowledge Katie, Melissa, Maria, Jinhye, Kyle, Brittany, Yan, Miao, Hsin-Wei, Rachel, and Tetsu. Maria and I spent a lot of time together on the farm in Sunderland, participating in CSA. Jinhye opened up the world of Korean pop music to me, which was playing constantly while writing this thesis. Brittany was always there when I needed an ear, and Rachel was always there to be my companion to church on Sundays. Additionally, I would like to thank Kyle and Tetsu for being my roommates over the last four years. Thank you all.

I would like to thank all of my Thai friends at UMass Amherst: Packy, Get, Kratae, Palm, Mon, Jumpee, Nok, Yui, Ploy, and Fah. Thanks for letting me join you at lunch, and for all the free Thai lessons that I was given. I look forward to seeing you all again on future trips to Thailand.

Without the constant support of those closest to me, this experience would not have been possible. Mom and Dad, thank you for supporting my education. Thanks for helping

me when I needed help, whether it was in a specific subject, or just pushing me to keep going and letting me know I could do it. I would like to thank Mary for showing me that the world is full of all kinds of people, and that everyone has value. Also, I would like to thank her for providing me an opportunity to talk for both of us, which I think gave me the ability to never let a room become silent. I would like to thank my extended family for always caring about me and asking about my research. Specifically I would like to thank John, who is probably my oldest friend, for keeping me grounded, and Lyuda, for showing me that family, even if separated by many years and miles, is still family. Finally, I'd like to thank Jess, who has been there for me since I decided to attend graduate school. Thanks for supporting my decision to get a PhD, and thank you for applying pressure when I needed it to finish my degree (sometimes the stick is more effective than the carrot). Words cannot truly express my gratitude.

ABSTRACT

FABRIC AND SOFT MATERIALS COMPOSITES
FOR BIO-INSPIRED ADHESIVES AND PROSTHETICS

MAY 2015

DANIEL RUDOLF KING, B.S., PENNSYLVANIA STATE UNIVERSITY

M.S., UNIVERSITY OF MASSACHUSETTS AMHERST

PH.D., UNIVERSITY OF MASSACHUSETTS AMHERST

DIRECTED BY: PROFESSOR ALFRED J. CROSBY

Adhesives have long been designed around a trade-off between adhesive strength and releasability. Within this spectrum, specialized materials have been designed to maximize adhesive ability for a given application. To overcome this trade-off, a new adhesive paradigm is required. Biologically inspired adhesives have been of interest over the past two decades, because organisms are seen using their adhesive pads to achieve high adhesive forces, while maintaining releasability and reusability. Many biological organisms possess microscopic fibrillar features on their toe-pads, which enables climbing. While much effort has been spent attempting to mimic these features, ultimately high force capacities have not been achieved. Recently, a new framework has been introduced which states that a specific surface morphology is not necessary for creating high force capacity, easy release adhesives. This framework states that for shear adhesives to achieve high force capacity, the ratio of contact area to compliance in the loading direction, *A/C*, must be increased. In this thesis we focus on expanding this framework to quantitatively understand both compliance and area, for a wide range of adhesive materials and geometries, and across a wide range of substrates with varying roughness. To increase the functionality of high strength, reusable adhesives, we have developed a new adhesive configuration which supports normal loading as well as shear loading. Finally, we expand to a new field, biological prosthetic materials, and develop fabric-based composites which are extremely tough, strong, and flexible, while containing water.

The foundation of the work presented in this thesis is based upon an analytical model developed to calculate the compliance of fabricated adhesives (Chapter 2). Combining this knowledge with the previously developed scaling theory allows a high degree of accuracy in calculating force capacity. While this method works well for smooth surfaces such as glass, it assumes that the nominal pad area is equal to the true area of contact, which is not true on rough surfaces. A model is developed to calculate the true area of contact based on surface roughness and adhesive materials properties (Chapter 3). The results of this model demonstrate that there is an optimum pad modulus for any given surface roughness to achieve maximum stress capacity. In some situations, high strength and easy release adhesives are required in normal loading situations. We develop a new adhesive configuration which enables shear adhesives to support normal loads (Chapter 4). This method results in a six-fold increase in normal force capacity. This provides tolerance in adhesives applications, greatly improving the commercial utility of these adhesives. Finally, we use techniques learned from the fabrication of adhesives to develop composites from polyampholyte gels and glass fiber fabrics (Chapter 5). These materials exhibit enhanced properties over the controls, including extremely high toughness and strength, while maintaining flexibility and containing water. A general mechanism is explained that results in these improved properties, opening up opportunities to develop enhanced composites from fabrics and soft materials in other fields.

TABLE OF CONTENTS

Page

LIST OF TABLES

Table Page

LIST OF FIGURES

CHAPTER 1

INTRODUCTION

1.1 Introduction to Adhesives

Adhesives are materials which possess an ability to bind two or more materials together.[1] Adhesives may be used for a wide variety of applications, from high strength, structural adhesives used in car frames,[2] to low strength, reusable adhesives in sticky notes,[3] to biocompatible adhesives used in wound closures for humans.[4] Other binding techniques exist, such as mechanical fasteners like rivets (for structural applications) and sutures (for wound closures), but these techniques cause damage to the materials which are bound together.[2] Even on freshly cleaned, smooth surfaces, strong bonds, such as covalent and ionic bonds, are often rendered inert by reactions with air.[5] Therefore, adhesives bind surfaces together by using weak, ubiquitous Van der Waals force, to create bonds between material surfaces.[3] This mechanism provides engineers with many methods for designing adhesives for applications.

Different techniques have been designed to achieve strong bonds between materials. Some of the simplest adhesives are epoxies, which consist of two liquid chemical components which react when mixed. The epoxy components are combined and placed between the materials to be adhered. The liquid epoxy wets the surfaces of the materials and flows to fill the joint. After a period of time (controlled by the chemistry of the components), the components react and form a solid joint, binding the materials together. These joints are very strong, but the chemical reaction is permanent. Another type of adhesive, pressure-sensitive adhesives (PSAs), which are used in tape consist of viscoelastic solids. These adhesive films are able to creep to conform to roughness to

create the bond. PSAs have been the focus of extensive research for over half a century, and many products are designed by tuning the viscoelastic properties to control adhesion strength.[3] By tuning the properties of the adhesive, a trade-off occurs between adhesion and releasability: as adhesive strength increases, the ability for adhesives to release decreases.[6] This trade-off is not just seen with PSAs, but throughout all commonly utilized adhesives. This provides an opportunity for new research: can adhesives be developed which are capable of supporting strong loads necessary for structural adhesive applications, yet possess the release properties of sticky notes?

1.2 Lessons from Nature

Humankind has long looked to nature for inspiration in developing new technology. In the 15th century, Leonardo da Vinci studied flight of birds, which inspired his designs of "flying machines."[7] In modern times, advances have come in a wide range of fields, with notable recent developments in super-hydrophobic materials resulting from studying the lotus leaf.[8–10] In biology, adhesive systems are used by many organisms for locomotion to expand to new habitats and escape from predators, as well as for reproductive purposes.[11–13] Adhesive pads in nature have very high safety factors, capable of supporting loads much greater than the mass of the organism.[5] Organisms are capable of climbing on many types of surfaces, regardless of roughness, and their adhesives can be used repeatedly without losing adhesive ability.[14–16] Finally they possess a unique self-cleaning capacity, allowing them to work well on fouled surfaces.[17–20] These characteristics make bio-inspired adhesives an interesting model for next generation adhesive systems.

Contrary to the spectrum of pressure sensitive adhesives which are designed around the trade-off between strong adhesion and releasability, adhesives in biology are capable

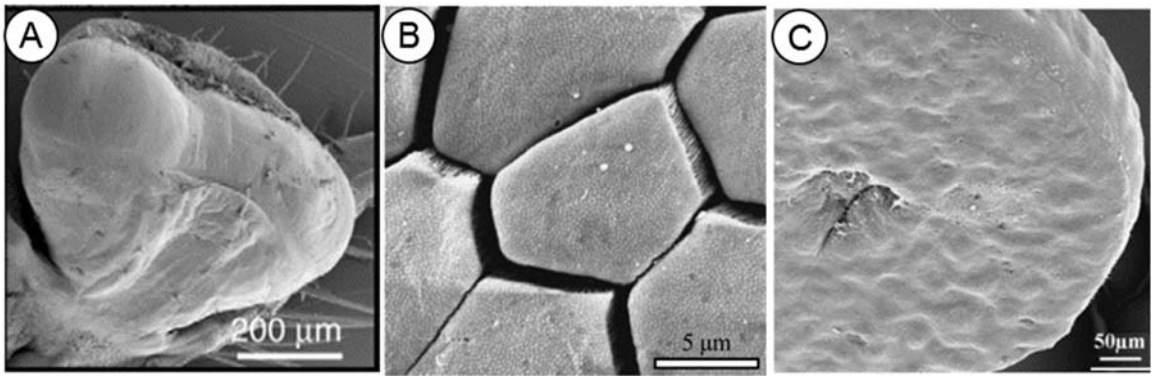

Figure 1.1 - Micrographs of smooth adhesive pads. Images are of (A) Stick insects (Reproduced with permission from J. M. R. Bullock, P. Drechsler, W. Federle, *Journal of Experimental Biology* **2008**, *211*, 3333),[21] (B) tree frogs (Reproduced with permission from B. N. J. Persson, *Journal of Physics: Condensed Matter* **2007**, *19*, 376110),[27]f and (C) Sea stars (Reproduced with permission from R. Santos, E. Hennebert, *Functional Surfaces in Biology* **2009**).[33]

of achieving high strength *and* easy release. These systems come in two types: smooth and "hairy."[21] Examples of organisms with smooth adhesive pads include cockroaches,[22,23] stick insects (Figure 1.1A),[21,24,25] tree frogs (figure 1.1B),[26–31] and sea stars (figure 1.1C).[32,33] These systems all at least partially depend on secretions to help increase adhesion to surfaces. However, the majority of research has focused on "hairy" dry adhesive systems, which are utilized by spiders,[34,35] leaf beatles,[36] and geckos (Figure 1.2).[12,37–40] Leaf beetles have three different adhesive pads which are each specialized for different surfaces.[21,36,41,42] Spiders on the other hand only utilize their adhesive pads on smooth surfaces, and use claws to climb on rough surfaces.[43,44] Geckos are the largest organisms capable of locomotion with adhesive pads. On the surface of the gecko toe are lamellar skin flaps called scansors (Figure 1.2B), which are covered in large arrays of very small fibrillar features called setae (Figure 1.2C), which each split into nanometer scale features called spatulae (figure 1.2D).[45,46] Despite being made of a high modulus material, keratin, these features are able to make intimate contact on surfaces.[14,18,47] It is important to note that geckos, like PSAs, adhere primarily through Van der Waals forces, and not

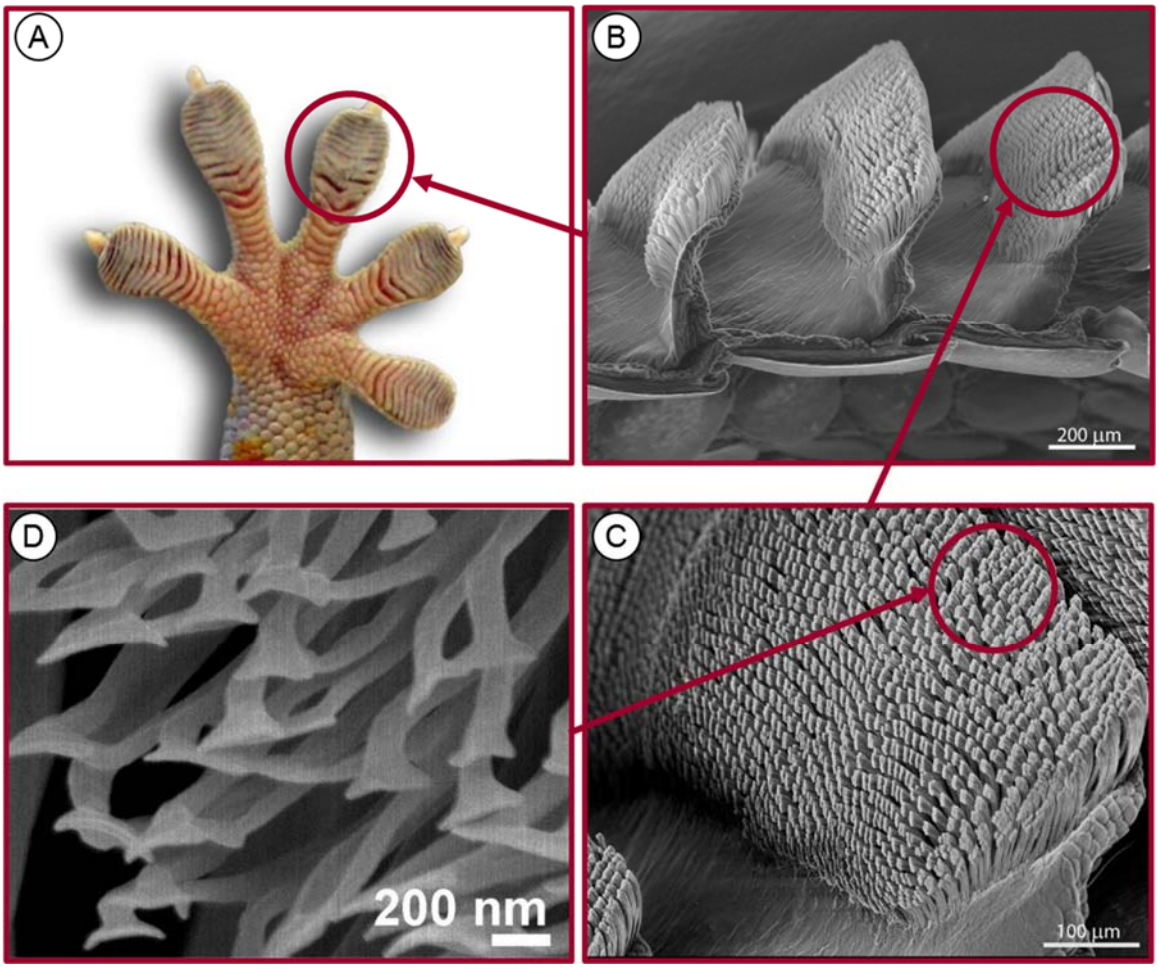

Figure 1.2 – Tokay gecko adhesive system. (A) An image of a Tokay gecko foot. (B) Focusing on an individual toe, multiple lamellar flaps are visible, which are called scansors. (C) Each scansor is covered with long and thin stalks called setae. (D) Each stalk is broken down into even smaller, triangular tipped features called spatulae. Used with Permission: Adv. Mater. 2012.[74]

capillary forces.[18,38,48] The adhesion of individual gecko setae has been examined in the past on surfaces of varying roughness, and broadly explored at the full body level.[15,49] The most unique and attractive characteristic of these adhesive systems is their consistently repeatable, high adhesive strength to a wide variety of surfaces, while still maintaining the ability to quickly and easily release. Despite consisting of different morphologies, the organisms described here each evolved in a manner that allows for locomotion across a range of surfaces.

Most researchers refer to "gecko inspired adhesives" as adhesives that attempt to mimic the features seen on gecko toe-pads.[48] Many research groups have created intricate adhesives utilizing photolithography, ion beam irradiation, micromachining, and other difficult manufacturing methods to mimic the nanoscopic features of gecko setae and spatula (Figure 1.3).[50–57] In some cases, very high adhesive stress values have been reported. However, these adhesives have generally been tested on smooth surfaces, and few groups have attempted to adhere these materials to surfaces encountered in daily life.

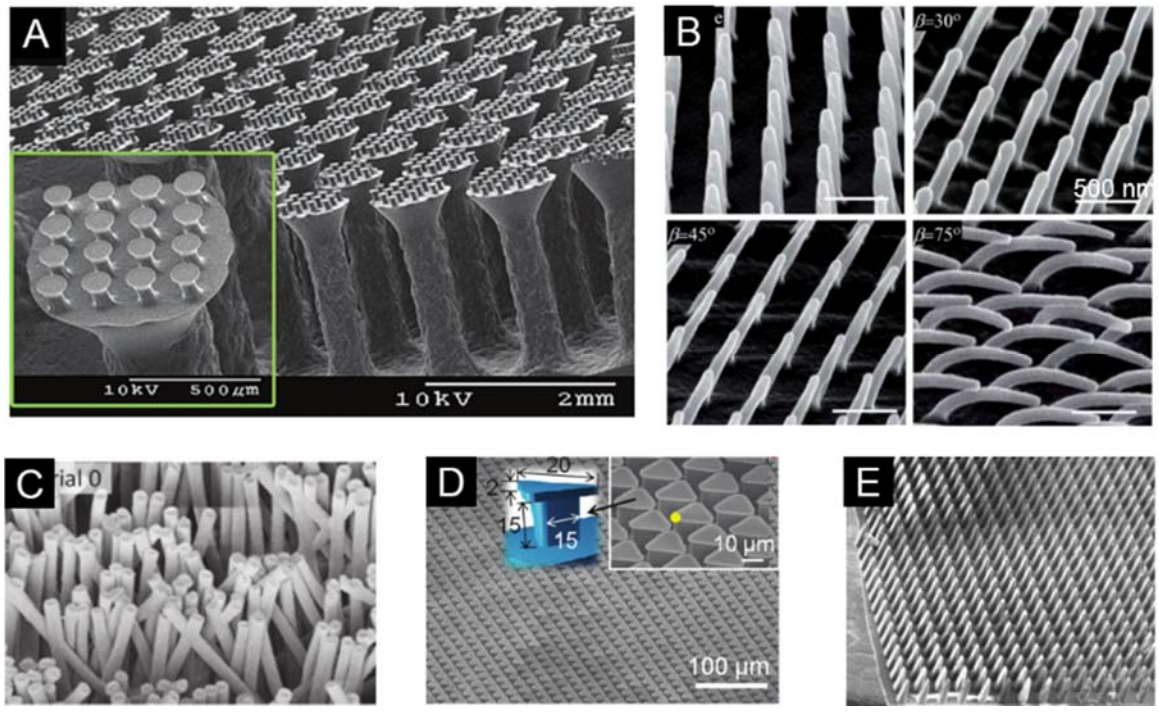

Figure 1.3 – Synthetic gecko-inspired adhesives. (A) Two-level hierarchical mushroom tipped pillars made with soft polyurethane elastomer. Reprinted with permission from M.P. Murphy, S. Kim, M. Sitti. *ACS Appl. Mater. Interfaces*, **2009**, pp 849–855,[50] Copyright 2009 American Chemical Society. (B) PUA pillars angled with ion beam irradiation. Reprinted with permission from Y. Rahmawan, T. Kim, S. J. Kim, K.-R. Lee, M.-W. Moon, K.-Y. Suh, *Soft Matter* **2012**, *8*, 1673.[51] (C) Pillars made from polypropylene. Reprinted with permission from A. G. Gillies, R. S. Fearing, *Langmuir* **2011**, *27*, 11278.[52] (D) Triangular tipped PUA pillars. Reprinted with permission from M. K. Kwak, H. E. Jeong, W. G. Bae, H. S. Jung, K. Y. Suh, *Small* **2011**, 2296.[53] (E) Microfabricated wedge-shaped adhesive arrays made from silicone elastomer. Reprinted with permission from A. Parness, D. Soto, N. Esparza, N. Gravish, M. Wilkinson, K. Autumn, M. Cutkosky, *Journal of the Royal Society, Interface* **2009**, *6*, 1223.[106]

Furthermore, these adhesives cannot be scaled to large sizes necessary for most commercial adhesive applications, and consequently high forces have not been achieved. Even if large scale fabrication methods were developed, some adhesives experience decrease performance with increased area.[58] A new approach is needed to overcome the shortcomings of fibril-based gecko-inspired adhesives. We will analyze adhesives from a fracture mechanics viewpoint to determine a method to scale gecko-inspired adhesives.

1.3 Adhesion Mechanisms

1.3.1 Pressure Sensitive Adhesives

To bind surfaces together, an adhesive creates molecular contact between surfaces, resulting in an ability to support load without debonding.[3,59] Traditional PSAs achieve this ability through the use of viscoelastic polymeric materials. At long times or large pressures, the polymeric adhesives are able to flow, creating contact between the surfaces and the adhesive.[60] Van der Waals forces are the main contributor of intermolecular forces, binding the surfaces together. The materials that can achieve these properties have been empirically understood for a long time, with PSA tapes being introduced in the early 1900s. Quantitative understanding of the important properties of PSA's would not be discovered until much later.

In the 1960's Dahlquist was one of the first to see that materials with a modulus below 10^5 Pa are able to exhibit strong "tack" and adhere well to surfaces.[61–63] "Tackiness" is one of the most important features of PSA materials, but is difficult to quantify.[64,65] Empirically, tackiness can be experienced by touching a piece of tape.[60] As one's finger tries to separate from the tape, the work required to cause this separation is experienced as tack. Zosel was one of the first researchers to attempt to quantify tack, by developing an

instrument capable of measuring the force, F, required to separate a steel probe of known area, A, being displaced at a known velocity, v, from a polymer sample, as a function of time, t.[66] The work of adhesion is then calculated as:

$$w = \frac{1}{A}\int Fv\,dt \tag{1.1}$$

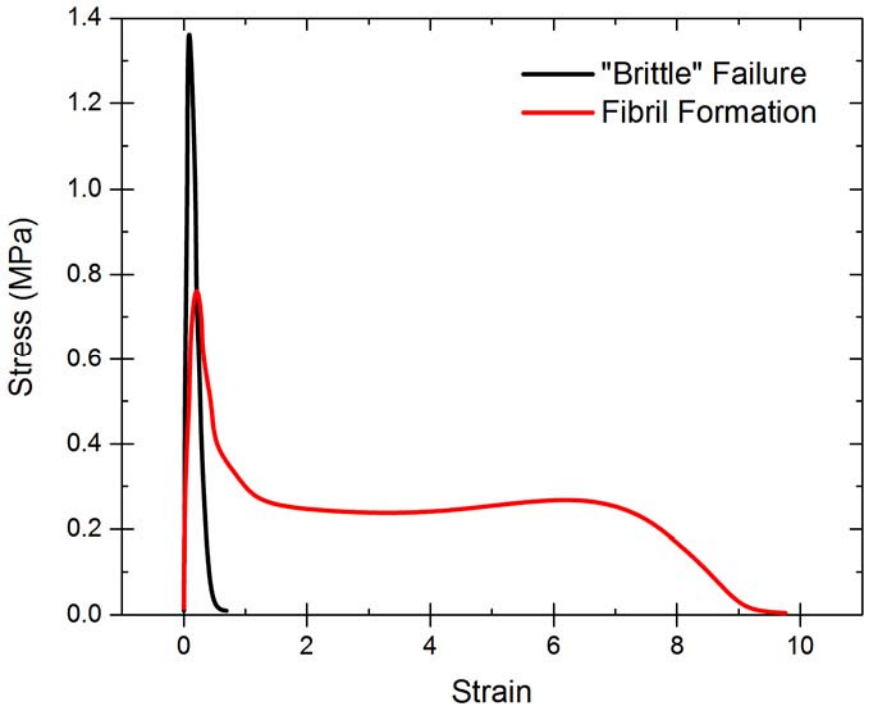

Figure 1.4 - Stress versus strain plots for two different polymer adhesives. One exhibits "brittle" failure, and the other undergoes fibril formation, generating large work of adhesion. Adapted with permission from A. Zosel, *The Journal of Adhesion* **1989**, *30*, 135.[66]

From this work, Zosel determined that, depending on the molecular architecture of the polymer adhesive, two different debonding mechanisms can take place (Figure 1.4). One, termed "brittle" failure occurrs when a high molecular weight rubber material is tested. A high initial stress is measured, with adhesive debonding occurring from the rubber. Due to the rapid debonding of the adhesive, the energy required to separate is very low. Conversely, a second debonding mechanism is observed with a lower molecular weight rubber, where again an initial peak in stress is observed, followed by a long shoulder region

Figure 1.5 - An example of fibril formation of an adhesive adhered between two plates of a parallel-plate rheometer.

of intermediate stress. During this region, fibrillation of the adhesive occurs between the probe and the base. An example of fibrillation is presented in Figure 1.5. This fibrillation mechanism greatly increases the work of adhesion,[67] and therefore is traditionally considered necessary to develop strong adhesives.

In some situations where strong work of adhesion is required, PSAs work extremely well. However, they also have many shortcomings. For example, failure is generally cohesive and permanent. Due to the large amount of creep PSAs undergo, after adhesion to a surface it cannot regain its original form. Also, to achieve moduli below the Dahlquist Criterion, a large amount of additives such as plasticizers and tackifiers are needed. Furthermore, not all situations benefit from adhesives which require large amounts of energy to debond. For example, it is easy to understand why PSAs do not exist on toe-

pads in Nature. If an organisms toes were covered with tacky materials, large amounts of energy would be required for locomotion. However even in Zosel's seminal paper he noted a second potential mechanism for adhesion: brittle adhesive failure with high failure forces, but low work of adhesion.[66]

1.3.2 Fibrillar Gecko-Inspired Adhesives

Geckos have inspired people with their ability to climb across surfaces for thousands of years. Originally, some people believed adhesion could occur through vacuum,[11] and even today some people argue over the importance of capillary forces.[48] In the early 2000s, it was discovered that Van der Waals forces primarily contribute to enable gecko adhesion.[38,39] An important mechanism for the high adhesive strength generated by the gecko foot is contact splitting.[18,48,68] Adhesive strength can be approximated using the theory presented by Johnson, Kendall, and Roberts, which states the pull-off force for an elastic solid is:

$$F_c = \frac{3}{2}\pi R\gamma \tag{1.2}$$

where R is the radius of the adhesive contact and γ is the adhesion energy per area. In the case of gecko adhesion, there is not one large area of contact. The surface of a gecko toe-pad is covered in millions of high aspect ratio features called spatulae. If the surface is broken up into n discrete segments, the radius of each segment is $R/\sqrt{n}$. Substituting into Equation 1.2 yields:

$$F_c' = \sqrt{n} \cdot F_c \tag{1.3}$$

In sum contact splitting principles state that for a given contact area that is broken up into n discrete segments, adhesive force will scale like $n^{1/2}$.[68] This mechanism provides a strong incentive for developing fibril-based gecko-inspired adhesives.

Besides contact splitting, other mechanisms make fibril-based gecko-inspired adhesives attractive. One benefit of these adhesives is that frequent initiation of cracks is required for a crack to propagate the full length of the adhesive. This results in interfacial failure occurring at higher stresses.[69,70] In the previous section the Dahlquist criterion stated that a modulus below 10^5 Pa is required for a material to exhibit tack. Due to geometry, the effective modulus of many high aspect ratio fibrillar adhesives have an effective modulus below 10^5 Pa, despite consisting of higher modulus materials.[5,47,48] Low modulus is achieved in rubbers by the introduction of additives, but is achievable for gecko-inspired adhesives purely through geometry.

Due to the many attractive theoretical abilities of fibril-based gecko-inspired adhesives, much effort has been exerted to synthetically develop them. However, the results have been lacking. In general, they have been difficult to fabricate, especially at large length scales. Even if large arrays of fibrils are fabricated, their performance may be sub-optimal due to fiber fracture (due to their aspect ratio, they lack mechanical strength), or fiber condensation (bunching, or self-adhesion of the fibrils).[48] This has resulted in many researchers describing extremely high loads at small contact areas,[71] but losing this ability at larger sizes.[58] To achieve the high stress and easy release abilities of gecko-inspired adhesives, while being capable of scaling to large areas requires a new type of adhesive system.

1.3.3 Looking Beyond Fibril-based Adhesives

While many biological systems are capable of high strength and easy release, it is interesting to note that they all do not consist of the same morphology. Therefore, hierarchical surface features are sufficient, but not necessary to achieve adhesive

locomotion. Rather than focusing on surface features, it is possible to ascertain the important parameters of biological adhesives by analyzing the fracture mechanics of these adhesives. The full derivation of this scaling equation is published in reference 72. This scaling theory is based on the work of Maugis and Barquins,[72] which is derived from Griffith crack theory.[73] For an adhesive of a discrete area, A, undergoing displacement, δ, the total energy, U_T, is the sum of the surface energy, U_S, the potential energy due to work, U_w, and the stored elastic energy of the deformed material U_E. The system is assumed to be in equilibrium, therefore:

$$\frac{\delta U_T}{\delta A} = \frac{\delta U_S}{\delta A} + \frac{\delta U_w}{\delta A} + \frac{\delta U_E}{\delta A} = 0 \tag{1.4}$$

In gecko adhesion, adhesive toe-pads quickly switch between engaged and a dis-engaged state. This will be incorporated as unstable failure, where:

$$\frac{\delta^2 U_T}{\delta A^2} < 0 \tag{1.5}$$

The adhesive is assumed to fail in one step, and therefore the differential terms are no longer necessary. Additionally, geckos are able to run across surfaces with little energetic penalty. For systems that do not exhibit hysteresis ($U_{final} - U_{initial} = 0$), energy is conserved. Any stored energy due to deformation of the adhesive is converted to surface energy at F_c. The initial energy of the systems is:

$$U_{initial} = U_E + U_w + \gamma_{12} A \tag{1.6}$$

And the final energy is:

$$U_{final} = A(\gamma_1 + \gamma_2) \tag{1.7}$$

Where the strain energy release rate G is defined:

$$G = \left(\frac{U_E}{A} + \frac{U_w}{A}\right) \tag{1.8}$$

And the surface energy is defined:

$$U_s = (\gamma_1 + \gamma_2 - \gamma_{12})A = G_c A \tag{1.9}$$

Solving for energy conservation, Equation 1.7 less Equation 1.6 yields:

$$U_{final} - U_{initial} = A(\gamma_1 + \gamma_2 - \gamma_{12}) - U_E - U_w \tag{1.10}$$

For the controlled displacement case where $U_w = 0$, substituting Equation 1.9 leads to:

$$G_c A - U_E = 0 \tag{1.11}$$

The elastic energy is determined:

$$U_E = \int F \, d\Delta = F\Delta \tag{1.12}$$

Where a linear elastic material behaves as:

$$F = \frac{1}{C}\Delta \tag{1.13}$$

To yield:

$$U_E = F^2 C \tag{1.14}$$

Substituting Equation 1.14 into Equation 1.11, and solving for the critical force, F_c, which occurs when $G = G_c$, gives the final scaling equation:

$$F_c \sim \sqrt{G_c}\sqrt{\frac{A}{C}} \tag{1.15}$$

From this scaling equation it is evident that the important parameter for controlling force capacity for gecko inspired adhesives is the ratio of $\sqrt{A/C}$ since G_c cannot be varied greatly while maintaining easy release. To achieve high force capacities, large area of contact is required, while minimizing compliance. Importantly, Equation 1.15 does not require specific surface geometry, such as contact splitting, or specific materials, such as those specified by the Dahlquist Criterion. As a general model, Equation 1.15 provides guidance to create adhesives with the properties of biological adhesives for large loads.

1.4 Scaling of Adhesives in Nature

To test whether this equation describes biological organisms, a simple experiment is performed utilizing live Tokay geckos.[74] The area of contact of the two front feet of a gecko specimen is measured, and the gecko is held by the torso and allowed to cling to a plate of glass which is attached to the load cell on the crosshead of an Instron tensile tester. The crosshead is displaced at constant velocity, and the maximum force and compliance of the gecko is calculated. Additional force and compliance data for other biological organisms is aggregated from the literature. These data agreed well with the derived scaling relation, Equation 1.15, and is presented in Figure 1.6.[74] Importantly, this plot demonstrates that for larger organisms to utilize adhesives, toe pad area must increase, but

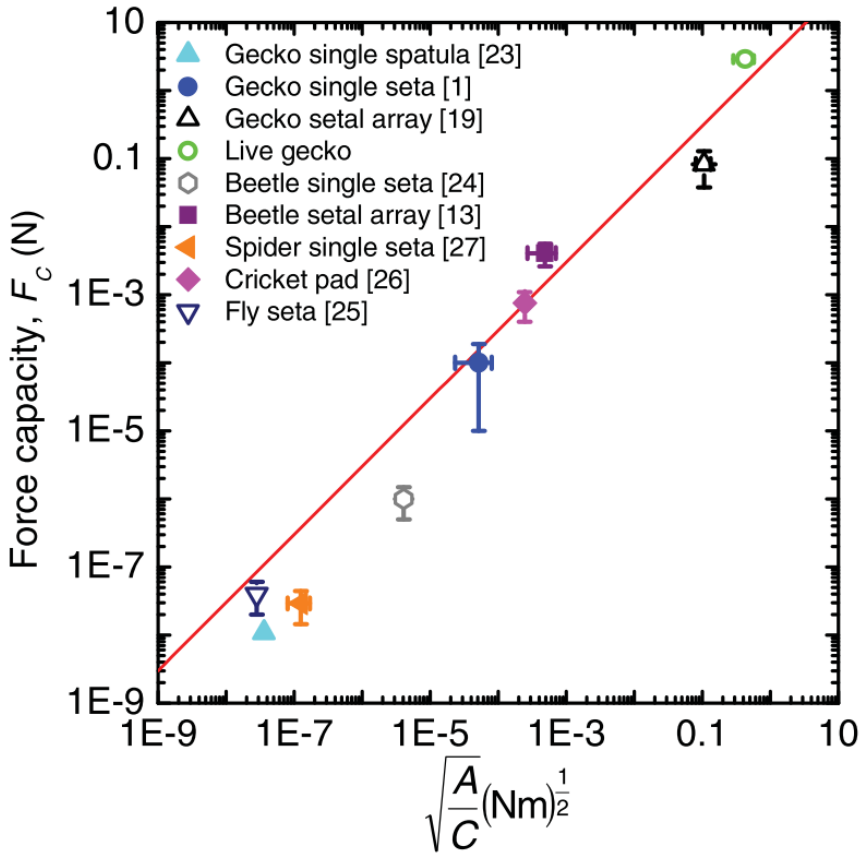

Figure 1.6 - Force capacity versus $\sqrt{A/C}$ for adhesive systems of different organisms, and components of their adhesive systems. The red line represents Equation 1.15. Used with Permission: Adv. Mater. 2012.[74]

also must become stiffer. This result has not been previously realized in the literature, and is important for understanding scaling of biological adhesives.

1.5 Fibril-less Gecko Inspired Adhesives

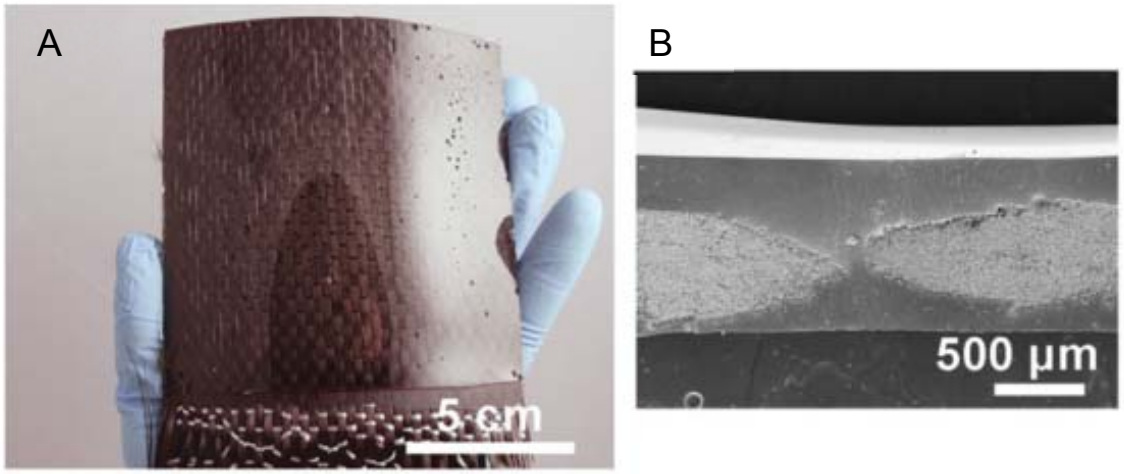

Figure 1.7 – Fibril-less gecko inspired adhesives. (A) Image of a carbon fiber fabric coated with polyurethane elastomer. (B) An SEM cross-section of the adhesive pad. Note that the elastomer fully covers the fibers, and that the surface is perfectly smooth, containing no features. Used with Permission: Adv. Mater. 2012.[74]

From this scaling equation it is evident that the important parameter for controlling force capacity for gecko inspired adhesives is the ratio of $\sqrt{A/C}$ since G_c cannot be varied greatly while maintaining easy release. To develop high force capacity adhesives, a large area of contact is required, without introducing compliance. To achieve these contrasting properties, composite adhesive materials consisting of stiff fabrics (to minimize *C*) and soft elastomers (to maximize *A*) are combined. Equation 1.15 does not depend on any specific features, and these adhesives have completely smooth surfaces. An example of these new gecko inspired adhesives is shown in figure 1.7A. This adhesive consists of carbon fiber fabric, and polyurethane elastomer. The surface of the elastomer pad is smooth (Figure 1.7B), and does not contain any features, like those seen on previously designed gecko-inspired adhesives. These new fibril-less, gecko-inspired adhesives are able to support

very high loads, over 2500 N for a 100 cm^2 contact area (Figure 1.8A). Additionally gecko-inspired adhesives should possess the ability to be reused many times, and Figure 1.8B demonstrates that over one hundred cycles, the average force did not significantly vary

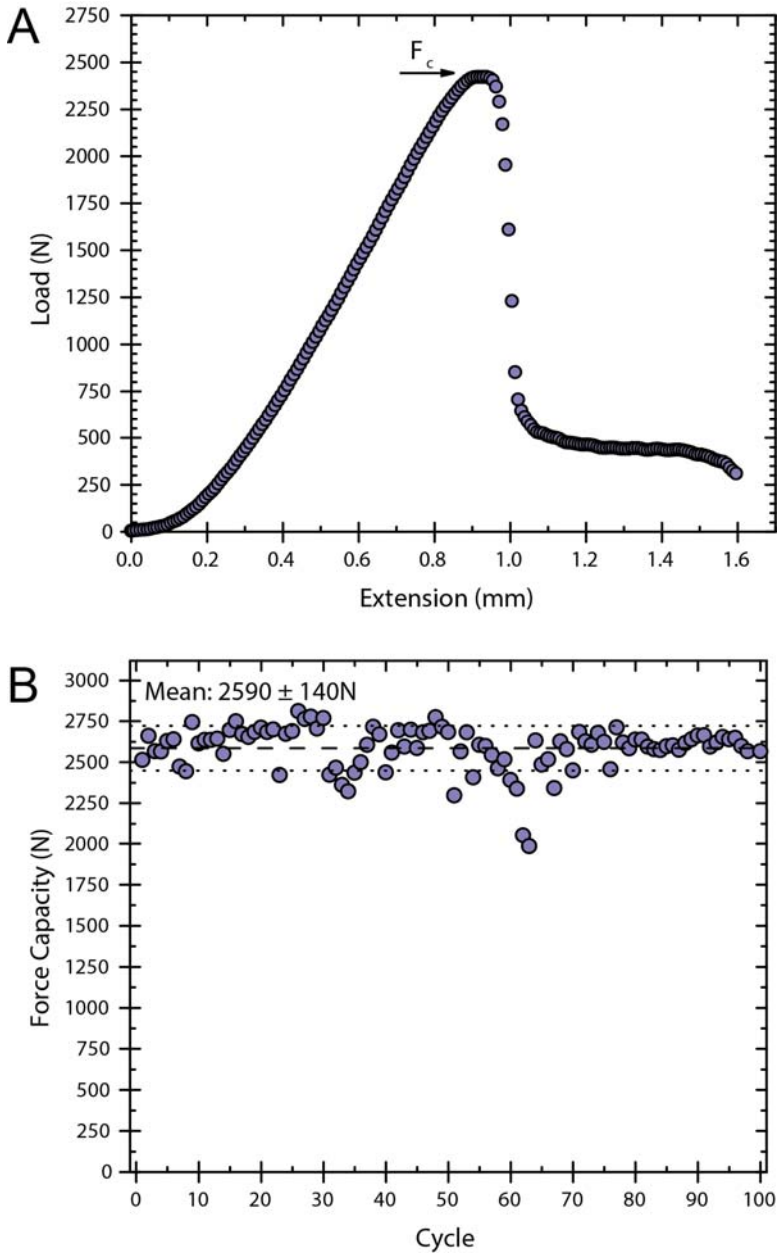

Figure 1.8 – High strength, reusable adhesives. (A) Load versus displacement curve for a fibril-less gecko-inspired adhesive consisting of unidirectional carbon fiber and polyurethane elastomer. The maximum force recorded represents the force capacity. (B) The same adhesive tested for 100 cycles. Even after one hundred tests the adhesive still performs at the mean force capacity, as determined by a one sample t-test with $P = 0.05$. Reproduced with Permission: Adv. Mater. 2012.[74]

Figure 1.9 - A 100 cm^2 adhesive pad supporting 130 kg of load. Used with Permission: Adv. Mater. 2012.[74]

from the mean force, as determined by a one sample t-test with $P = 0.05$.[74] The remarkable adhesive strength of these adhesives is displayed in Figure 1.9, where a fibril-less gecko inspired adhesive is used to support 130 kg of weights on a glass surface.

Figure 1.6 demonstrated that the derived scaling equation describes force capacity over many orders of magnitude for organisms with adhesive pads found in Nature. Interestingly, the synthetic adhesives fabricated also follow this scaling equation, and follows the same trend line. Figure 1.10 is a plot of both biological data and synthetic data. The successfulness of Equation 1.15 over fourteen orders of magnitude demonstrates the general applicability of using $\sqrt{A/C}$ to scale force capacity.

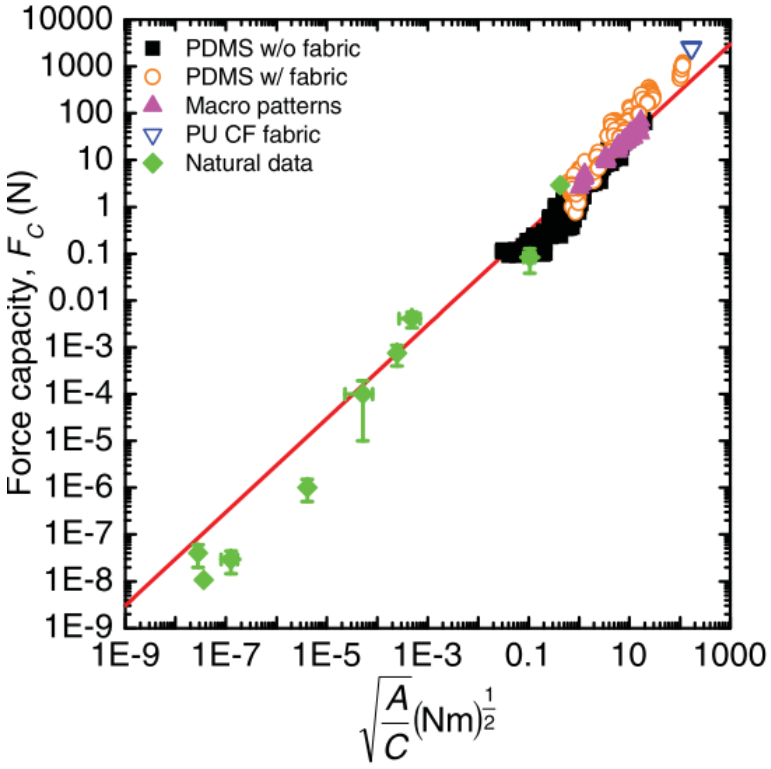

Figure 1.10 – Force capacity versus $\sqrt{A/C}$ for both biological and synthetic data. Used with Permission: Adv. Mater. 2012.[74]

When designing gecko-inspired adhesives, many researchers focus on mimicking the features which are visible on the surface. However, inspiration can occur at many levels. For example, while airplanes are capable of flight which is inspired by Nature, they do not require feathers or flapping wings. With fibril-less gecko-inspired adhesives, there are no surface features which mimic those of the gecko. However, a deeper analogy exists, where this adhesive device follows the entire morphology of the gecko toe. In the gecko adhesive system, tendons connect the skeleton of the gecko to the lamellar skin flaps called scansors, which break down into the smaller setae and spatulae features on the surface of the toe.[45] Because there is a direct connection from the skeleton, to the skin, to the pad features, compliance is minimized in the system, which is shown to be crucially important to scale force capacity in Equation 1.15. A schematic of this system is shown in Figure

1.11. Hence, fibril-less gecko-inspired adhesives are still gecko-inspired because they consist of a compliant surface "pad," which connects to the stiff fabric "tendon" through the composite elastomer/fabric "skin." In future chapters the different components of the adhesives will be described using these biomimetic terms of "pad," "skin," and "tendon."

Further research has been performed on these new gecko-inspired adhesives. Design criteria has been described for these adhesives under shear loading,[75] and methods for creating these adhesives out of "green" materials have been reported.[76] The scaling equation described in Equation 1.15 also describes scaling of normal adhesion.[77] In light of the success of these adhesives, we have pushed forward to expand the understanding of adhesion in biology and how it can inspire the development of better adhesives.

Figure 1.11 - A view of a gecko toe with an overlay of the underlying tendon structure. Tendons connect from the skeleton, through the skin, to the surface features of the gecko. Used with Permission: Adv. Mater. 2012.[74]

1.6 Dissertation Organization

We have introduced the scaling parameter, $\sqrt{A/C}$, as a proven guideline for creating high strength, easy release adhesives. In this thesis we will increase our

understanding of the variables that make up this parameter to produce adhesives with higher force capacity, for a wide range of surfaces, in any loading orientation. We additionally use lessons learned from the adhesive fabrication process to venture into a new field, creating extremely high toughness, biocompatible materials for prosthetic applications.

Chapter 2 introduces a calculated compliance equation, which is used to calculate $\sqrt{A/C}$, and therefore adhesive force capacity. The compliance equation is experimentally verified by accurately predicting the force capacity of adhesives made with two different materials, ranging from 50 N to over 2500 N. The compliance equation is used to show that optimized shapes exist which increase force capacity. Additionally, it proves that components of the adhesive far away from the interface still influence force capacity. Through understanding the materials and geometric properties of the adhesive, it is possible to calculate force capacity, reducing the need for prototyping.

Chapter 3 focuses on the A term of the $\sqrt{A/C}$ scaling parameter. To understand force capacity, the true area of contact must be known. Previous experiments focused on glass, where the true area approaches the measured adhesive area. Many desirable adhesive substrates, such as metals or painted surfaces, possess surface roughness which influences adhesion. A model is introduced that takes into account the adhesive materials as well as surface roughness to predict adhesive stress capacity, and is experimentally verified. The results of this chapter demonstrate the wide applicability of the fibril-less gecko-inspired adhesives.

Chapter 4 moves away from focusing purely on shear adhesion, and introduced double pad adhesives, a new adhesive configuration designed to increasing normal force

capacity. Important variables are introduced, including pad gap length, tendon width, and tendon materials. The best double pad adhesives demonstrate a factor of six increase in normal force capacity, without compromising shear force capacity and reusability.

Chapter 5 combines the fabrication techniques learned in developing fabric based adhesives with new polyampholyte hydrogels to create extremely tough composite materials. The composites exhibit tear strengths that are two orders of magnitude greater than the neat polyampholyte hydrogels, and four orders of magnitude greater than traditional single network hydrogels. The proposed mechanism provides a general technique for making composite materials with increased toughness.

Chapter 6 concludes with lessons learned in this thesis. Additional future work is presented, to further improve these materials. While the advances in this thesis have greatly improved fibril-less gecko inspired adhesives and materials for biological prosthetics, there is still much more to learn in these fields.

CHAPTER 2

OPTIMIZING ADHESIVE DESIGN BY UNDERSTANDING COMPLIANCE

2.1 Introduction

Adhesives are used to bind surfaces together, yet they have long suffered from a trade-off between joint strength and joint reversibility. Interestingly this tradeoff is not seen in biologically inspired adhesives.[78] Tree frogs,[27,29,31] stick insects,[24,25] and sea stars[33] are able to use smooth adhesives for locomotion, while spiders,[34,43,79] leaf beetles,[36,80] and geckos[37,38,40,81] utilize "hairy" features to climb across walls and ceilings. Previous research from our group has connected these different adhesion mechanisms by a simple scaling theory, which states that adhesive force scales with $\sqrt{A/C}$, where A is the area of contact and C is the compliance of the adhesive.[74–77] Taking advantage of this scaling parameter, we have created adhesives from simple elastomers and fabrics which are capable of extremely high adhesive forces, yet are releasable and reusable. Additionally, the materials and geometric properties of the elastomers have been shown to greatly influence force capacity.[75] However, this work focused on the limit where the elastomers are more compliant than the fabric. In this chapter we include the compliance of all components, including the fabric, as well as the test setup. Through understanding the importance of total compliance, we develop an equation to calculate force capacity, and use this framework to fabricate improved fibril-less gecko-inspired adhesives.

2.2 Background

The adhesion strength under shear deformation has long been investigated for polymeric,[82] metallic,[83,84] and composite systems.[85] A lap shear joint involves two materials that are overlapped and connected together by an adhesive member.[86–88] Two

main joint domains exist, structural adhesive lap joints and flexible adhesive lap joints.[87] Structural adhesive lap joints consist of a very thin adhesive between the two stiff adherends, with strong adhesion between the adhesive layer and the adherends. In this extensively studied regime, where the length of the joint is much longer than the thickness, the strength of the joint is controlled by the mechanical strength of the adherends.[87–92] Both analytical[93] and finite element modelling has been performed for lap shear joints.[94–96] While these models work well for rigid joints, they do not accurately describe the reversible adhesives seen in nature.

In the reversible adhesive systems studied here, the adhesive layer is a soft elastomer. Until recently there has been very little research on structures which fall into the flexible adhesives category, where deformation in the adhesive layer limits the mechanical properties of the joint. It has been shown that the geometry of the adhesive layer controls the adhesive strength of a flexible lap shear adhesive.[75] Two important lessons for designing the adhesive layer have been determined for flexible joints, and will be incorporated into our model: decreasing thickness reduces the compliance of the adhesive, resulting in higher force capacity, and combining the different deformation mechanisms using superposition determines the compliance of a joint. In high strength reversible adhesives however, this clear distinction between structural and flexible lap shear joints is lost. Deformation occurs in both adherends and adhesive, resulting in neither a fully structural or flexible adhesive joint. To predict the performance of a reversible adhesive, we must take into account the geometry and materials of both the adherend (fabric) and the adhesive layer (elastomer).

2.3 Approach

2.3.1 Deriving a Total Compliance Model

To analyze this system, we assume that a discrete rectangular "block" of elastomer (pad) is connected parallel to a composite "block" of fabric and elastomer (skin), which is connected to an additional "block" of fabric attached at the bottom (tendon, 3D schematic and 2D projection in Figure 2.1A and Figure 2.1B). The names given to each component refer to the component of the gecko adhesive system which it mimics. Each block has a discrete width, *w*, length, *L*, thickness, *t*, and Young's modulus, *E*. Three different

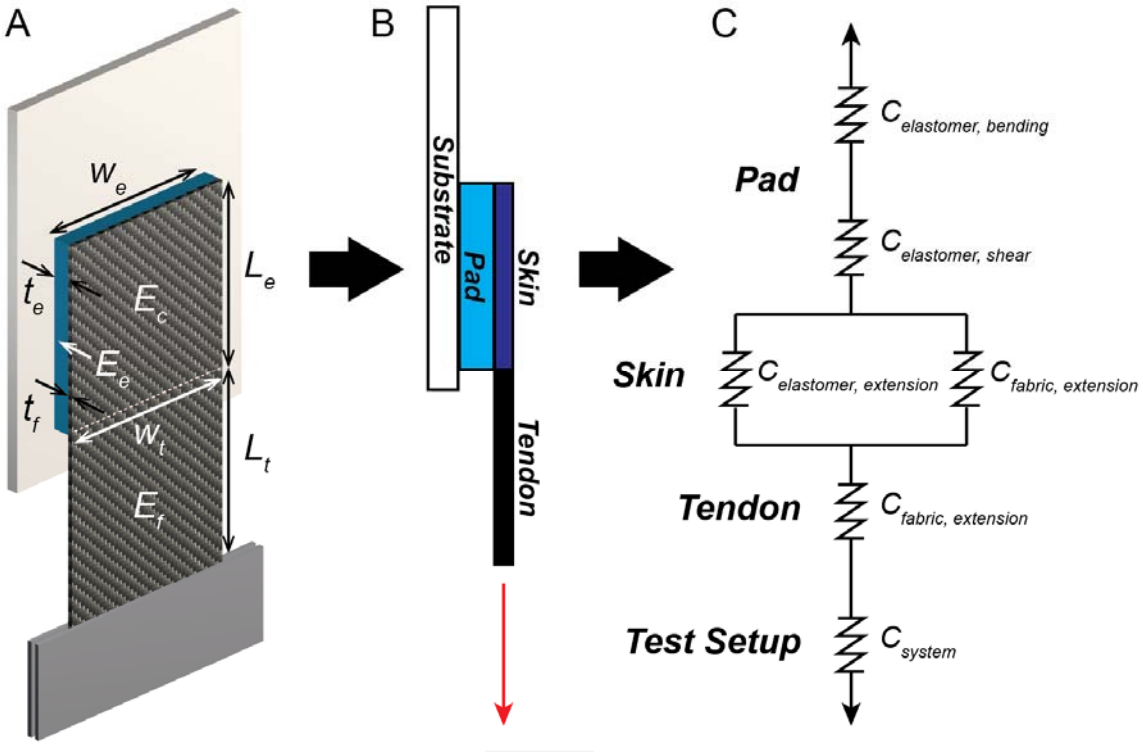

Figure 2.1 – Schematic of an adhesive pad on a substrate. (A) Relevant geometric and materials properties are noted. (B) 2D schematic projection of an adhesive pad, with the important components labeled. (C) A representation of the compliance for each adhesive component, denoted as springs in the overall system.

deformation modes will be assumed: extension, shear, and bending.[75,93]

Extension will be modeled using Hooke's Law:

$$\sigma = \frac{F}{A} = E\varepsilon \tag{2.1}$$

Where σ is stress, ε is strain, F is force, and A is area. Compliance, is written as $C = \Delta/F$, where Δ is displacement. In extension, $\varepsilon = \delta/L$, and $A = wt$ giving:

$$C_{extension} = \frac{L}{wtE} \tag{2.2}$$

In shear, strain is defined as $\varepsilon = \delta/t$, with $A = wL$, and $E \approx 3G$ (assuming Poisson's ratio = 0.5), where G is the shear modulus. Using Hooke's Law for shear, $\sigma = F/A = G\varepsilon$, giving:

$$C_{shear} = \frac{3t}{wLE} \tag{2.3}$$

When $t > L$, bending significantly contributes to the total compliance.[75] This compliance is:

$$C_{bending} = \frac{4t^3}{wL^3E} \tag{2.4}$$

The adhesives are tested in a lap shear configuration. For the pad, the applied force is parallel to the attachment surface. When $t < L$, shear compliance dominates, and when $t > L$, bending compliance dominates.[75] By combining Equation 2.3 and Equation 2.4, the pad compliance is obtained:

$$C_{pad} = \frac{4{t_e}^3}{w_e{L_e}^3E_e} + \frac{3t_e}{w_eL_eE_e} \tag{2.5}$$

For the adhesives fabricated here, the skin is a composite component consisting of elastomer and fabric. This component is fixed along its length to the pad. The force is applied to the wt cross-section of the skin, and this results in extensional deformation of the skin and the attached pad. The extensional compliance of the skin is:

$$C_{skin,ext} = \frac{L_e}{w_et_fE_c} \tag{2.6}$$

Where E_c is the composite modulus of the fabric and elastomer, which depends on the volume fraction, φ, of the elastomer in the fabric. As a first approximation, a Voigt model

composite is used to model this component because the fabric and elastomer both deform with equal strain.[97] More complicated models also exist for modeling composites.[98] Using the Voigt model gives the composite modulus:

$$E_c = E_e\varphi_e + E_f\varphi_f \tag{2.7}$$

$$\varphi_i = \frac{V_i}{V_T} \tag{2.8}$$

Where E_f is the Young's modulus of the fabric. V_i is volume of the elastomer, *e,* or fabric, *f*. V_T is the total volume. Because the skin is directly connected to the pad, any extension that occurs in this component will result in extension of the pad, which must also be included:

$$C_{pad,ext} = \frac{L_e}{w_e t_e E_e} \tag{2.9}$$

Equation 2.6 and Equation 2.9 are added in parallel to determine the total compliance of the skin:

$$\frac{1}{C} = \frac{w_e t_f E_c}{L_e} + \frac{w_e t_e E_e}{L_e} \tag{2.10a}$$

$$C_{skin} = \frac{L_e}{w_e}\left[\frac{1}{t_f E_c + t_e E_e}\right] \tag{2.10b}$$

The last component of the adhesive is the tendon, which consists of fabric and is attached to the skin. This component exhibits extensional compliance, which is therefore expressed:

$$C_{tendon} = \frac{L_t}{w_t t_f E_f} \tag{2.11}$$

Finally, we must include the compliance of the test setup, C_{system}, which is measured experimentally. The pad, skin, tendon, and system are in series (where compliances are additive) and superposition principles are used to add their compliances together to

calculate a total combined compliance (Figure 2.1C). Therefore, the sum of Equation 2.5, Equation 2.10, and Equation 2.11 yields:

$$C_{calculated} = \frac{4{t_e}^3}{w_e{L_e}^3 E_e} + \frac{3t_e}{w_e L_e E_e} + \frac{L_e}{w_e}\left[\frac{1}{t_f E_c + t_e E_e}\right] + \frac{L_t}{w_t t_f E_f} + C_{system} \qquad (2.12)$$

Each term in Equation 2.12 depends on both geometric and materials properties which are easily measured directly. We have previously shown that force capacity is calculated:[74]

$$F_c = \sqrt{2G_c}\sqrt{\frac{A}{C}} \qquad (2.13)$$

where G_c is the critical strain energy release rate for shear adhesion, and will be used as a fitting parameter. To determine F_c, we substitute Equation 2.12 into Equation 2.13, to give:

$$F_c = \sqrt{2G_c}\sqrt{\frac{w_e L_e}{\frac{4{t_e}^3}{w_e{L_e}^3 E_e} + \frac{3t_e}{w_e L_e E_e} + \frac{L_e}{w_e}\left[\frac{1}{t_f E_c + t_e E_e}\right] + \frac{L_t}{w_t t_f E_f} + C_{system}}} \qquad (2.14)$$

Equation 2.14 demonstrates that both geometric and materials properties play a role in the compliance of each system component. Using this equation, it is possible to estimate which materials will result in high strength adhesives. Figure 2.2 is a contour map of the elastomer modulus versus the effective fabric modulus, where the color denotes the calculated force capacity, assuming G_c = 170 N/m. In this plot, blue represents the lowest force capacities, and red represents the highest force capacities. The geometry of the adhesive pad is fixed, with a 10 cm x 10 cm pad with a thickness of 0.4 mm, and a 10 cm tendon length. To achieve high force capacities, visible in the upper right, both the fabric and the elastomer modulus must be increased. Combining a low modulus elastomer with any modulus fabric results in low force capacity, because the pad compliance is too high. Likewise, combining a low modulus fabric with any modulus elastomer also results in low

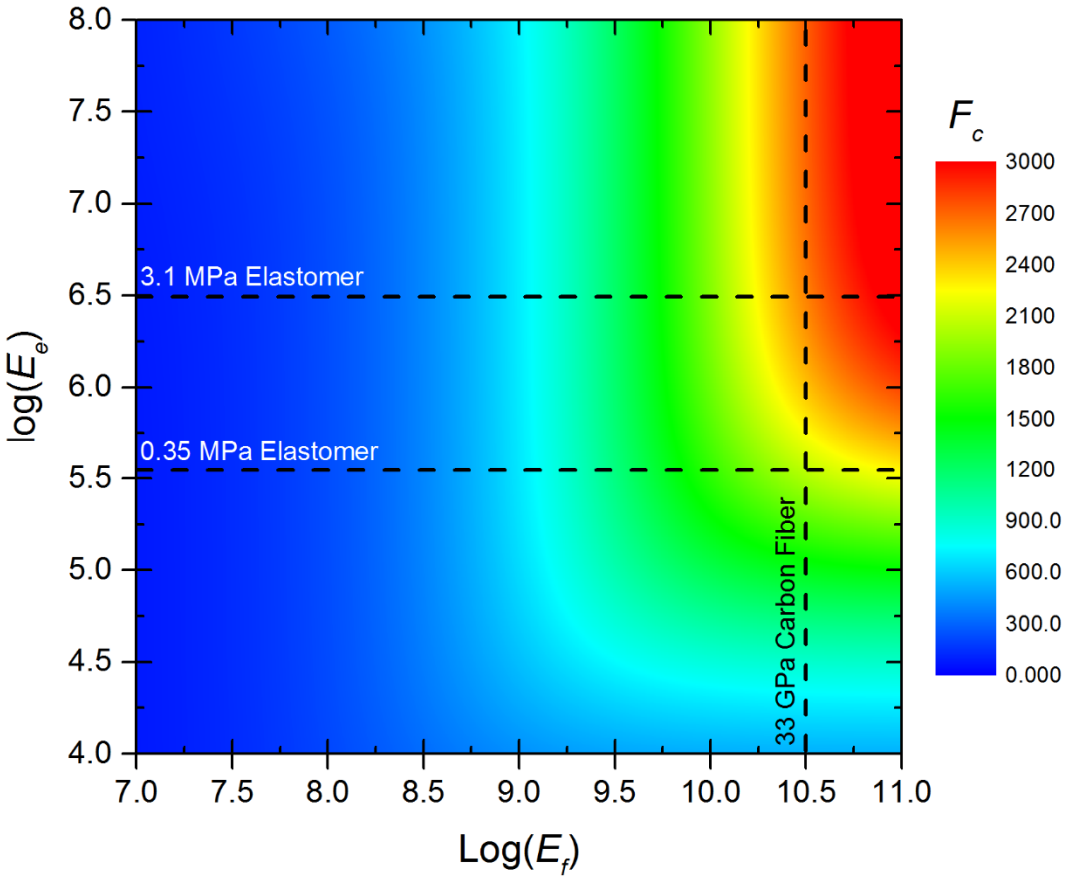

Figure 2.2 - Plot of force capacity as a function of elastomer modulus and effective fabric modulus. Color represents the force capacity for the combination of elastomer and fabric modulus with fixed geometry, L_e = 10 cm, w_e = 10 cm, t_e = 0.4 mm, L_t = 10 cm, and G_c = 170 N/m.

force capacity, because the skin and tendon compliance is high. Combining a high modulus elastomer and a high modulus fabric however, results in high force capacities as the compliance of all components are minimized. This is counter-intuitive to traditional adhesive design, which states that the modulus must be below the Dahlquist Criterion (10^5 Pa) to create good contact with the surface and increase the work of adhesion. Even with the stiffest fabrics, the maximum force capacity that can be achieved with elastomers below the Dahlquist Criterion is less than half of the maximum force capacity predicted when using high modulus elastomers. Focusing only on materials with a modulus below the

Dahlquist Criterion prevents the fabrication of adhesives which are capable of the highest force capacities.

Based on this plot, materials are chosen for fabricating adhesives. Since the highest force capacities occur with the highest modulus fabrics, carbon fiber fabric will be used for the synthetic adhesives. A vertical line is drawn on Figure 2.2, which represents the modulus of the unidirectional carbon fiber. On this line, as elastomer modulus increases, force capacity increases by an order of magnitude. Two elastomers are chosen. One elastomer, with a modulus of 3.1 MPa is chosen, as this is the modulus at which force capacity begins to saturate. Additionally, a 0.35 MPa elastomer is chosen, as this material is close to, but slightly above the Dahlquist Criterion. This method for choosing adhesive materials demonstrates the power of Equation 2.14, as it allows for force capacity prediction, without requiring time consuming and expensive prototyping.

2.4 Experimental

2.4.1 Materials

Materials for fabricating the elastomer pads are purchased from BJB Enterprises. The following elastomers were chosen: ST1060, F15, ST3040, ST1075, and ST1085. The two components are mixed together in a plastic cup (60 mL for two adhesives), and degassed in a desiccator until bubbles disappeared. The mixture is then reintroduced to air, with an approximate work time of 20 minutes before gelation occurred. Moduli are determined by dynamic mechanical analysis (DMA) at 0.40 Hz, the frequency that corresponds to the adhesives testing rate for the 0.40 mm thick elastomers (mastercurves for ST1060 and F15 are shown in Figure 2.3). The elastomer moduli are 3.1 MPa for

ST1060, 0.35 MPa for F15, 1.0 MPa for ST3040, 6.9 MPa for ST1075 and 22.1 MPa for

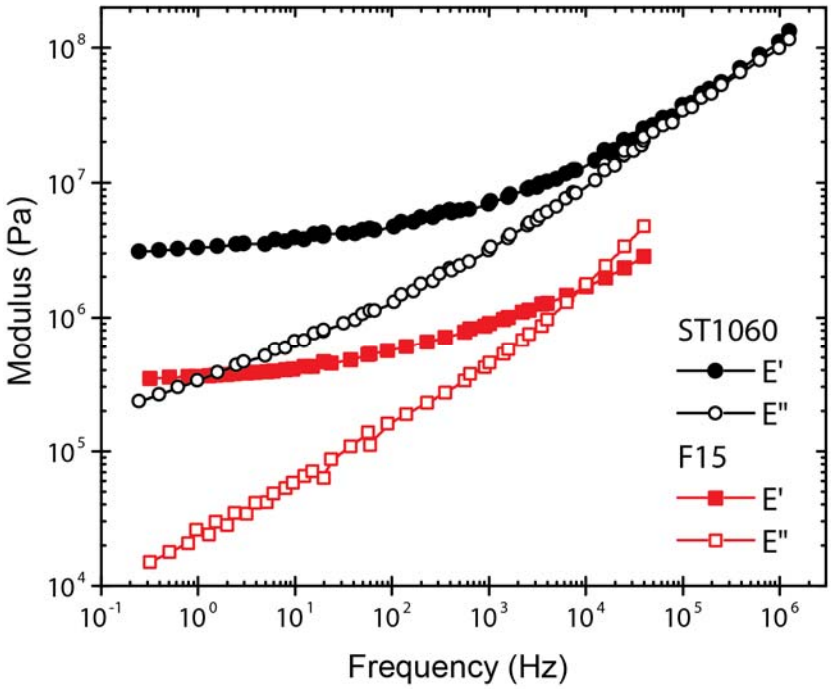

Figure 2.3 - Dynamic mechanical analysis (DMA) results for the two elastomers used in this chapter. E' (solid data) represents the storage modulus, and E" (hollow data) represents the loss modulus. The modulus at 0.4 Hz corresponds with the mechanical response of the elastomers used in the fabricated adhesives.

ST1085.

24K unidirectional carbon fiber tape was purchased from Soller Composites, with a nominal thickness of 0.3 mm, measured with calipers. Modulus was determined by uniaxial tension experiments. 25 mm x 100 mm (l x w) samples were gripped and displaced at 10 mm/min until a load of 1800N was reached. The effective modulus of the fabric was determined by the linear regression of the slope of the stress versus strain curve. The effective modulus was 33 ± 2 GPa, averaged from five individual specimens.

2.4.2 Fabrication

Bemis 3231 adhesive film (50 μm thick with paper release liner) is adhered to the top and bottom of the fabric with an iron set at approximately 200°C, denoting the top and

bottom of the adhesive pad region. This thin adhesives film prevents fraying of the fabric. The release liner is left on until after sample fabrication was complete. On polyethylene (PE) coated glass, the carbon fiber fabric is taped into place, with three pieces of 3M packing tape, over the Bemis adhesive film release liner. The uncured elastomer is poured onto the fabric, and smoothed with a glass slide. A thin PE film is placed on top of the thin layer of uncured polymer. A glass plate is then placed on top of the film, and 25 pounds of force is applied to create a smooth adhesive surface. Samples are cured at room temperature overnight (at least 12 hours), then placed in a 70°C oven for at least 12 hours. After curing is complete a rotary blade cutter is used to cut the samples to the desired size, and the release liner is removed. Two pieces of 3 mm thick polycarbonate (purchased from McMaster Carr) are adhered to the bottom of the fabric using a cyanoacrylate glue, leaving a 10 cm gap between the polycarbonate anchor and the adhesive pad. Two 5/8" diameter holes are drilled through the polycarbonate anchor to attach to the custom built adhesive anchor.

2.4.3 Testing

An Instron 5500R tensile tester is utilized for testing. The adhesive is anchored to the base of the tensile tester with a custom built adhesive anchor, which allows for rotational freedom in the plane of the adhesive (Figure 2.4). The glass substrate is held in place by a custom built substrate holder, which is tightly attached to the crosshead, and displaced at a rate of 10 mm/min, until the sample detaches from the surface. The adhesive test setup has a measured compliance of 2.5×10^{-7} m/N. Each test is performed at least 5

times, and the first test is excluded to allow for conditioning of the test setup and adhesive pad.

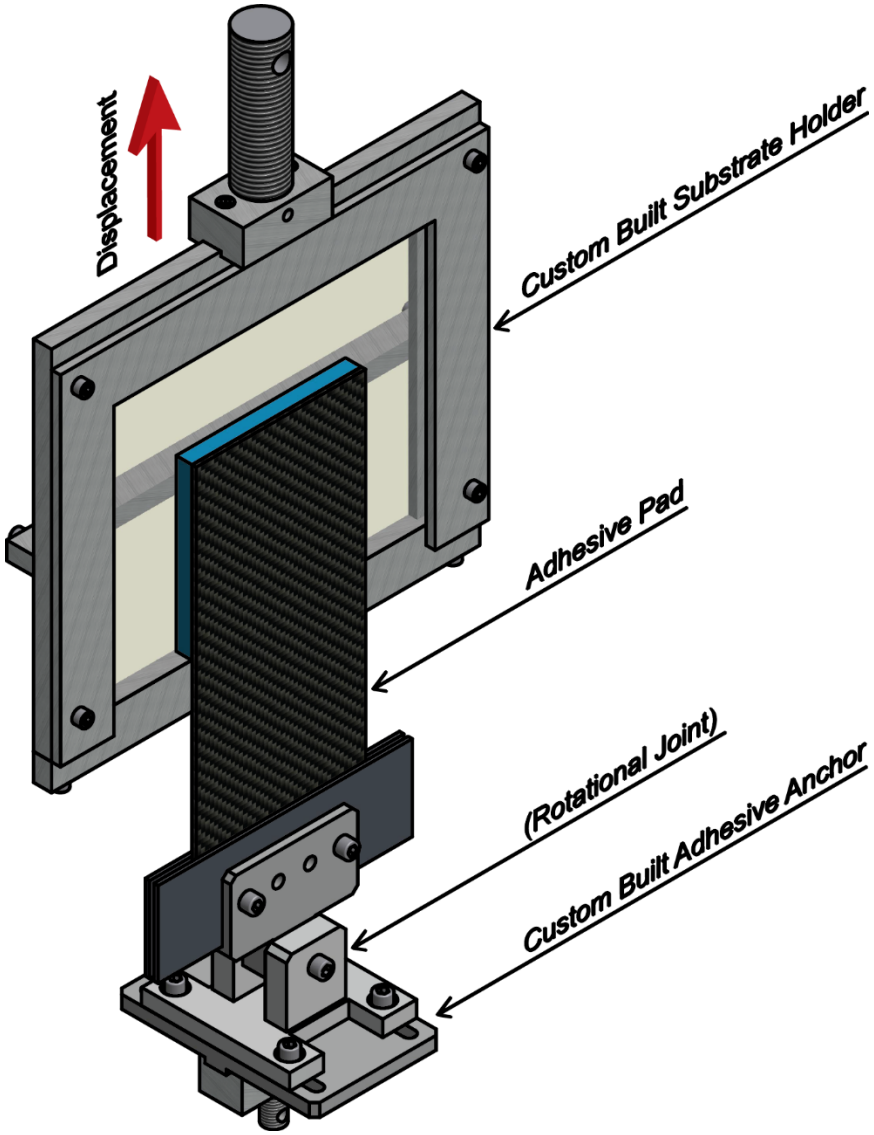

Figure 2.4 – Schematic of the test setup. The custom built substrate holder and adhesive anchor were machined with 6061 Aluminum.

2.5 Results

2.5.1 Verifying Equation 2.14

Equation 2.14 is used to select materials for creating high strength, reusable adhesives. Each sample was tested with $L_e = 10$ and $w = 10$, then cut to a smaller size and

retested, maintaining $L_e = w_e = 1$. The sizes tested are 100 cm^2, 64 cm^2, 49 cm^2, 36 cm^2, 25 cm^2, 16 cm^2, 9 cm^2 and 4 cm^2, and at each size at least 5 tests are performed. A representative force versus displacement curve for each pad area is shown in Figure 2.5, for both 3.1 MPa and 0.35 MPa elastomer samples. As pad area is reduced, force capacity decreases, and the adhesive compliance increases. Additionally, sample to sample variability is minimal for the prepared adhesives, which is presented in Figure 2.6.

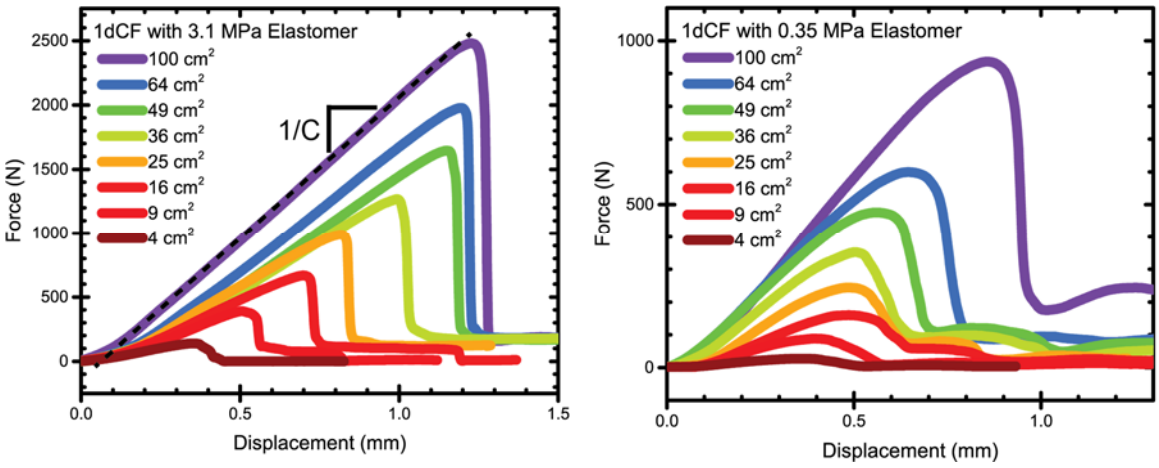

Figure 2.5 - Representative force versus displacement curves for adhesives made with both the 3.1 MPa and the 0.35 MPa elastomer. On the left, a representative best fit line for compliance is drawn on the 100 cm^2 adhesive test.

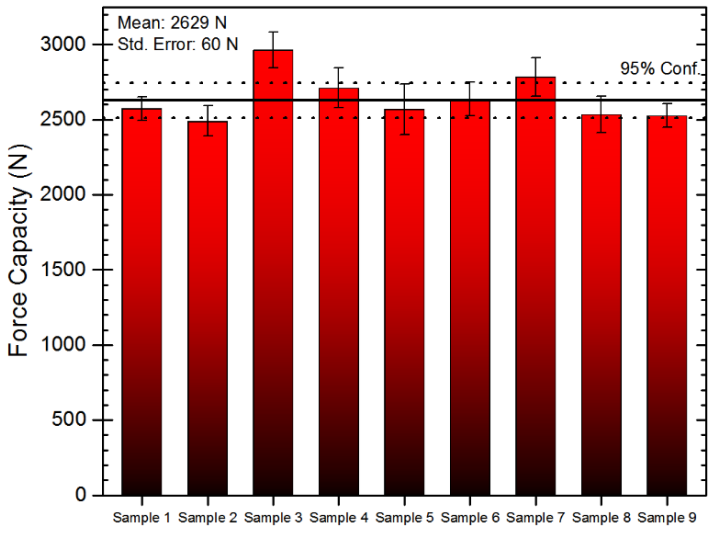

Figure 2.6 - Sample to sample variability for 9 samples made with unidirectional carbon fiber and the 3.1 MPa modulus elastomer.

From the force versus displacement curves, a compliance is calculated from the inverse of the slope of the loading curve, which is fitted with a linear regression from a load of 2 N to the maximum load. Because the elastomers are soft and visibly wet the glass, the measure area is assumed to be the true area of contact. The area is divided by the compliance to determine the experimental scaling parameter, $\sqrt{A/C}$. In Figure 2.7, the measured experimental values of $\sqrt{A/C}$ versus the calculated $\sqrt{A/C}$ from Equation 2.14 are compared. The dotted line in the plot represents a slope of 1, which represents a true agreement between experimental and calculated values. The solid black line is a linear regression of all experiments, and has a slope of 0.99, displaying almost perfect prediction of $\sqrt{A/C}$.

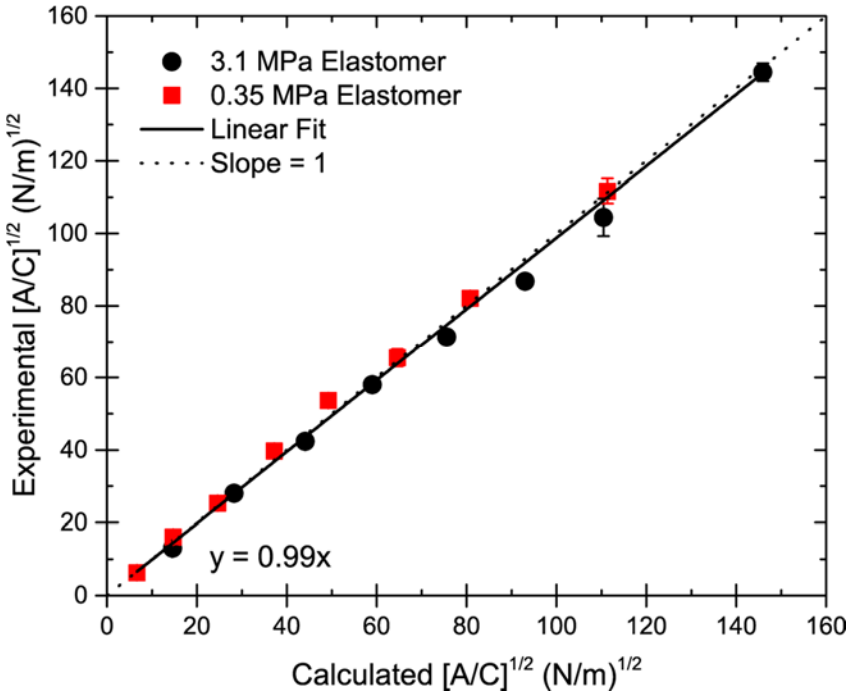

Figure 2.7 - A plot of experimental $\sqrt{A/C}$ versus calculated $\sqrt{A/C}$, for the two different adhesive pads. A slope of 1 represents perfect agreement between the calculated and experimental results, and the resulting linear regression has a slope of 0.99.

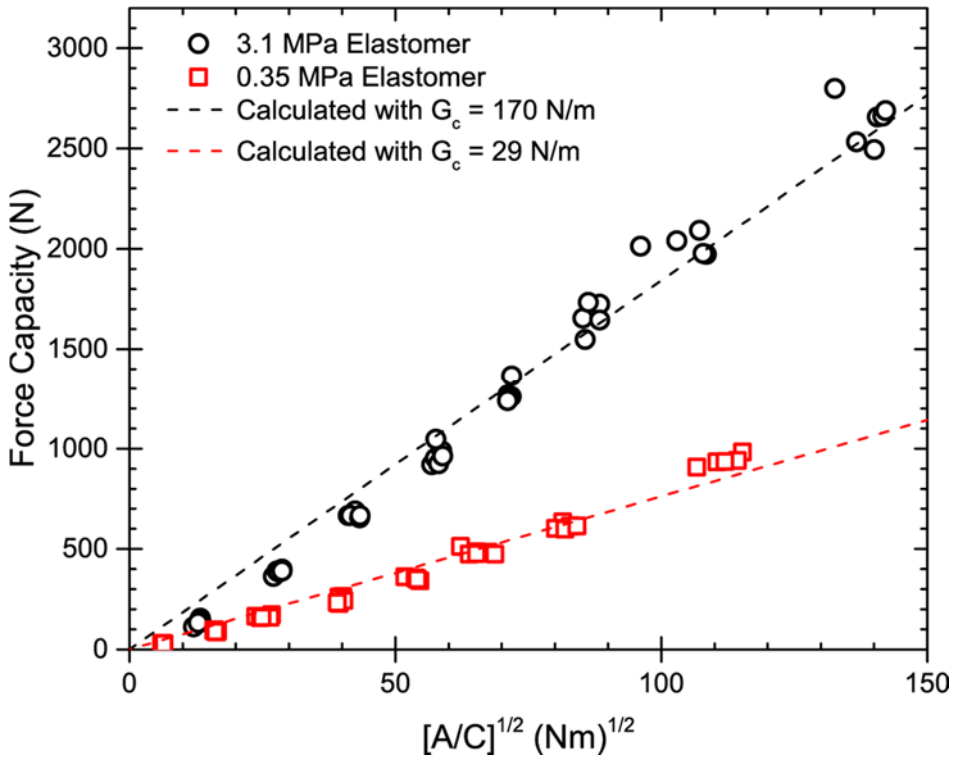

Figure 2.8 - A plot of force capacity versus $\sqrt{A/C}$. As $\sqrt{A/C}$ increases, force capacity increases for both adhesives. The rate of increase in force is the G_c of the system. Using Equation 2.13 and fitting for G_c allows us to accurately predict the force capacity

Being able to predict $\sqrt{A/C}$ is an important step towards calculating force capacity. To quantitatively calculate a force capacity, the critical strain energy release rate (under shear loading conditions), G_c, must be determined. Equation 2.13 states that by plotting force capacity versus $\sqrt{A/C}$, G_c for the adhesive can be calculated from the slope. This is performed in Figure 2.8. Interestingly, the two different formulations have dramatically different values of G_c: 170 N/m for the 3.1 MPa elastomer, and 29 N/m for the 0.35 MPa elastomer. This can be attributed to the two pad materials consisting of different material chemistries. For both sample formulations, force capacity scales linearly, as described by Equation 2.13. The dashed lines in the plot represent a calculated value of F_c from Equation

2.14. After determining a G_c for each adhesive, Equation 2.13 can be used to accurately calculate force capacity for the fabricated adhesives.

2.5.2 Importance of Shape

2.5.2.1 Shape Ratio

For commercially available adhesives, shape is generally determined by form rather than function. To maximize adhesive force capacity, compliance must be minimized, and geometric variables are an important component of compliance. For example, the compliance of the skin component of the adhesive decreases with increasing width and decreasing length. Therefore, understanding the importance of adhesive shape is necessary to optimize force capacity for adhesives of a given size.

Shape ratio, SR, of an adhesive is defined as the length (L_e) of the pad divided by the width (w_e). The impact of geometry for each adhesive component is described in Equation 2.12. Pad bending and pad shearing do not depend on shape ratio. However, the skin in extension is directly proportional to the shape ratio with a slope of 1, and the tendon in extension is dependent with a slope of 0.5. Based on this understanding, shape ratio must be decreased until a minimum compliance is achieved to maximize force capacity.

Samples are created with varying shape ratios to verify the hypothesis that decreasing shape ratio will increase force capacity. Each sample is first tested with $SR = 1$ and $L_e * w_e = 100$ cm^2 as a benchmark, to verify that the sample was fabricated successfully. Sample size is then reduced by cutting the adhesive into pads with varying shape ratios. Since 10 cm is the maximum available width and length, the available shape ratio range becomes larger as pad area decreases. Samples are tested at three pad areas, 49 cm^2, 25 cm^2, and 9 cm^2. For the 49 cm^2 pad shape ratio varies from 0.49 to 2.04, for the 25 cm^2 pad

shape ratio varies from 0.25 to 4, and for the 9 cm^2 pad shape ratio varies from 0.09 to 11.1. These areas are chosen to determine whether shape ratio is significant for both small and large pads, and to provide a wide range of achievable shape ratios.

Equation 2.14 is used to calculate the force capacity for adhesives with varying shape ratios. This is plotted in Figure 2.9 for the experimentally tested areas. Calculated forces are compared to experimental results for adhesives with five shape ratios at each sample area. As shape ratio decreases, the force capacity generally increases across the entire range of shape ratios for all pad areas. The 49 cm^2 adhesive pads exhibit a very strong dependence on shape ratio, with force capacity increasing 45% from highest to lowest

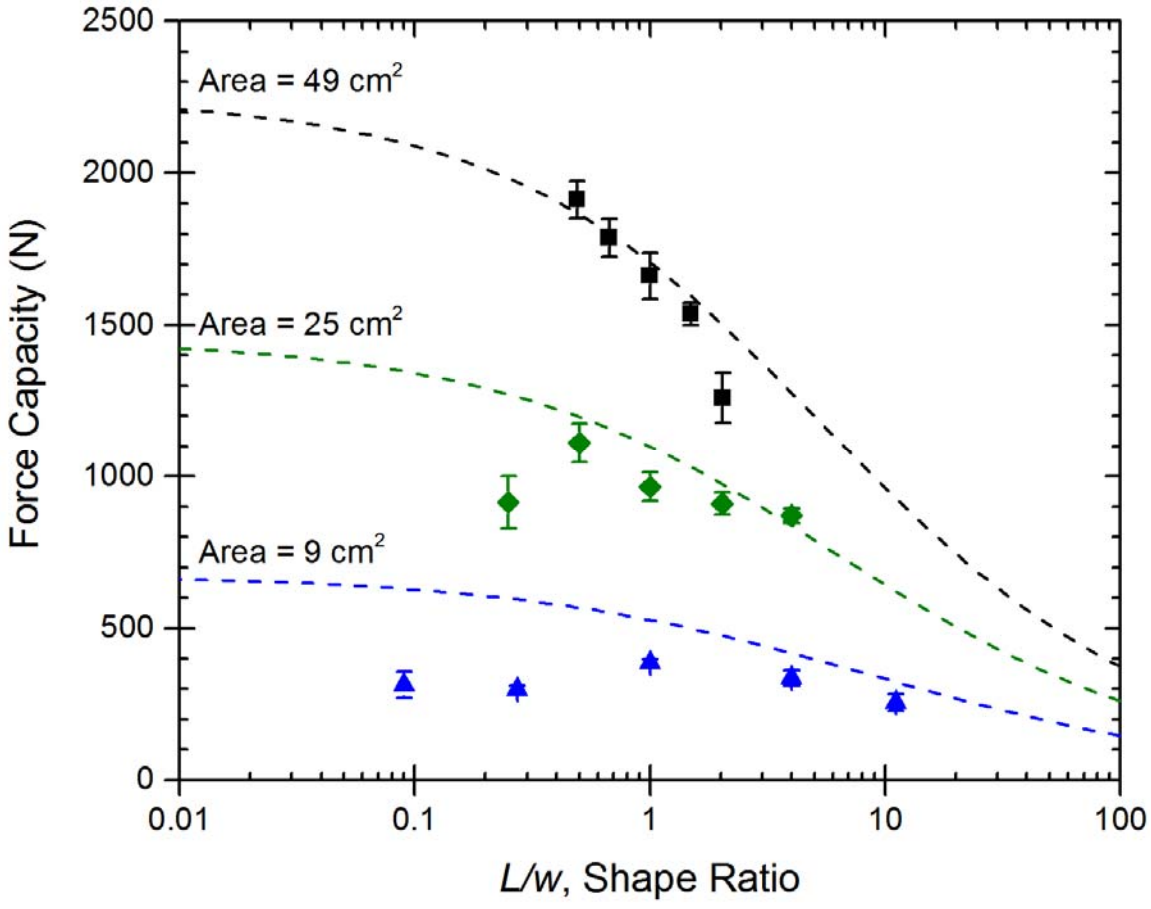

Figure 2.9 - A plot of force capacity versus shape ratio for 3.1 MPa elastomer adhesives. Dotted lines represent calculated force capacity for varying pad areas. Solid data points represent experimental results.

shape ratio. For the 25 cm^2 adhesive pads, a weaker dependence on shape ratio is calculated. This dependence agrees with the experimental results until $SR = 0.5$. For $SR = 0.5$, the force capacity greatly drops to a level equal with the force of the highest shape ratio sample. In the case of the 9 cm^2 adhesive pads, only a slight increase in force capacity is predicted with decreasing shape ratio. Again, a slight increase in force capacity is seen as shape ratio decreases, until shape ratio decreases below 0.5. As sample width increases and pad length decreases, load distribution across the width of the pad becomes increasingly more difficult. This poor load distribution results in stress concentrations within the pad, and crack growth begins in these locations. Once crack growth begins, due to short pad lengths and the elastic nature of the adhesives, the sample quickly fails through the whole sample. A tradeoff is clearly evident between shape ratio and sample loading ability; low shape ratio minimizes compliance, which is necessary to increase force capacity, but must not be so low that sample loading is negatively influenced.

Decreasing compliance increases force capacity, but if the adhesive component being tuned is already sufficiently stiff, the total system compliance will not change. Observing how the compliance of each component varies with shape ratio reveals which components most greatly influence force capacity. In Figure 2.10, the compliance of each component is plotted as a function of shape ratio, for each pad area. The black line represents Equation 2.12, the sum of the compliance for each component, and the data points represent the experimental compliance for each adhesive. The compliance of the pad does not change with shape ratio. However, the compliance of the skin is strongly dependent on the shape ratio, increasing with a slope of 1 as shape ratio increases. The

tendon is also dependent on width, but not length, and increases with a slope of 0.5 as shape

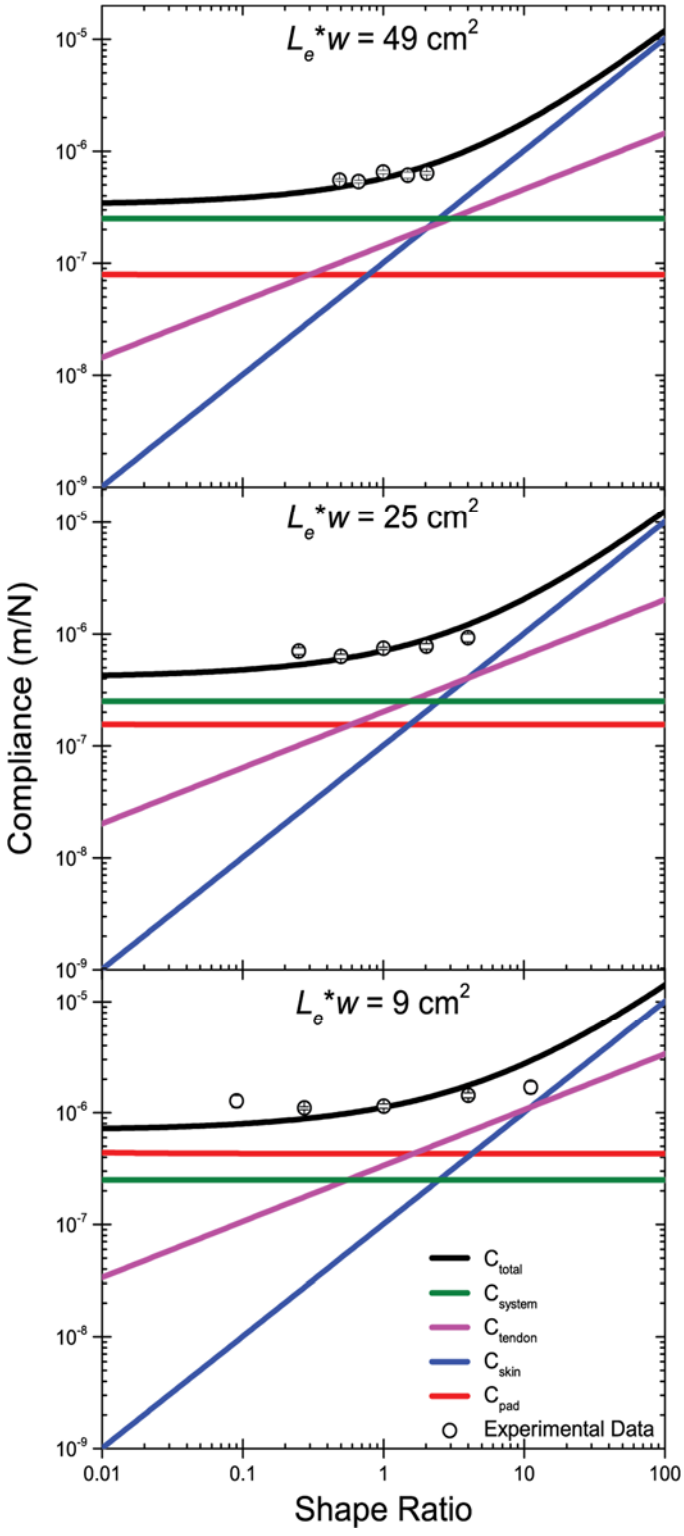

Figure 2.10 - Plots of compliance versus shape ratio for adhesives with three different pad areas. The sum of each individual component results in the total compliance for the adhesive. Open data points represent experimental results.

ratio increases. Finally, the compliance of the test system must also be included, because any source of compliance, regardless of distance from the adhesive interface, influences force capacity. The plots of compliance versus shape ratio for varying pad areas demonstrate which adhesives benefit from tuning shape ratio.

Understanding the compliance of each component allows for optimization of shape ratio for a given pad area. For the 49 cm^2 adhesive pads at high shape ratios, skin undergoing extension is the most compliant component of the system. As shape ratio decreases to $SR = 2$, the test system becomes the most compliant component. Therefore, at $SR < 2$, the adhesive pad approaches the minimum attainable compliance, which is seen as a plateau in the total compliance as shape ratio decreases. For the 25 cm^2 adhesive pads at $SR > 3$ the skin is again most compliant, followed by a short region ($1.5 < SR < 3$) where the tendon is most compliant. When $SR < 1.5$, the system and the pad are the most compliant components of the entire system. Interestingly, at $SR = 0.6$ the tendon compliance drops below the pad compliance, and the pad then becomes the most compliant part of the adhesive. Below this shape ratio force capacity decreases, because the sample peels locally from an isolated crack at the pad interface. This result is consistent with the pad being the most compliant component of the adhesive. Finally, for the 9 cm^2 adhesive pads, when $SR > 10$ the skin is the most compliant component. When $1.5 < SR < 10$, the tendon is the most compliant component of the system. Despite being made of carbon fiber, a material with modulus four orders of magnitude greater than the elastomer, the tendon is the limiting factor of adhesive force capacity. For $SR < 1.5$, the pad is the most compliant component of the system, and for $SR < 0.6$ only the pad and system greatly influence compliance. In this region a decrease in force capacity is observed due to poor loading

across the width of the sample, which is a result of high pad compliance. Failure mechanisms which result in lower than expected force capacities can be prevented by controlling the most compliant component of the adhesive system.

2.5.2.2 Calculating Compliance of Non-rectangle Adhesives

In some situations, pads with rectangular geometry may not be ideal. Equation 2.14 is derived specifically to calculate the force capacity for reversible adhesive systems with rectangular geometry. By altering the compliance equation, Equation 2.12, to allow for shapes where the length changes with the width of the sample, e.g. triangle or pentagon shaped adhesive pads, compliance for any shape can be calculated. For these adhesives, compliance is calculated by integrating over a finite sample width, x, where L_e is a function of x, to determine the compliance:

$$C_{calculated} = \int_0^x \left(\frac{4{t_e}^3}{L_e(x)^3 E_e} + \frac{3t_e}{L_e(x) E_e} + L_e(x) \left[\frac{1}{t_f E_c + t_e E_e} \right] + \frac{L_t}{t_f E_f} \right) d\left(\frac{1}{w_e} \right) \quad (2.15)$$

Equation 2.15 is substituted into Equation 2.13 to calculate force capacity. In Figure 2.11, for samples of varying shape with areas of approximately 49 cm^2, the calculated $\sqrt{A/C}$ ratios are plotted, along with the resulting force capacities. Geometric properties of the triangle and pentagon shaped adhesives are listed in the caption of Figure 2.11. As previously mentioned, high shape ratio rectangles are not preferred, and $\sqrt{A/C}$ for the *SR* = 2 adhesive pad is low. However, for the pentagon and triangle a slight increase in $\sqrt{A/C}$ is calculated, with the triangle slightly less than the *SR* = 0.5 rectangle. The force capacity results generally agree with the $\sqrt{A/C}$ ratio calculations. The force of the *SR* = 2 rectangle is the lowest. No statistical significance was determined between the square and the pentagon ($P = 0.025$). The triangle exhibited a higher force capacity, statistically equivalent

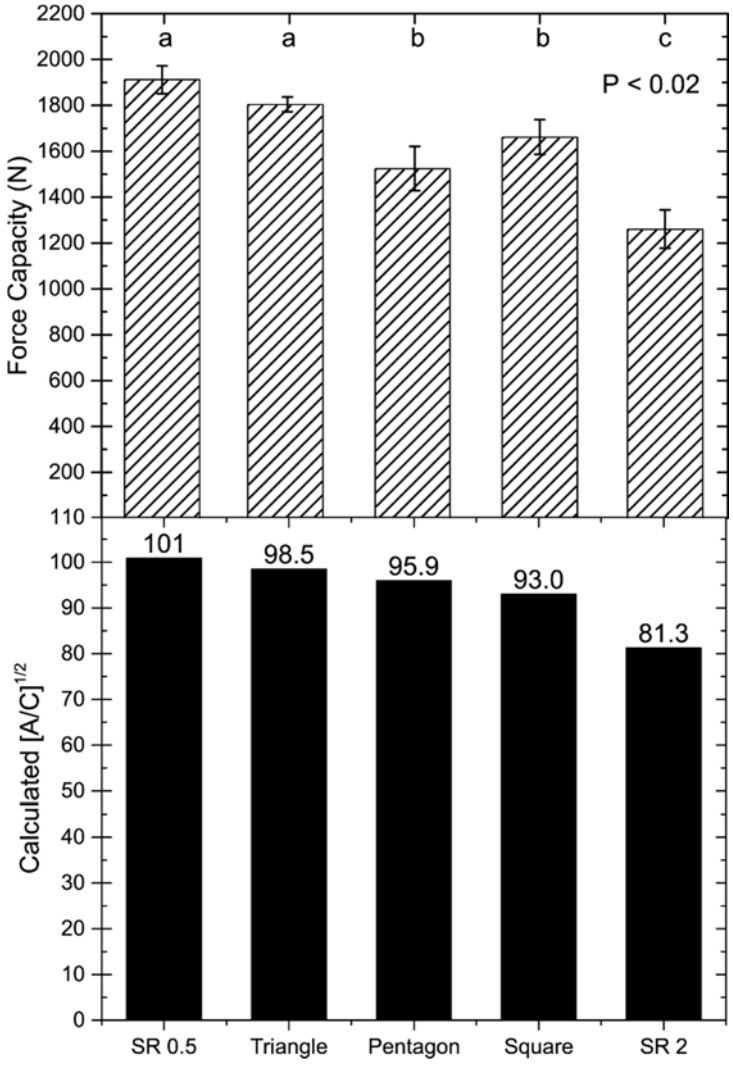

Figure 2.11 - A plot of $\sqrt{A/C}$ and force capacity for adhesives of varying geometry. Dimensions for the triangle are base = 10 cm and height = 10 cm, and for the pentagon is edge height = 4.9 cm, center height = 8 cm, and width = 7.8 cm. ANOVA analysis with a post-hoc Tukey test for $P < 0.02$ is used to determine significance. *SR* 0.5 rectangle and triangle adhesives are found to provide the best performance for a pad area of 49 cm^2.

to that of the $SR = 0.5$ adhesive ($P = 0.09$). The triangle has an additional benefit: more adhesive area is located towards the middle of the pad, whereas a rectangular pad has equally distributed pad area. Failure often initiates at the edges of the adhesive, and therefore triangular adhesives avoid failure due to crack initiation from the edges of the sample.

2.5.3 Importance of the Tendon

2.5.3.1 Tendon Length

In some circumstances the tendon is the most compliant component of the system, limiting force capacity. To test the impact of tendon length, an adhesive with area = 100 cm^2, $SR = 1$ and $L_t = 40$ cm is fabricated, and the tendon length is systematically decreased to determine the impact of tendon length on measured compliance and force capacity. Figure 2.12 presents both $\sqrt{A/C}$ and the force capacity as a function of tendon length. As

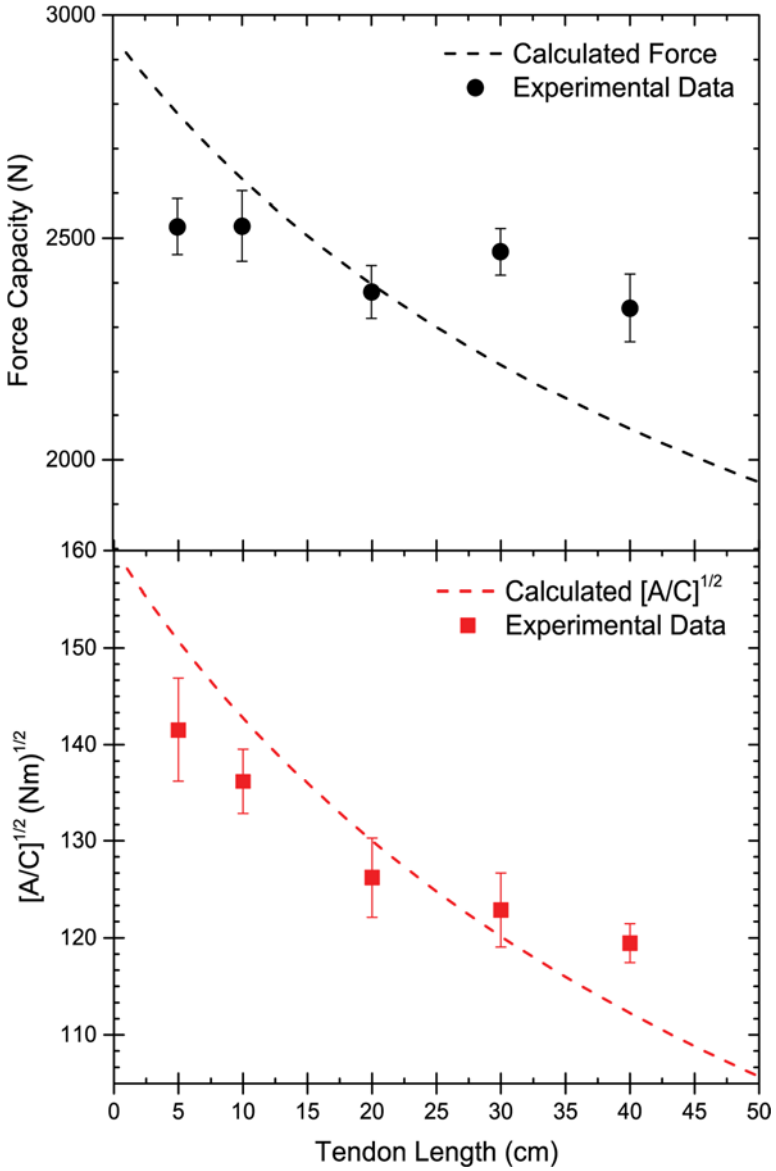

Figure 2.12 - A plot of $\sqrt{A/C}$ and force capacity versus tendon length. As tendon length increases, both $\sqrt{A/C}$ and force capacity are expected to decrease (dashed lines).

tendon length increases, $\sqrt{A/C}$ is calculated to decrease dramatically, with a 35% decrease expected from 5 cm to 40 cm tendon lengths. However, over this tendon length range, only a 20% decrease is observed. Even more surprisingly, this drop in $\sqrt{A/C}$ did not directly translate to a drop in force capacity; only an 8% decrease in force capacity is experienced. The individual compliance of each component is analyzed to determine which components contribute the most to the total compliance. In Figure 2.13 the compliance of each component is plotted as a function of tendon length. As tendon length varies, the compliance of the pad, skin, and system are constant, while the tendon compliance increases with increasing tendon length. However, the tendon is only the most compliant component for L_t > 25 cm. Below 25 cm, the test setup is the most compliant component, limiting the force capacity increase with decreasing tendon length. Below 10 cm, the skin

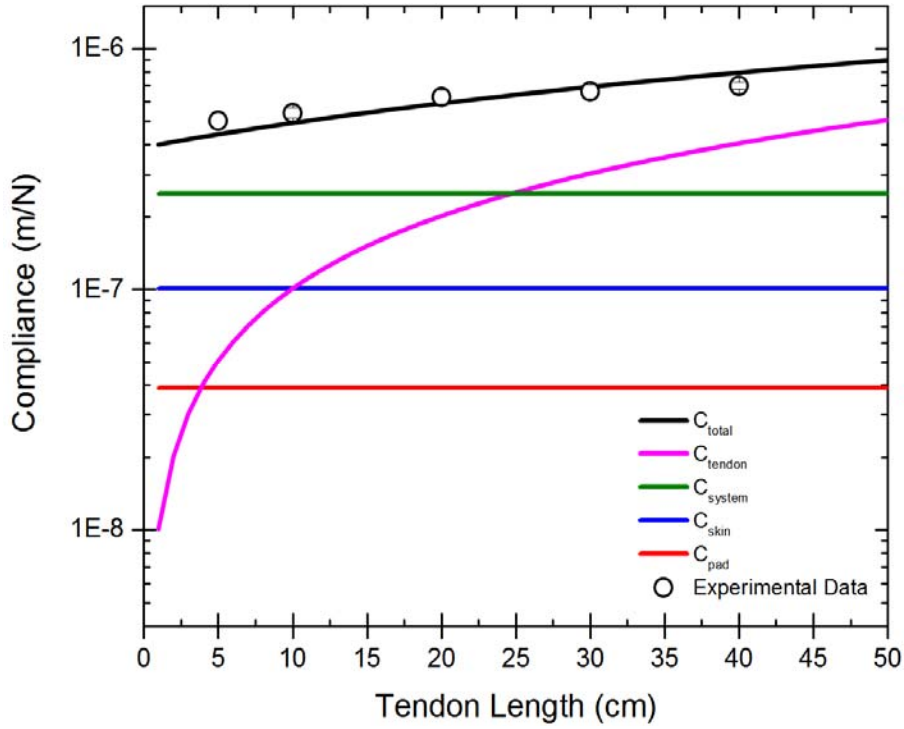

Figure 2.13 - Compliance as a function of tendon length, for each of the system components. The black line is the sum of the components. Open data points represent experimental data.

also becomes more compliant than the tendon. Despite a wide range of tendon length tested, only a small region exists where the tendon is the most compliant component of the system.

The slight dependence of force capacity on tendon length may be caused by two simultaneous events. One reason is that at short tendon lengths the contributions of system and skin compliance, not the tendon compliance, dominates the overall adhesive pad compliance. If compliance of the tendon is not a primary contributor to the total compliance, the influence of tendon length is negligible. An additional contribution is due to the failure mechanism of the adhesives. At long tendon lengths the peel angle will be very low, resulting in the adhesive pad undergoing predominantly pure shear deformation. However, as tendon lengths decrease, small deviations in loading displacements can result in larger loading angles. Only a few degrees of peel is required to deviate from a lap shear test to a peel test, and this could result in the deviation from expected force capacity at short tendon lengths.[99] In general, it is important to minimize tendon length to reduce compliance, but provide a sufficiently long tendon to prevent introducing large peel angles.

2.5.3.2 Tendon Width

While tendon length minimally influences force capacity, tendon width strongly controls force capacity. In all previous tests, tendon width is fixed with the pad width ($w_e = w_t$). Equation 2.12 is formed from combining the compliance of the pad, skin, and tendon in series. If the geometry of the tendon is varied independently from the pad and skin, a minimal impact on force capacity is expected as long as compliance remains low compared to the pad and skin. However, for this to be true, the load applied to the tendon must be able to distribute to the whole pad region of the adhesive. Figure 2.14 shows the results for

a 10 cm x 10 cm adhesive pad with a 10 cm tendon, where the width of the tendon is reduced systematically. The tendon remains nominally in the center of the adhesive. As tendon width decreases, the force capacity drops. Two trend lines are drawn: the blue line represents full load transfer from the tendon to the whole pad area (w_e = 10 cm), while the red trend line represents load transfer only to the pad area directly connected to the tendon ($w_e = w_t$). The results demonstrate that the data follows the calculation where no load is able to be distributed across the width of the adhesive; only the portion of the pad directly

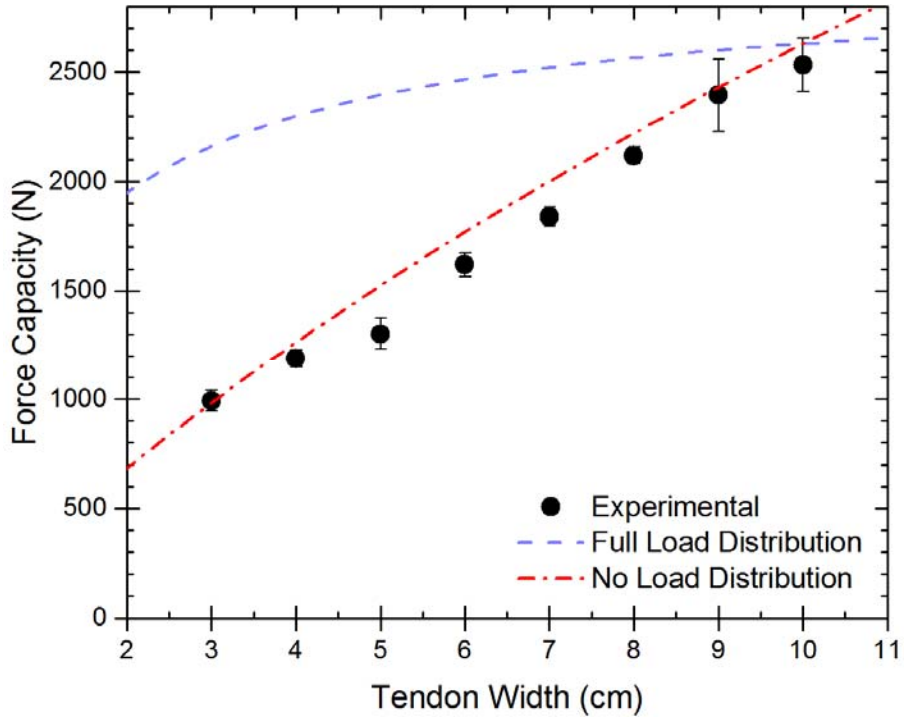

Figure 2.14 - A plot of force capacity versus tendon width. As tendon width increases, approaching the total pad width, force capacity increases. Two calculated force lines are plotted, where the load is able to be fully distributed across the width (blue), and where the tendon is able to only load the pad immediately above the tendon (red).

loaded influences the force capacity of the adhesive system. To maximize force capacity for an adhesive, it is important that the tendon is able to fully distribute load to the entire pad area.

2.5.4 Elastomer and Fabric Modulus

Using Equation 2.14 to generate Figure 2.2 demonstrated that for a stiff fabric like carbon fiber force capacity is expected to increase as elastomer modulus increases. As elastomer modulus increases, the pad and skin component compliances decrease. At some point the compliance from these components become so low that the impact is negligible, and force capacity plateaus (denoted by the saturated red region in the upper right). To test this

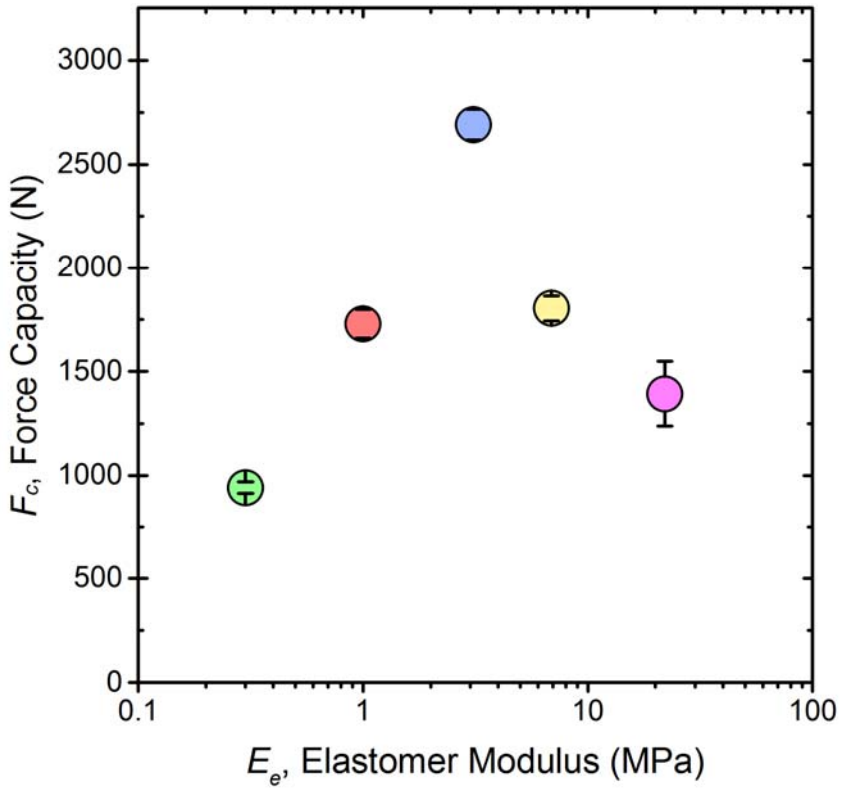

Figure 2.15 - A plot of force capacity as a function of elastomer modulus. Force capacity initially increases as modulus increases, but above 3.1 MPa force capacity drops with increasing elastomer modulus.

hypothesis, adhesives are made with unidirectional carbon fiber and additional elastomers, spanning into the region where force is expected to plateau. The results are presented in Figure 2.15. As modulus increases, force capacity increases until it reaches the 3.1 MPa elastomer. The force capacity of adhesives made with higher modulus elastomer is much lower, disagreeing with the expected trend from Figure 2.2. The reason for this decrease will be discussed in more detail in the Chapter 3.

2.6 Discussion

The results from these experiments provide lessons for optimizing the design of adhesive pads. For an adhesive supporting load, every component influences the force capacity, even those far from the adhesive interface. To create the highest force capacity adhesive joints, compliance must be reduced, so that the adhesive is as stiff as the adherends. For a given system, there is a minimum attainable compliance, and if the adhesive compliance is decreased further, the adhesive joint will be stronger than the adhered materials. If an adhesive is strong, but it is adhering to a compliant material, the entire system cannot become strong. The methods outlined in this chapter for reducing adhesive compliance provides multiple methods to tune adhesives to approach the minimum attainable compliance, which represents an optimally designed adhesive for a given application. For a system which has achieved the minimum attainable compliance for an application, any further decrease in compliance, for example by continuing to reduce shape ratio, will not result in a decreased total compliance, and may cause poor loading properties, resulting in a decreased force capacity. Regardless of shape, an adhesive is optimal if the measured compliance approaches minimum attainable compliance.

Even if the minimum attainable compliance has been reached, force capacity can still be scaled. Equation 2.1 states that minimizing compliance increases force capacity, but increasing area also increases force capacity. After an optimized adhesive shape is designed, the area of the pad can be increased if additional force capacity is required. The framework introduced in this chapter, when combined with previously published research on gecko-inspired adhesive scaling, provides powerful guidance for high strength, reversible adhesive design.

Shapes beyond the square pads previously developed can be fabricated to improve adhesive force capacity. Here, rectangles, triangles, and pentagons are demonstrated to provide improved adhesive qualities compared to square adhesive pads. While triangle and pentagon pads exhibit reduced compliance compared to a square pad, there are downsides to using die-cut samples. These pads are difficult to manufacture, because a large area must first be coated, then punched to the desired shape, which results in material waste. If manufactured at large scales, it would be important to weigh the tradeoffs of a preferred design to a larger adhesive pad without production waste.

Despite being located far from the adhesive interface, the geometry of the tendon plays an important role in adhesive force capacity. Kendall's peel model states that as peel angle decreases, peel strength increases.[99] A long tendon is useful because it reduces the loading angle, allowing the adhesive to maintain predominantly shear deformation, which results in the highest peeling forces. However, a shorter tendon decreases compliance, helping the system reach the minimum attainable compliance. Understanding this tradeoff is important to designing adhesives with appropriate tendon geometry. Furthermore, tendon width is important. A wider tendon is stiffer than a narrow tendon, decreasing compliance. Even more importantly, the tendon distributes the load to the pad, and a narrow tendon is incapable of complete load sharing. To maximize force capacity, the tendon must span the full width of the pad. These results provide useful guidelines for tendon design in adhesives.

2.7 Conclusion

The findings presented in this chapter enable the prediction of adhesive force capacity for different materials and different geometries to a high degree of accuracy. This

allows for optimization of the system and helps avoid inefficient bottlenecks, where decreasing the compliance of a component results in no gain in adhesive force capacity. By decreasing shape ratio, adhesives achieve higher force capacity for the same pad area. Complex shapes are fabricated and force prediction is still possible, with these shapes capable of exceeding the force capacity of regular square adhesives. Finally, even though located far from the interface, tendon geometry can play an important role in adhesive force capacity. Understanding these finding allows for the fabrication of optimized adhesive devices, and provides a general framework for understanding the importance of individual materials and geometric properties in gecko-inspired adhesives.

2.8 Acknowledgements

This work was funded by the Human Frontiers Science Program and the University of Massachusetts CVIP Technology Development Fund. We also thank NSF MRSEC (NSF DMR-2820506) for facilities support. I would like to thank M.D. Bartlett, and M. J. Imburgia for their thoughtful discussions, and C.J. Carey and A.V. Cugini proofreading support.

CHAPTER 3

CREATING GECKO-LIKE ADHESIVES FOR "REAL WORLD" SURFACES

3.1 Introduction

In Chapter 2, force capacity is optimized by minimizing the compliance of the adhesives. Previous research on reusable adhesives is performed on glass substrates, where the true area of contact approaches the nominal contact area of the pad. On rough surfaces, making contact with elastic materials is much more difficult. Based on this problem, viscoelastic materials are traditionally used to complete contact with surfaces regardless of roughness. Strong, reusable, non-damaging materials that adhere quickly and effortlessly to a wide range of surfaces are highly desirable; however, their development has proven significantly challenging. In this chapter gecko-inspired adhesives are presented that fulfill these criteria. Performance across a range of "real world" surfaces, including glass, Teflon™, and painted drywall is quantified. Geckos are known to climb across a variety of surfaces, and synthetic adhesives are compared to live Tokay geckos. Our findings are significant because they show that a synthetic design can achieve high adhesive stress on rough surfaces while maintaining reusability. Further, these adhesives surpass the adhesive stress capacity of Tokay geckos across all tested substrates without the use of any surface features, indicating that high reversible adhesive performance can be obtained without directly mimicking fibrillar features found on geckos. These results should expand the application of adhesives in commercial and industrial arenas.

3.2 Background

While traditional pressure sensitive adhesives (PSA) are capable of adhering to a variety of surfaces by creeping to accommodate multiple scales of roughness, they present

many drawbacks, including difficult removal (when designed to support high shear loads), minimal to no reusability, and surface fouling or damage.[3,59,67] As a result of these drawbacks, there has been a concerted international effort to devise "dry", high-capacity, reusable adhesives, such as those present on gecko toe-pads. Geckos can exert moderate to high adhesive forces over repeated cycles[37–39,100] while maintaining an ability to easily release and prevent fouling. This enables them to cling to and climb on substrates spanning a wide range of roughness and chemistries including wood, painted drywall, and concrete. **(**Figure 3.1A-C).[11,20,45,81,101,102] Many research groups have attempted to replicate the performance of the gecko adhesive system by focusing on mimicking their setae, which are arrays of very small, fibrillar features that divide into nanometer-sized spatulae.[54,71,103,104] The geometric arrangement of setae enable them to function as a soft material, thus allowing contact on micron scale surface roughness[14,15] despite being made of keratin, a high modulus material.[47,105] This approach has been valuable for understanding gecko-like adhesion and providing a framework for future studies. Although significant advances have been made in the fabrication of gecko-like microfibrils[50,58,106,107], these adhesives are often difficult to manufacture, have limited reusability, and cannot produce high force capacities on "real world" surfaces that have large scale roughness.

To generate high forces on millimeter and centimeter length scales, geckos possess a unique sub-surface morphology of stiff tendon tissue integrated directly into the skin, creating lamellar flaps referred to as scansors. These scansors enable a "draping" property for the skin, allowing the gecko to generate strong forces over macroscopic length scales.[45,74,108] "Draping" is characterized by the ability to conform while maintaining in-plane stiffness.[74,109] Russell had initially reported this unique morphology[45], and our group

recently revealed its importance in the generation of high adhesive forces across large length scales.[74] Understanding the properties and roles of the sub-surface structures has enabled the creation of larger gecko-like adhesives.

Recently our research group has demonstrated synthetic, reusable gecko-like adhesives that exhibit high shear adhesive force capacities (~300 kg for a 100 cm^2 adhesive) and release with very little force (<1 kg in peel).[74] These adhesives are created by integrating a soft elastomer pad with a stiff fabric, such as carbon fiber, which possesses many of the important "draping" properties developed in the sub-surface morphology of geckos. This integrated adhesive material conforms to the surface, without relying upon fibrillar surface features, while still resisting deformation in the loading direction parallel to the surface. Although these adhesives are shown to perform impressively on glass, their performance has not been explored on rougher surfaces that are commonly encountered in "real world" applications. Here we develop a new, enabling extension of this "draping" adhesive principle and use it to demonstrate gecko-like adhesives comprised of elastomers and stiff fabrics that can adhere robustly across a wide range of "real world" surfaces.

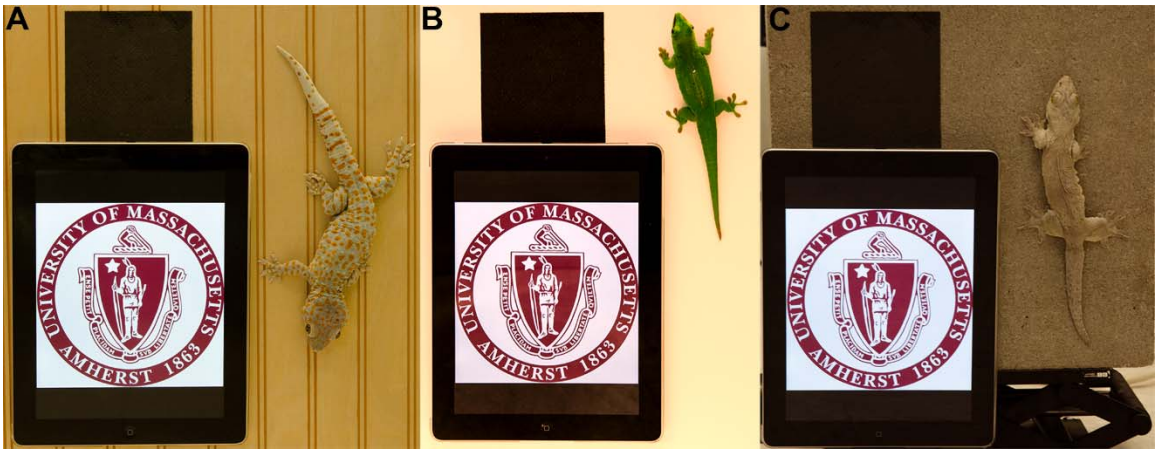

Figure 3.1 - An iPad tablet with a 3K plain weave carbon fiber/PU-B gecko-inspired adhesive adhering to "real world" surfaces next to geckos. (A) wood paneling with *Gekko gecko*, (B) painted drywall, with *Phelsuma grandis*, (C) concrete stone with *Gehyra vorax*. Used with Permission: Adv. Mater. 2014.[119]

3.3 Approach

Previous work[74–77] found that a simple equation describes the adhesive force capacity, F_c, of reversible adhesives:

$$F_c = \sqrt{2G_c}\sqrt{A/C} \tag{3.1}$$

Three variables control this relation: G_c is the critical strain energy release rate for interfacial fracture in the prescribed mode of failure, A is the true contact area, and C is the compliance in the loading direction. G_c is an ineffective control parameter because it cannot be varied greatly for reversible adhesive interfaces. The $\sqrt{A/C}$ ratio is a generalized reversible scaling parameter, which is used to scale adhesive force over many orders of magnitude, not only for synthetic materials but also for many different biological structures, including those of geckos, beetles, flies, and spiders.[74] In the previous chapter this equation was experimentally verified on smooth surfaces, where the true area of contact (A) is nearly equal to the full nominal area of the adhesive (A_n). On rough surfaces, however, we cannot expect this assumption to remain valid.[110,111] To extend this relationship to rough surfaces, the change in contact area must be accounted for to accurately predict force capacity.

According to Equation 3.1, strong adhesives require the adhesive material to be 1) soft enough to create intimate contact with the surface (large A), and 2) stiff enough to enable low shear compliance (low C). When contacting a rough surface, the area of contact, A, is a fraction, f, of the nominal area:

$$A = fA_n \tag{3.2}$$

This fraction is defined by a probabilistic function that accounts for the probability of surface forces being capable of exceeding the elastic restoring force required to bring the

adhesive into contact over a surface asperity with amplitude, β.[110,112] This probability function is approximated:

$$f \cong \exp\left(\frac{-\beta}{G_{c,N}/E_e}\right) \tag{3.3}$$

where $G_{c,N}$ is the critical strain energy release rate, or adhesion energy, normal to the surface, and E_e is the Young's modulus of the elastomer pad. $G_{c,N}/E_e$ describes the length scale over which a material will adhere to a surface.[113,114]

To calculate force capacity, the compliance of the adhesives must be known. In Chapter 2 adhesives were designed using carbon fiber because utilizing stiff fabrics minimizes the compliance of the adhesives. In this chapter, carbon fiber fabrics will again be used. Here the compliance contributions of the pad bending, the tendon, and the system, are not included, because these components are sufficiently stiff that they will negligibly influence the compliance. The compliance of the adhesive structure (Figure 2.2A and Figure 2.2B) in the direction of loading is calculated by accounting for the shear (Equation 2.5, second term) and extension (Equation 2.10) deformation modes:[75]

$$C_{calculated} = \left[\frac{3t_e}{AE_e} + \frac{{L_e}^2}{A}\left(\frac{1}{t_eE_e+t_fE_c}\right)\right] = \frac{1}{fA_n}\left[\frac{3t_e}{E_e} + {L_e}^2\left(\frac{1}{t_eE_e+t_fE_f}\right)\right] \tag{3.4}$$

where L_e is the length of the elastomer pad, E_c is the composite modulus of the fabric, and t_i is the thickness with i equal to e or f, referring to the elastomer pad or fabric, respectively. Rearranging with Equation 3.2, we see that:

$$C_{real} = \frac{1}{f}C_{calculated} \tag{3.5}$$

Substituting Equation 3.2, and 3.5, into Equation 3.1 gives:

$$F_c = f\sqrt{2G_c}\sqrt{A_n/C_{calculated}} \tag{3.6}$$

Interestingly, we see that the only difference from the original equation, Equation 3.1, is the addition of the fractional area of contact variable, *f*. Solving for the stress capacity, $\sigma_c = F_c/A_n$, and inserting Equation 3.3 and Equation 3.4 yields:

$$\sigma_c = \exp\left(\frac{-\beta}{G_{c,N}/E_p}\right)\left(\frac{2G_{c,S}}{{L_p}^2\left(\frac{1}{t_p E_p + t_f E_f}\right)+\frac{3t_p}{E_p}}\right)^{1/2} \tag{3.7}$$

Here we set $G_c = G_{c,S}$, which is defined as the critical strain energy release rate for pure shear, which is the loading mode of these experiments. Equation 3.7 will be used to calculate adhesive stress capacity for fabricated adhesives across a range of surface roughness.

3.4 Experimental

3.4.1 Materials

Polyurethane elastomer pad materials are purchased from BJB Enterprises. The mix ratios of 'A' and 'B' components are used as follows: PU-A: ST1060 100:55, PU-B: ST3040 100:97.5, PU-C: F15 45:100. The components are mixed together in a plastic cup, and degassed in a desiccator until bubbles disappeared; the mixture is then reintroduced to air and used. 24K unidirectional carbon fiber tape is purchased from Soller Composites (E_f = 40 GPa), 3K plain weave carbon fiber fabric (E_f = 20 GPa) is purchased from Soller Composites and used for figure 3.1. Effective fabric modulus is determined by taking the linear portion of a force vs displacement curve for a 10 cm by 20 cm strip of fabric, tested at 10 mm/min with a 50 kN load cell on a Instron 5500R tensilometer. Elastomer modulus (E_e) values are determined by dynamic mechanical analysis (DMA) at room temperature with 0.1% strain at a frequency corresponding to the adhesives lap shear testing rate, which

for t_e values of 0.42 mm, 0.90 mm, and 0.41 mm results in frequencies of 0.40, 0.19, and 0.41 Hz, for PU-A, PU-B, and PU-C, respectively. To quantify an effective $G_{c,N}$, a material property proportional to the surface energy, a glass half-sphere (R = 3.6 mm) is indented on the polyurethane elastomers following the methodology of Johnson, Kendall, and Roberts, at velocities of 109, 112, and 163 μm/s for elastomers PU-A, PU-B, and PU-C, respectively, which approximately matches the average strain rate experienced within the tests.[115,116] 3M VHB™ tape is tested at 100 μm/s as a point of comparison. These results are presented in Figure 3.2, and indicate that there is relatively little variability between materials with respect to G_c, especially compared to 3M VHB™ tape.

3.4.2 Adhesive Fabrication

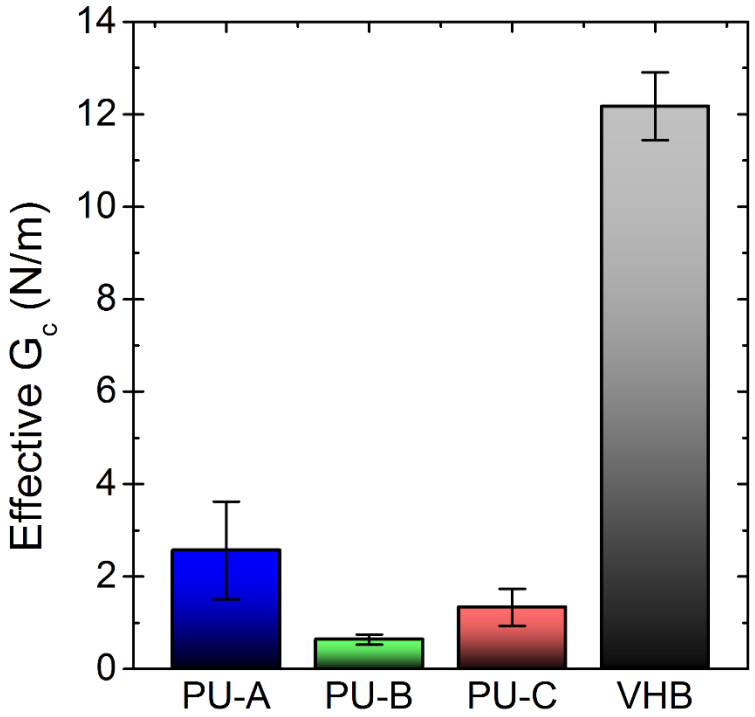

Figure 3.2 - Effective G_c for different materials. 3M VHB™ tape is included for comparison, as a traditional PSA. Strain rates are chosen to correspond with rates used in the shear adhesion tests. Data is shown as the mean with error bars representing ± standard deviation. Used with Permission: Adv. Mater. 2014.[119]

The fabrication method used here is the same as in Chapter 2. In brief, on polyethylene coated glass, fabric is taped into place. A spacer is cut and taped onto the fabric. The uncured elastomer is poured into this spacer, and smoothed with a glass slide. A thin PE film is placed on top of the thin layer of prepolymer, and 25 pounds of force is applied to create a smooth surface. Samples are cured at room temperature overnight (at least 12 hours), then placed in a 70°C oven for 24 hours. After curing, a rotary blade cutter is used to cut the samples to the desired size. Two pieces of 3 mm thick polycarbonate (McMaster Carr) are adhered using a cyanoacrylate based adhesive to the bottom of the fabric.

3.4.3 Substrate Preparation

The substrates chosen for investigation are glass, acetate film, Teflon™, aluminum, painted drywall, and frosted glass. 20 cm by 25 cm by 0.63 cm thick glass (Amherst Glass) is utilized as the glass testing substrate. A 250 μm thick piece of adhesive-backed PTFE (McMaster Carr) is placed onto another glass substrate to make the Teflon testing substrate. A piece of acetate film (McMaster Carr) is adhered to a plate of glass using Elmer's spray glue to create the acetate testing substrate. A bar of 0.63 cm thick Aluminum (Alloy 6061, unpolished finish) (McMaster Carr) is cut to 20 cm by 25 cm. Finally 0.63 cm thick drywall (Home Depot) is painted with high gloss white paint (Benjamin Moore). Glass and Aluminum surfaces are cleaned with acetone, and the remaining substrates are wiped with a Kimwipe tissue (Kimberly Clark) when adhesives are changed (every six tests). Surface profiles from white light interferometry (Zygo NewView 7300) are shown in Figure 3.3A. Image areas greater than 2 mm^2 are captured by stitching multiple images together.

3.4.4 Testing

Testing is performed using a similar procedure as in Chapter 2. In brief, an Instron 5500R tensilometer is utilized for testing, with a 50 kN load cell for 100 cm^2, 36 cm^2, and 9 cm^2 sample sizes, and a 1 kN load cell for 4 cm^2 and 1 cm^2 sample size. Substrates are held in place by a custom built substrate holder (Figure 2.4), which is tightly attached to the crosshead, and displaced at a rate of 10 mm/min, until the sample detached from the surface. The adhesive is gripped using a mechanical grip on the bottom, and applied to the substrate by hand. Each test is performed 5 times, and all sizes and substrates are testing using one adhesive (180 tests per adhesive). All tests for each adhesive are performed on the same day, and no noticeable change is measured from test to test, resulting in the small error bars in Figure 3.10. Similarly, 90 degree peel tests are performed with a 1 kN load cell with the same substrates oriented perpendicular to the adhesives at a rate of 100 mm/min.

3.4.5 Animal Care

Geckos are maintained individually in 10-ga glass aquaria in the Irschick lab at the University of Massachusetts Amherst (under IACUC protocol 2009-0051). Each cage is heated with a 60-watt bulb on a timer switch that provides light from 9 AM to 5 PM. They are each fed 12 large vitamin-dusted crickets per week. Gecko experiments are performed by holding the animal's torso while the two front feet are attached to a glass plate, which is displaced at 300 mm/min. The force is measured until it reaches a maximum. At this point the gecko begins to slip, denoted by a plateau or decrease in force, at which point the handler's grip is reset and the test is repeated. For more information on this testing protocol, see reference 72.

3.5 Results

3.5.1 Experimental Surfaces Analysis

As verification of the relationship outlined in Equation 3.7, six substrates comprising a range of surface roughness and chemistries are prepared: glass, poly(vinyl acetate), Teflon™, aluminum, painted drywall, and frosted glass. The roughness of these

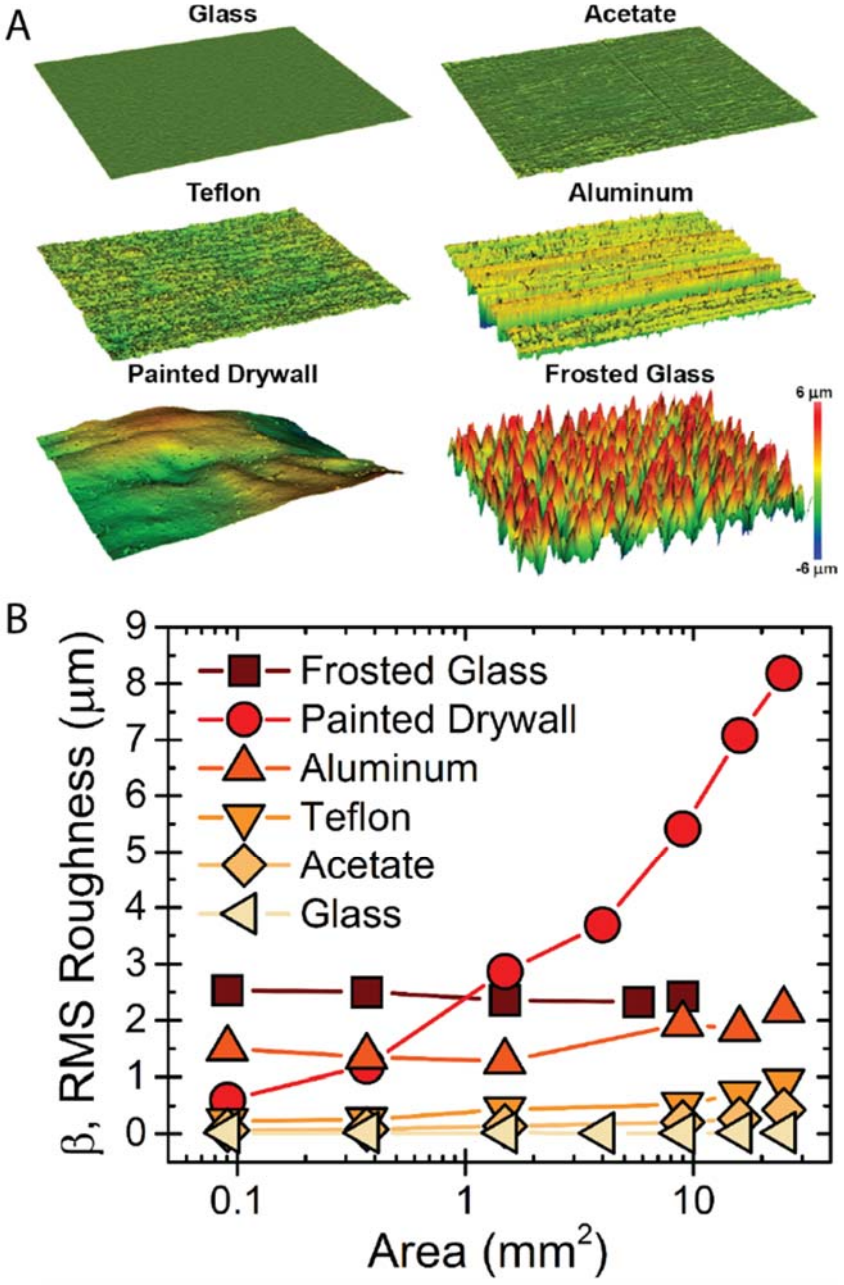

Figure 3.3 - White light interferometry profiles of the prepared substrates. (A) Visual representation. (B) A plot of measured RMS roughness versus the area of contact measured. Painted drywall varied dramatically with area, while the remaining substrates did not depend on the area of contact. Used with Permission: Adv. Mater. 2014.[119]

surfaces is measured with white light interferometry, and the surface profiles are provided in Figure 3.3A. β for these surfaces is found by taking the average of RMS values at three magnifications corresponding to 1.31, 0.37, and 0.09 mm^2 surface areas (Figure 3.3B). These substrates provide a wide range of roughness, from $\beta = 0.01$ μm for glass, to $\beta = 2.5$ μm for frosted glass. Performance on painted drywall is also of interest due to its combination of short length scale and long length scale roughness, as well as being a common surface for which adhesives are desired.

3.5.2 Theoretical Predictions

In Chapter 2, it is noted that as elastomer modulus increases, compliance decreases, and therefore adhesive strength should increase (Figure 2.2). However, in experiments performed on glass with adhesives above a certain modulus, force capacity decreased (Figure 2.15). Photographs of the surface of pads with moduli of 0.3 MPa and 10 MPa is

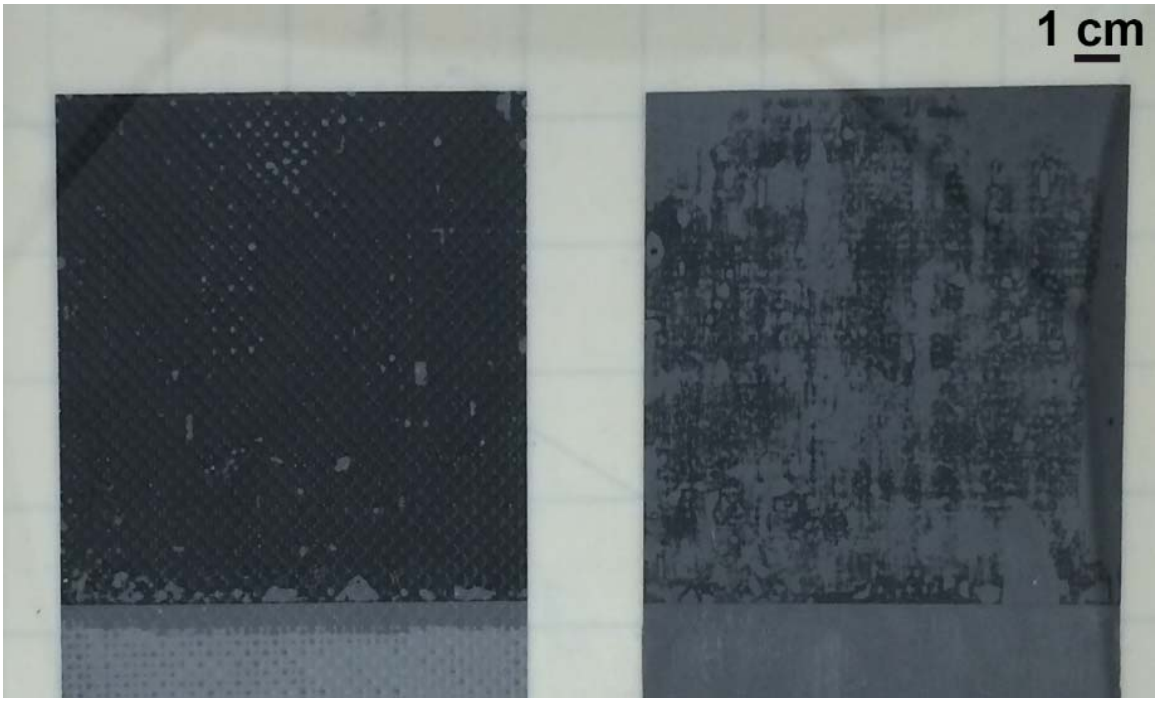

Figure 3.4 - Photographs of a 0.3 MPa elastomer adhesive (left) and a 10.0 MPa elastomer adhesive (right). Dark color represents contact with the glass plate. The 0.3 MPa elastomer makes much more complete area of contact than the 10.0 MPa elastomer.

shown in Figure 3.4. While the 0.3 MPa adhesive makes large areas of contact, only a small area of contact is made with the 10 MPa adhesive. When only a small area of contact is made, force capacity is low, regardless of elastomer modulus. Using Equation 3.6, Figure 2.2 can be replotted, taking into account the fractional area of contact resulting from surface roughness of the glass ($\beta = 0.01$ μm). The resulting plot is shown in Figure 3.5. For carbon fiber, as elastomer modulus increases the force capacity increases until a maximum is reached, and then force capacity decreases. When the elastomer modulus becomes high, the area of contact, as predicted by Equation 3.2, decreases, and the adhesives are no longer

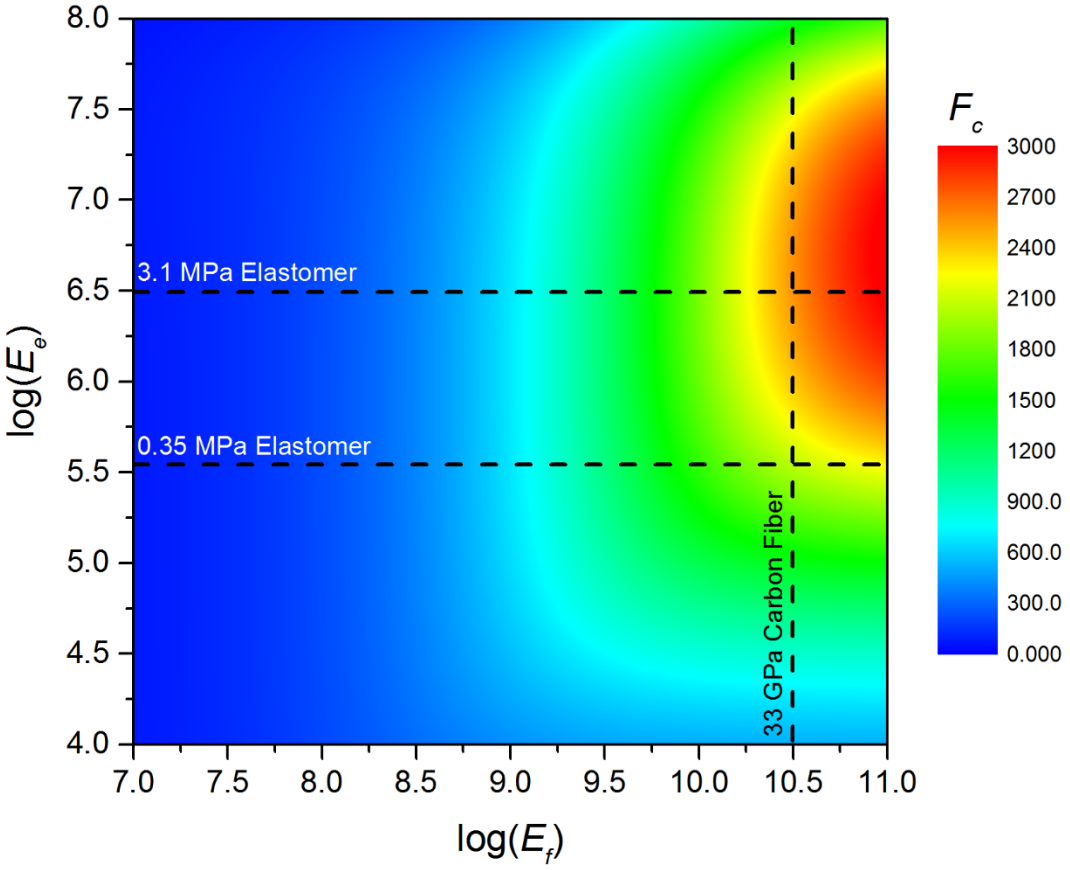

Figure 3.5 - Plot of force capacity as a function of elastomer modulus and effective fabric modulus, taking into account surface roughness of glass, $\beta = 0.01$ μm. Color represents the magnitude of force capacity.

able to support large loads. The results of Figure 3.5 agree with the trend seen in Figure 2.15. The highest force capacities are achieved with the highest modulus elastomers, which

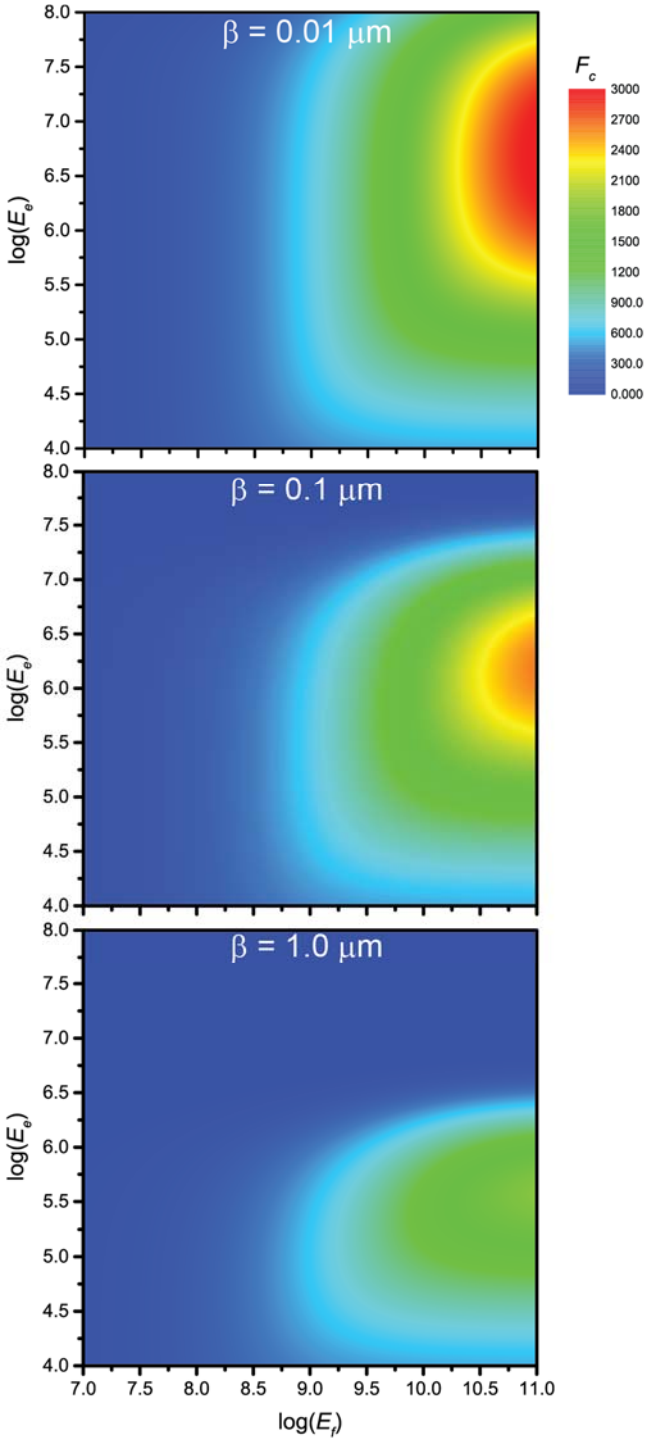

Figure 3.6 - Contour plots of force capacity as a function of elastomer modulus and effective fabric modulus. As roughness increases, the maximum achievable force capacity decreases, and the elastomer modulus at which this value occurs decreases.

are still capable of completely wetting the substrate.

Extending this idea, it is possible to predict how adhesives will perform on increasingly rough surfaces. In Figure 3.6, three contour maps are plotted, for $\beta = 0.01$ μm, 0.1 μm, and 1.0 μm. As roughness increases, two changes occur. First, the maximum achievable force capacity decreases. Second, the elastomer modulus where maximum force capacity occurs decreases. This provides a general guideline for developing adhesives for rough surfaces.

For all surfaces roughness values within the range tested, maximum force capacity occurs with the stiffest fabrics. For this reason, we use carbon fiber, as the fabric material for all samples. Additionally, analysis focuses on adhesives with $A_n = 4$ cm^2, to allow for comparison of the adhesives to the clinging ability of live Tokay geckos. Figure 3.7 illustrates the dependence of adhesive stress capacity as a function of elastomer pad modulus, E_e, for several surface roughness values, β, where L_e, t_e, t_f, E_f , $G_{c,N}$, and $G_{c,S}$ are measured quantities for the adhesives described in this chapter and are listed in Figure 3.7.

From the plot in Figure 3.7, several predictions are constructed. While keeping lengths, L_e, and L_t, thicknesses, t_e, and t_f, and fabric modulus, E_f of the adhesives constant, there is an optimal modulus that results in maximum adhesive stress capacity for any given surface roughness. As roughness increases, the optimal modulus decreases, and the maximum achievable adhesive stress decreases. From this basic relationship, a general spectrum for releasable adhesives is revealed; at one end of this spectrum exist extremely high strength, optimized adhesives suitable for smooth substrates, and at the other end are moderate strength adhesives which are capable of adhering to a wide range of surfaces. Perhaps most interestingly, this spectrum demonstrates that the optimal elastomer modulus

for gecko-like adhesives that adhere to surfaces with roughness values up to 2.5 μm is greater than the Dahlquist Criterion[3,62,67], which is widely used in the development of conventional pressure-sensitive adhesives. Whereas the Dahlquist Criterion was established to provide large deformations to effectively "blunt" a developing peel front, the gecko-like adhesives described here take advantage of extremely high stiffness carbon fiber

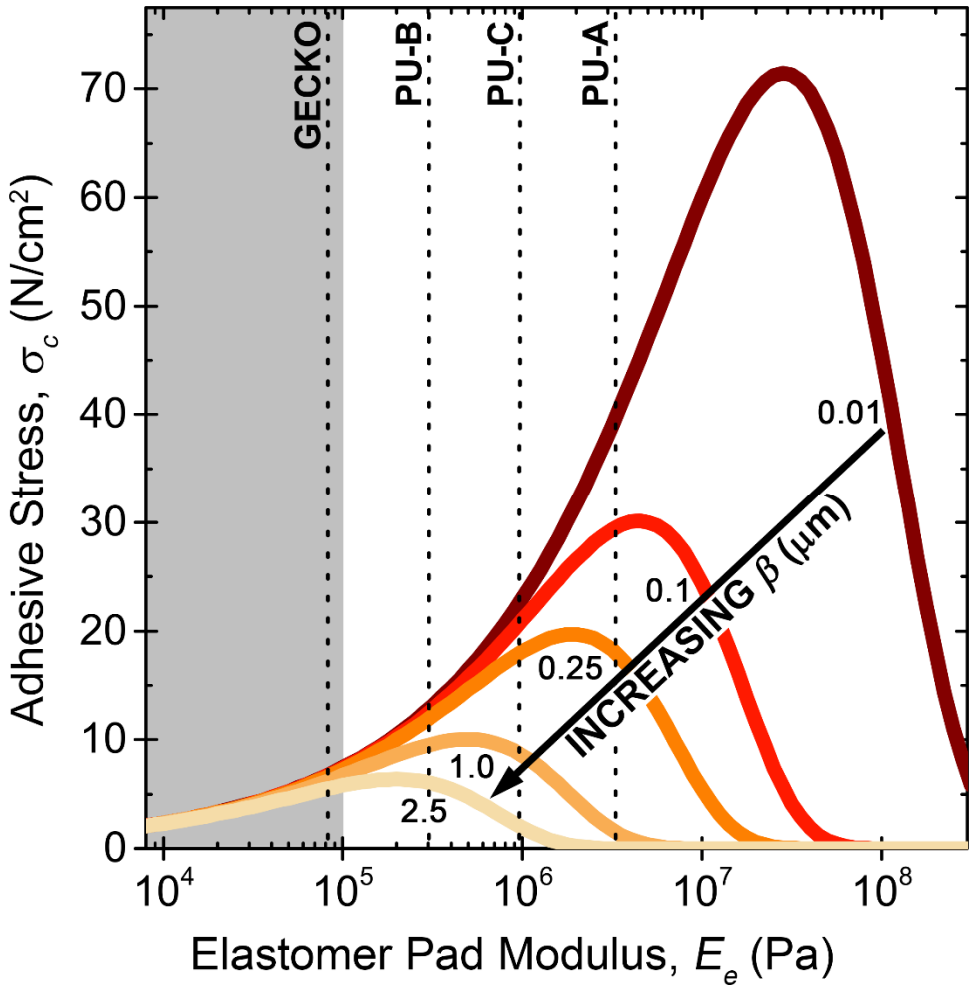

Figure 3.7 - Adhesive stress capacity versus elastomer pad modulus for varying roughness surfaces, with A_n = 4 cm^2, L_e = 2 cm, t_e = 0.42 mm, t_f = 0.3 mm, E_f = 40 GPa, $G_{c,N}$ = 1.51 N/m, and $G_{c,S}$ = 35 N/m. As roughness increases, the optimal elastomer pad modulus shifts to a lower modulus and adhesive stress capacity decreases. The shaded region represents modulus values most often associated with pressure sensitive adhesives. Used with Permission: Adv. Mater. 2014.[119]

fabric to distribute shear forces across a large area, and thus the elastomers are not required to achieve large deformations like traditional PSAs.

3.5.3 Synthetic Results

To fabricate the best adhesive for rough surfaces, Figure 3.7 is used to guide elastomer choice for stiff fabric tendons. Adhesives are prepared with uniaxially aligned 24K tow carbon fiber fabric. Elastomers with moduli of 3.1 MPa, 0.35 MPa, and 1.0 MPa as determined by Dynamic Mechanical Analysis (DMA) are used and are referred to as PU-A, PU-B, and PU-C, respectively. Samples are prepared with A_n = 100 cm^2 with L_e = w = 10 cm, and are cut to smaller sizes for testing, while maintaining L_e/w = 1. Predicted performance for these adhesives is denoted in Figure 3.7 as vertical lines.

A representative force, F, versus applied displacement, Δ, plot is shown in Figure 3.8A. Force increases with displacement, ultimately reaching a maximum value, F_c, followed by a rapid decrease, corresponding to the adhesive's detachment from the surface. F_c is normalized by A_n and presented as adhesive stress capacity, σ_c in Figure 3.8B, for samples of A_n = 4 cm^2. Adhesive stress capacities for PU-A are very high on glass and decreases with increasing surface roughness, with no significant adhesion observed on frosted glass. PU-B, which has the lowest modulus, exhibits the lowest adhesive stress on glass, but is able to maintain this adhesive stress with only 30% deviation even on rough surfaces. The results for PU-C show a combination of characteristics; the intermediate modulus elastomer achieves high adhesive stresses on glass while still maintaining an ability to adhere to rough surfaces. The resulting adhesive stress capacities for the three adhesives agree well with the trends predicted by Equation 3.7; for the smoothest substrate (glass), the highest modulus elastomer pad material results in the highest adhesive

performance and as roughness increases the adhesive capacity of PU-A quickly decreases to zero. In contrast PU-B and PU-C maintain moderate adhesive strength on rougher

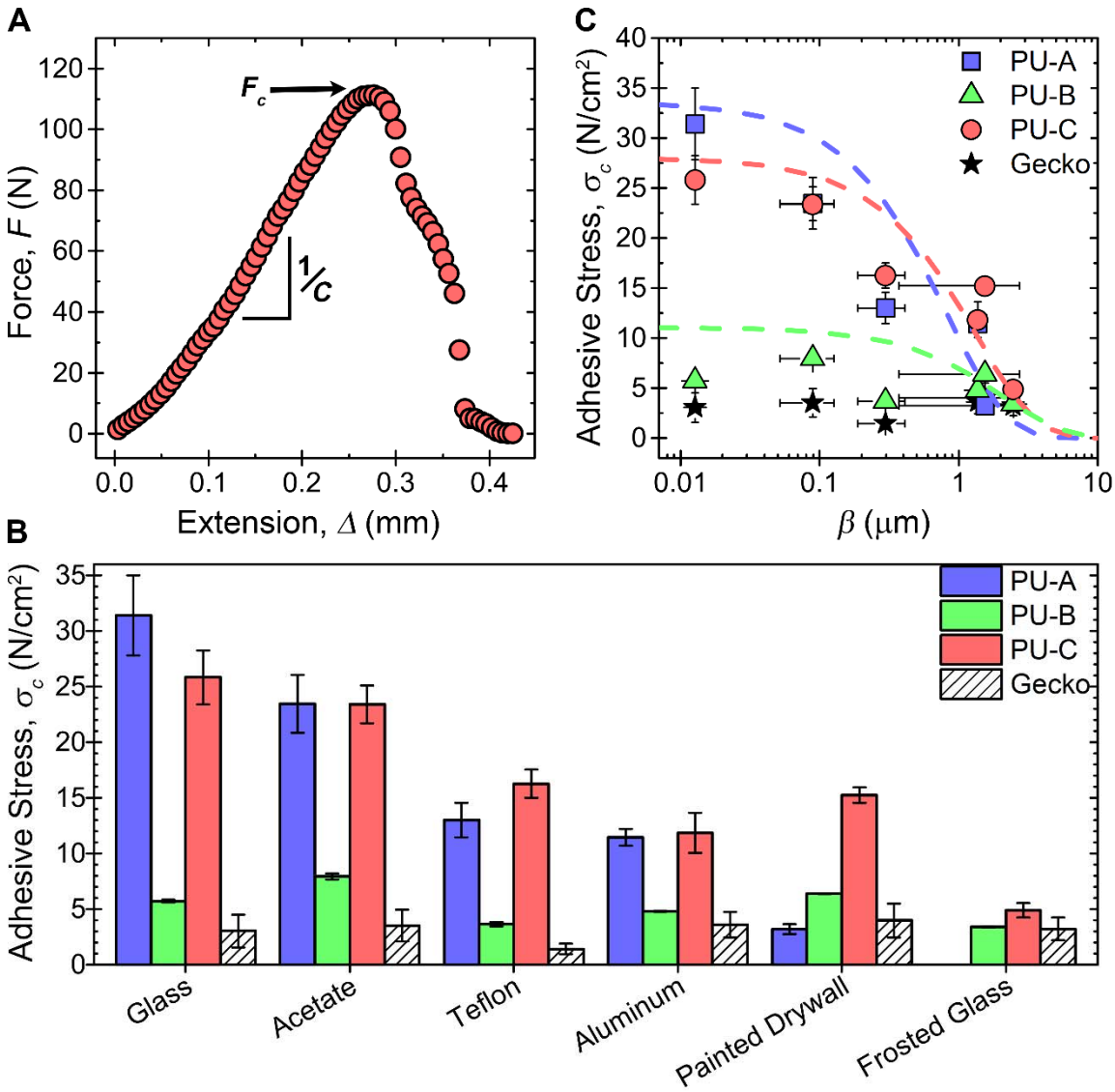

Figure 3.8 - A representative force versus extension plot for PU-C. As extension increases, load increases linearly ($d\Delta/dF = C$) until a maximum force is reached (F_c), where the adhesive quickly detaches from the surface. (B) Adhesive stress capacity for different substrates, for both synthetic adhesives and live geckos, with data representing the mean ± standard deviation. Synthetic adhesives have contact areas of 4 cm^2, similar to gecko toe pads. Gecko toe-pad area was measured for each specimen. (C) Shear adhesive stress capacity versus surface roughness, for both synthetic and live geckos. Data is shown as the mean with error bars representing standard deviation for σ_c (y-axis) and β (x-axis). Dashed lines represent fits of Equation 3.7 with experimental parameters from Table 1 and $G_{c,S}$ values of 24.9, 55.4 and 49.7 N/m for PU-A, PU-B, and PU-C respectively. Used with Permission: Adv. Mater. 2014.[119]

surfaces, most notably on frosted glass. These results are summarized in Figure 3.8C, where the average adhesive stress is plotted against the surface roughness, β. Values for Equation 3.7 can be found in Table 3.1, and $G_{c,S}$ is used as a fitting parameter. The resulting fits agree well with the data verifying the ability of Equation 3.7 to capture the key elements of these gecko-inspired adhesives.

Table 3.1 - Experimental parameters for synthetic adhesives used in Figure 3.8. From fitting to Equation 3.7, $G_{c,S}$ values of 24.9, 55.4 and 49.7 N/m were obtained.

	PU-A	**PU-B**	**PU-C**
Elastomer Pad Thickness, t_e (mm)	0.42	0.90	0.41
Elastomer Pad Width, w (cm)	2	2	2
Elastomer Pad Length, L_e (cm)	2	2	2
***Pad Modulus*, E_e (MPa)**	3.1	0.3	1
Tendon Length, L_t (cm)	10	10	10
Fabric Thickness, t_f (mm)	0.3	0.3	0.3
Effective Fabric Modulus, E_f (GPa)	40	40	40
$G_{c,N}$ (N/m)	2.57±1.06	0.638±0.11	1.33±0.40

Our results for surfaces of varying roughness demonstrate the benefit of utilizing draping adhesives. Roughness is complex, as it can vary over many length scales, and RMS roughness is only one parameter that can be used to describe how surface topography affects adhesion.[111,112] As shown in Figure 3.3B, the measured RMS roughness for drywall is the highest of all substrates when measurement areas are greater than 1 mm^2, but decreases as measurement area decreases. By contrast, frosted glass roughness is uniform over many length scales, and is the roughest substrate for measurement areas less than 1 mm^2. Interestingly, adhesive strength is substantially higher on painted drywall. We interpret this result as arising from millimeter or larger scale roughness being

accommodated by draping of the adhesive fabric, whereas accommodation of micron or smaller scale roughness is dependent on the elastomer properties.

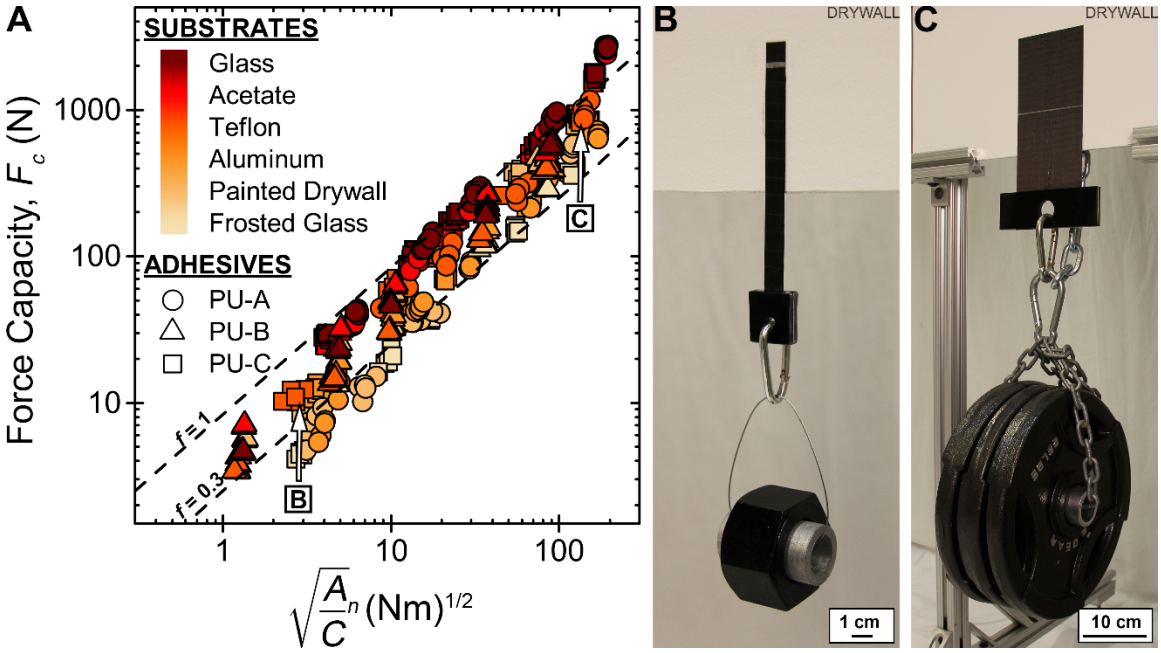

Figure 3.9 – Scaling adhesive strength on rough surfaces. (A) Force capacity, F_c, versus $\sqrt{A_n/C}$ for all synthetic adhesives tested, ranging from areas of 1 cm^2 to 100 cm^2. Data point color represents adhesive substrate, while shape represents adhesive material. Even as surface roughness increases, force capacity continues to scale as $F_c \sim f\sqrt{G_c}\sqrt{A_n/C}$. Fitting lines represent upper and lower bounds of adhesive contact, with the upper line (f = 1) fitting approximately 100% contact, and the lower line (f = 0.3) fitting approximately 30% contact. The letters B and C refer to the adhesives utilized in part (B) and (C). (B) 1 cm^2 adhesive holding a 340 g mass, and (C) 100 cm^2 adhesive holding a 34 kg mass on painted drywall. The chain behind the adhesive and drywall is used for lifting the weights. Used with Permission: Adv. Mater. 2014.[119]

Furthermore, our adhesive results conform to the general scaling relationship described by Bartlett et al. (Figure 3.9).[74–77] The variability of these data is attributed to the fact that the area used to plot the data is the *nominal area*, A_n, of the adhesive, not the *true contact area* of the adhesive, which is decreased due to roughness. In Figure 3.9A, two lines are shown which represent the upper bound of an adhesive making full contact (f = 1) and lower bound of an adhesive making only 30% contact (f = 0.3). Even on surfaces where true contact area is reduced, the force capacity still scales with $\sqrt{A_n/C}$. As a simple

example of scaling, Figure 3.9B and Figure 3.9C demonstrate that increasing the size of a PU-C adhesive from 1 cm^2 to 100 cm^2 allows for an increasing in hanging load from 340 g to 34 kg. These findings firmly establish $\sqrt{A_n/C}$ as the key scaling parameter for reversible, gecko-like adhesives on both smooth and rough substrates, thus allowing performance to be maintained over a large range of adhesive sizes.

While high force capacity is an important characteristic for an adhesive, easy release is also essential for many applications. To quantify the release force of the fabricated adhesives, 90 degree peel experiments are performed. The force required to remove these adhesives is two orders of magnitude lower than the shear adhesive force capacity (Figure 3.10), and is less than 1 kg. One reason for this low peel force, or easy release, is that the storage modulus is substantially greater than the loss modulus, resulting

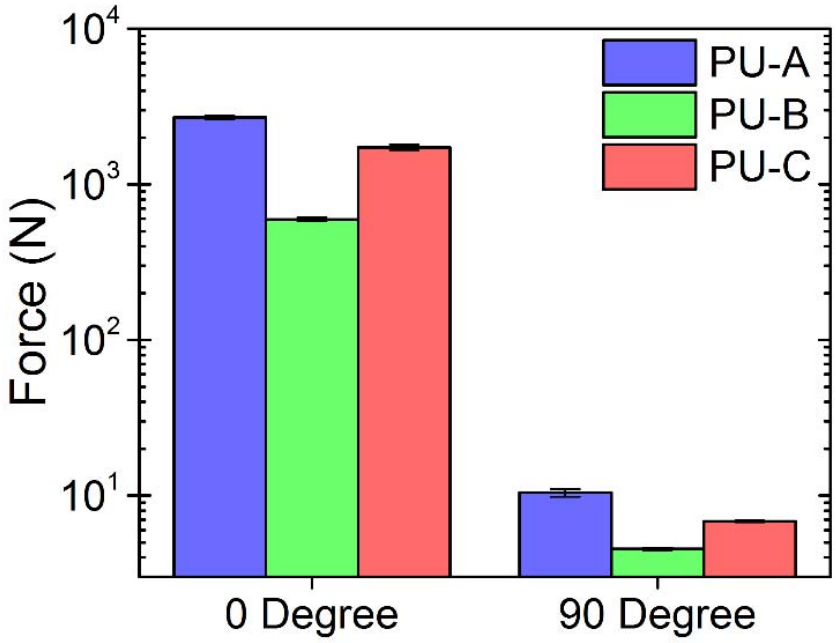

Figure 3.10 - Force capacity at 0 degree and 90 degree peel angles, for three different elastomer pad materials. Significantly lower peeling force at 90 degrees allows for easy release of the adhesives. Data is shown as the mean with error bars representing ± standard deviation. Used with Permission: Adv. Mater. 2014.[119]

Figure 3.11 - Photograph of a LCD computer monitor hanging on drywall with a gecko-inspired adhesive. Adhesive consists of glass fiber fabric and PU-C.

in low $\tan(\delta)$ values of 0.083, 0.043, and 0.12 at rates corresponding with the lap shear testing strain rates for PU-A, PU-B, and PU-C, respectively. This small $\tan(\delta)$ implies that minimal energy loss occurs during peel, an attribute that contrasts starkly to conventionally strong pressure sensitive adhesives.[3] This predominance of elasticity allows for easy release at high angles,[87] but even more importantly, the ability to maintain the same force capacity over multiple cycles of attachment and release on numerous surfaces. We have demonstrated a proof-of-concept for adhesive reusability by attaching an LCD computer monitor on various indoor and outdoor surfaces (example in Figure 3.11), without cleaning the adhesive or preparing any of the surfaces. This demonstrates one potential application for high strength, reversible adhesives which are not currently available in the commercial or industrial marketplace.

3.5.4 Live Gecko Results

Adhesive experiments are also performed on five adult live Tokay geckos (*Gekko gecko*) across the same range of surfaces to provide a point of comparison for the fabricated synthetic adhesives. While geckos are well known for their climbing ability, most studies have focused on their adhesive abilities on smooth surfaces, such as glass. Despite variability in roughness of the substrates, gecko force capacities were relatively constant across substrates for each individual (Figure 3.12). Variation in body size is accounted for amongst geckos by dividing force capacity, F_c, by toe-pad area. The average adhesive stress capacity for Tokay gecko specimens is 3.1 N cm^{-2} across all six surfaces (Figure

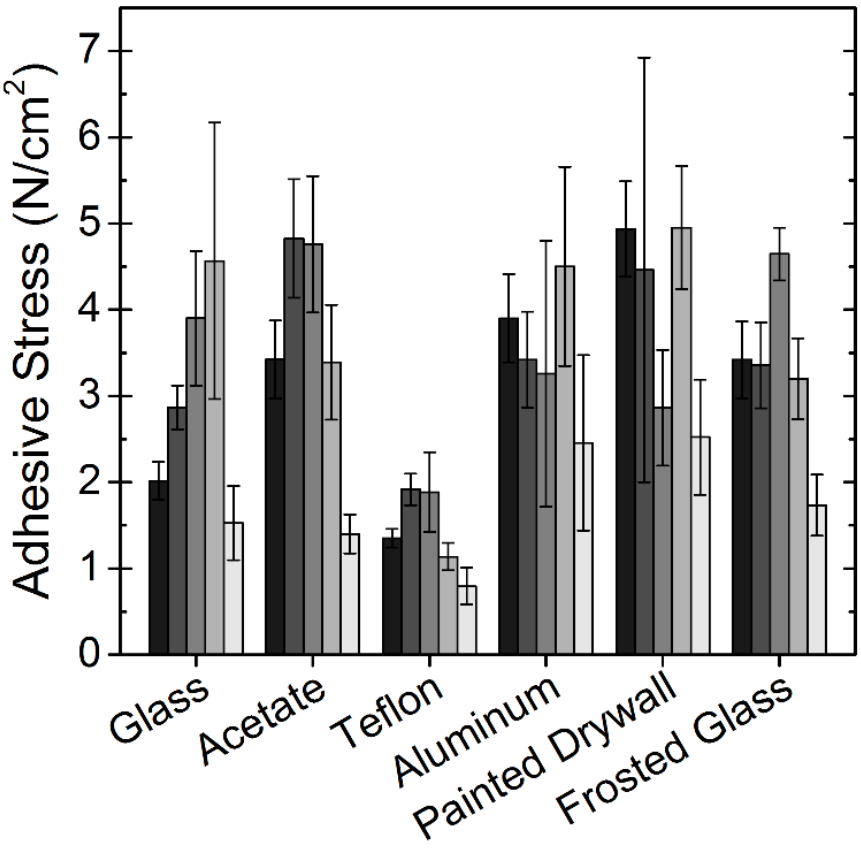

Figure 3.12 - Adhesive stress versus substrates for the Tokay gecko specimens. Each bar represents a single specimen. Data is shown as the mean with error bars representing ± standard deviation. Used with Permission: Adv. Mater. 2014.[119]

3.8B). Tokay geckos do not adhere strongly to the Teflon surface, which is likely a consequence of the surface chemistry of this substrate, and not roughness.

The consistent adhesive stress capacity across substrates for Tokay geckos can be attributed to both the sophisticated neuromuscular system of gecko feet and toes[12,45,101,117,118], and also the basic structure of their toe-pads. Geckos carefully position themselves prior to surface contact, which might aid in achieving optimal contact. Because each toe-pad is covered in microscopic fibrillar features, they have very high compliance normal to the substrate and easily establish intimate contact with the surface, even on higher roughness surfaces.[5,47] Calculations performed by Autumn et al. have shown that Tokay gecko setae have an effective modulus of 86 kPa.[47] Figure 3.7 demonstrates that for this modulus across all roughness values there is little variability in adhesive stress. It is important to note that this plot is contingent on the fabric compliance being much less than the elastomer pad compliance, while still maintaining the ability to drape. In geckos, the sub-surface tendon system acts in a similar manner as the fabric in our adhesives. Accordingly, it can be expected that low effective modulus of the setae allows gecko toe-pads to establish conformal contact on micron and sub-micron length scales, analogous to the elastomer pad in our materials, while the unique coupling of the gecko's sub-surface tendon system minimizes compliance and simultaneously provides draping on larger length scales. This empowering combination is one feature that allows the gecko to cling and climb proficiently across many length scales of roughness, although there remains a significant amount of research that needs to be performed to fully understand how geckos climb.

3.6 Discussion

The adhesive stress capacity of our adhesives is capable of surpassing geckos for all of the surfaces examined (Figure 3.8B). We note that gecko-like adhesion is not merely about strength; it also includes reusability, easy peel, and the ability to resist fouling. Our adhesives achieve some of these (easy peel, reusability), and can be easily cleaned if dirt accumulates over its lifetime. While utilizing highly compliant fibrils is an effective specialization for geckos, our approach of varying elastomer softness enables us to alter surface compliance without the additional complicating step of synthesizing fibrils, which requires difficult manufacturing techniques and complicates scaling to large sizes. This allows us to compensate for micron and smaller scale roughness. Additionally, carbon fiber fabrics are able to affectively mimic the "draping" ability, while maintaining the high stiffness seen in gecko toe-pads, enabling adhesion over millimeter and larger scale roughness. By combining these features, like the gecko, we obtain nearly equal adhesive stress capacities across surfaces with one of our elastomers (PU-B). Tuning our materials system further, we surpass this capability with PU-C, maintaining the ability to adhere to all surfaces but with high adhesive stress capacity on smooth surfaces. Therefore, by changing the materials systems utilized in the adhesive and following draping adhesive principles, we can optimize the adhesive characteristics for a variety of surfaces. This capability is an important characteristic for gecko-like adhesives, which has not been previously achieved with synthetic fibrillar adhesive systems.[54,58]

3.7 Conclusions

Our adhesives show that the ability to adhere to a wide range of surfaces can be achieved without fabrication of fibrillar structures and suggests that this ability is due to low effective modulus in combination with low compliance in the direction of loading. The

mathematical constructs described within this manuscript should guide the construction of future high strength reversible adhesives. The ability for ultra-stiff carbon fiber fabrics to drape over macroscopic length scales, and elastomers to deform at microscopic length scales enables strong adhesion on "real world" surfaces. Our results are consistent with previously described scaling equations, reinforcing the ability for this method to achieve extremely high force capacities. We believe that the "dry" and high-capacity gecko-like adhesives demonstrated here can be utilized for a wide range of commercial and industrial applications, such as wall-hanging in homes or adhesion to fragile surfaces for manufacturing.

3.8 Acknowledgements

This work was funded by the Human Frontiers Science Program and the University of Massachusetts CVIP Technology Development Fund. We also thank NSF MRSEC (NSF DMR-2820506) for facilities support. I would like to thank S. B. Hutchens, J. T. Pham, and C. S. Davis for their thoughtful discussions, N. P. Bende for help with photography, and C. A. Gilman for help performing the live gecko testing experiments. Additionally I would like to thank M. D. Bartlett, D. J. Irschick, and A. J. Crosby for their contributions to the published manuscript and B. M. deRonde for proofreading support.

CHAPTER 4

USING SHEAR ADHESIVES TO SUPPORT NORMAL LOADS

4.1 Introduction

Bottom-loaded fibril-less adhesives are an efficient design for creating high strength, reusable adhesives for a variety of surfaces.[74–76,119] However, these adhesives are only designed for shear adhesion. In many applications, a zero degree loading angle is not possible to achieve; for example, in wall hanging applications, the adhesive hangs along the surface of the wall, not directly beneath it, resulting in a peel angle. The adhesives presented in Chapter 2 and Chapter 3 are designed to easily peel when forces are applied at high angles, limiting their usefulness in wall hanging application. Therefore, a new design is required to create adhesives that resist peeling from non-shear forces.

Again, Nature is used as a guide for new adhesive designs. Biological organisms are capable of climbing across ceilings, yet their adhesive toe-pads achieve the highest adhesive forces under shear loading conditions. Some organisms use their muscular systems to generate shear forces. Geckos specifically are seen to widely spread their limbs and toes, allowing them to generate shear force to maintain adhesion on walls or inverted surfaces. The adhesives introduced in this chapter are designed to mimic this ability to minimize loading angle when normal loads are applied.

This chapter presents new adhesive devices which show a more than six-fold increase in normal adhesive force capacity, compared to bottom loaded adhesives. Two elastomer pads are coated at opposite ends of a single piece of fabric, referred to as a "double pad" and force is applied from the center of the fabric. The design developed here is similar to the radially distributed toes in the gecko. This new adhesive device enables

high strength, reversible adhesives for use in a wide range of situations where pure shear loading conditions cannot be achieved.

4.2 Background

Previous research on fibril-less gecko-inspired adhesives shows that connecting the tendon to the center of the skin, rather than to the bottom, prevents a rapid decrease in force capacity with increasing applied load angles.[74] However, this method has some complications, which limits its applicability. One problem with this design is fabrication is difficult, and each sample must be prepared individually. An additional problem is that the joint connecting the tendon to the skin can act as a limiting component; if the fabric is very stiff it becomes difficult for adhesion to occur under the joint, and if it is too compliant the adhesive can tear at the joint. These difficulties led to the development of new adhesives which possess an ability to support loads at high loading angles, with a simpler fabrication process.

Biology again provides inspiration for adhesive design. Geckos and other organisms crawl across ceilings or other horizontal surfaces, where the effective loading angle on the toe-pads is much greater than zero degrees.[11,37,81] Researchers have proposed that their ability to adhere on horizontal surfaces is due to the high aspect ratio features which cover their toes, called setae. High adhesive strength is achieved due to a phenomenon known as contact splitting.[48,68,120] Contact splitting principles state that for a given contact area that is broken up into n discrete segments, adhesive force will scale like $n^{1/2}$.[68] However, this method necessitates the use of small, hierarchical features which are difficult to manufacture at large scales.

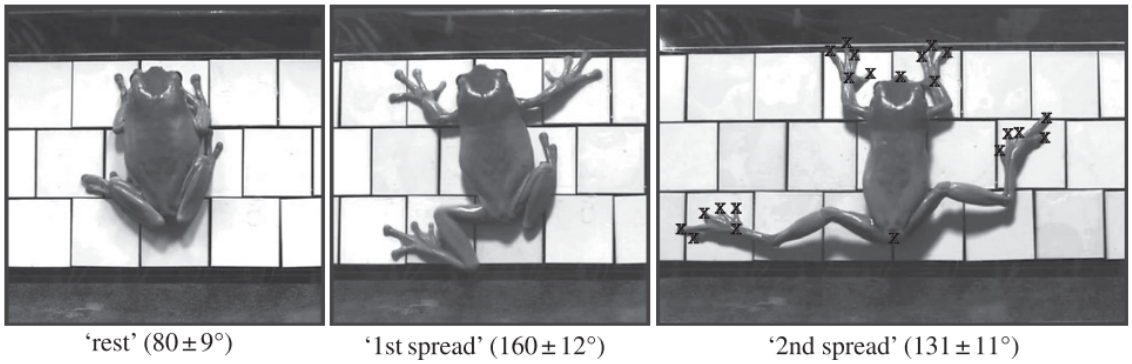

Figure 4.1 – Positional change of a tree frog from a vertical surface (left) to a partially inverted surface (right). [31] Used with permission: Endlein, T.; Ji, A.; Samuel, D.; Yao, N.; Wang, Z.; Barnes, W. J. P.; Federle, W.; Kappl, M.; Dai, Z. *Journal of the Royal Society, Interface* **2013**.

There is also evidence that organisms climb across ceilings by extend their limbs, to emphasize shear forces (Figure 4.1).[22,31,35] This method allows organisms to use adhesive pads which work best under shear conditions, to support normal loads. Results from Kendall demonstrate that the peel strength of adhesives greatly decreases with increasing peel angle (Figure 4.2).[99] To create reversible adhesives that work under normal

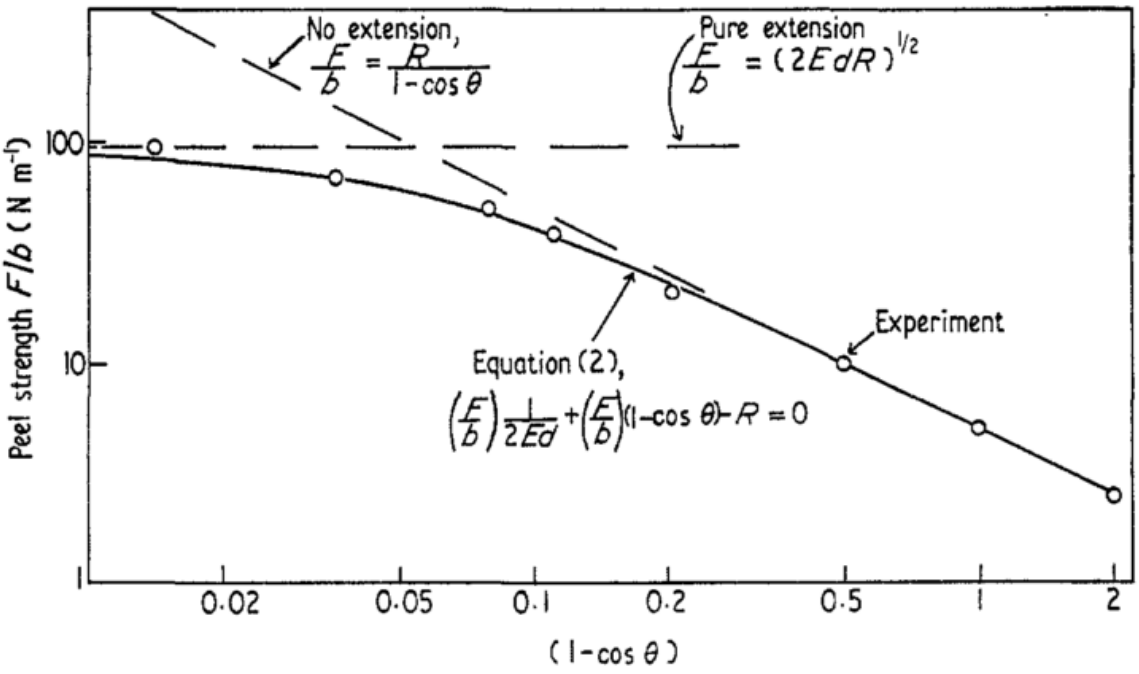

Figure 4.2 - Peel strength as a function of loading angle.[99] Used with permission: K. Kendall, Thin-film peeling- the elastic term. *J. Phys. D: Appl. Phys.* **1975**, 8, 1449.

loading conditions, a design is required that minimizes the effective loading angle on the pads. These adhesives are not enabled by contact splitting, or by altering the adhesive materials. The adhesives fabricated here support normal loads by generating shear forces and minimizing the loading angle of the adhesives.

4.3 Approach

A diagram of a double pad adhesive system, with a 90 degree applied load is shown in Figure 4.3. A 90 degree load is applied as it represents the highest possible loading angle on both pads. A simple model of the effective loading angle, θ, is used to predict the important variables to increase normal force capacity, $F_{c,normal}$. θ, the angle generated by the applied force is given as:

$$\cos\theta = \frac{\overline{A'B}}{\overline{A'B'}} = \frac{\overline{AB} - \overline{AA'}}{\overline{AB} + \delta_{fabric}} \tag{4.1}$$

Where $\overline{A'B}$ is the initial pad gap length, L_g ($\overline{AB}$) minus some length due to deformation of the pad ($\overline{AA'}$). Likewise, $\overline{A'B'}$ is L_g plus some additional displacement due to the applied force stretching the fabric. The displacement length $\overline{AA'}$ is the x-axis component of the applied force multiplied by the pad compliance, and the displacement, δ_{fabric}, is the hypotenuse force multiplied by the fabric compliance:

$$\cos\theta = \frac{L_g - F_x C_{pad}}{L_g + F_h C_{fabric}} = \frac{L_g - \frac{FC_{pad}}{2\tan\theta}}{L_g + \frac{FC_{fabric}}{2\sin\theta}} \tag{4.2}$$

Using trigonometry it is possible to solve for these component values of the applied force. This equation is simplified further, yielding:

$$1 - \cos\theta = \frac{F(C_{pad} + C_{fabric})}{2L_g \tan\theta} \tag{4.3}$$

$$\tan\theta - \sin\theta = \frac{F(C_{pad} + C_{fabric})}{2L_g} \tag{4.4}$$

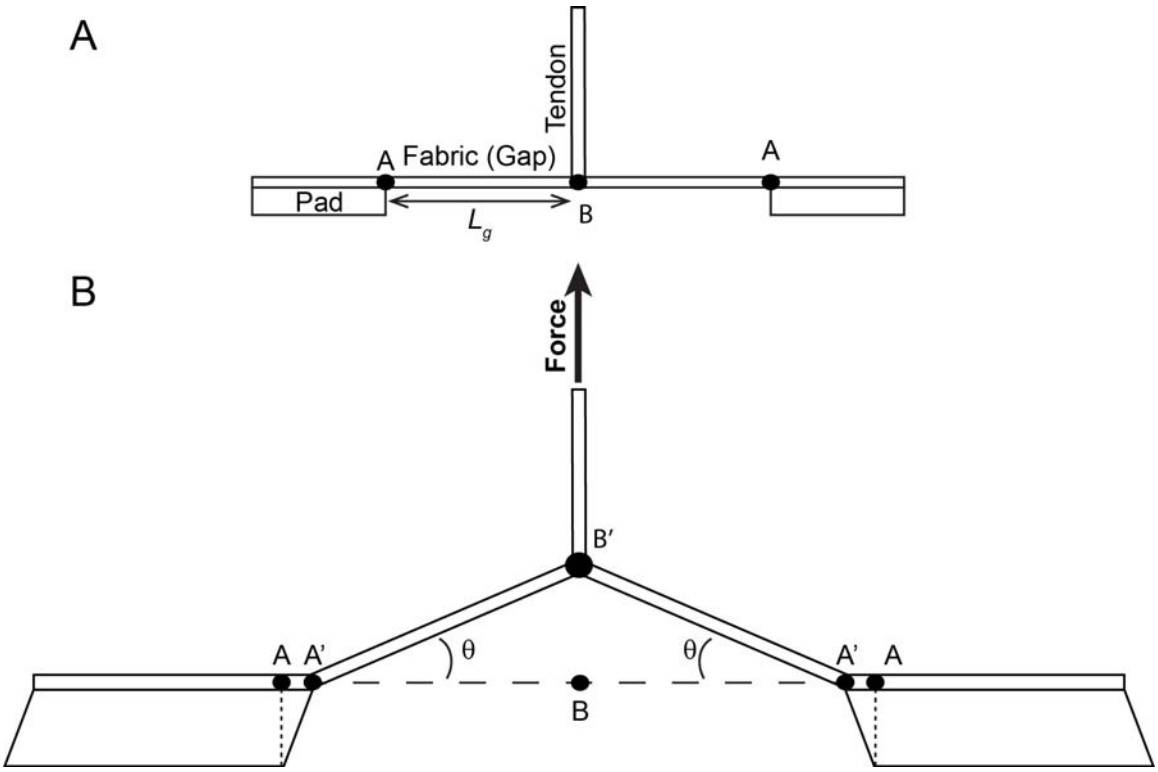

Figure 4.3 - Schematic of a double pad (A) at rest, and (B) after a force is applied normal to the adhesive.

θ is approximated by Taylor expansion:

$$\frac{\theta^3}{2} + \frac{\theta^5}{8} + \frac{13\theta^7}{240} + \cdots = \frac{F(C_{pad} + C_{fabric})}{2L_g} \tag{4.5}$$

And for the low angle limit, where θ < 45°, the expansion can be limited to just the first term:

$$\theta \approx \left[\frac{F}{L_g}(C_{pad} + C_{fabric})\right]^{1/3} \tag{4.6}$$

Substituting (C_{pad} + C_{fabric}) ≈ $C_{calculated}$ (Equation 2.12) to give:

$$\theta \approx \left[\frac{FC_{calculated}}{L_g}\right]^{1/3} \tag{4.7}$$

This equation allows for predictions of loading angle to be made based on different properties of the double pad system. As would be expected, increasing the applied load will increase the effective loading angle, which ultimately causes the sample to release

from the substrate. Based on Equation 4.7, there are a few methods which will be used to increased normal force capacity:

1. Decreasing the compliance of the system. This increases the force required to deform the adhesive to increase the peeling angle.
2. Increasing the pad gap length. Longer L_g results in a smaller loading angle for the same amount of deformation.
3. Insuring a zero degree loading angle when the sample is adhered to the surface. The assumption within this chapter is that loading angle is the main parameter controlling normal force capacity, and it is therefore important that no *initial* peel angle is imposed during application of the sample.

4.4 Experimental

4.4.1 Materials

Elastomer are purchased from BJB Enterprises and used for the pads. ST1060 is prepared by mixing 'A' and 'B' components with a ratio of 100:55. Modulus of the elastomer is determined by dynamic mechanical analysis (DMA) at a frequency corresponding to the adhesives testing rate, 0.40 Hz for the 0.40 mm thick samples. The ST1060 elastomer has a storage modulus of 3.1 MPa (mastercurve is presented in Figure 2.3). The components are mixed together in a plastic cup, and degassed in a desiccator until bubbles disappeared; the mixture is then reintroduced to air, with an approximate work time of 20 minutes before gelation occurs.

15 cm wide 24K unidirectional carbon fiber tape is purchased from Soller Composites. Cotton fabric is purchased from Joann Fabrics. 7.5 cm wide Kevlar fabric tape is purchased from US Composites. To bond the fabrics together, Bemis 3231 adhesive

film (60 μm thickness) on release paper is used, and applied with an iron, set to approximately 200ºC.

4.4.2 Fabrication

Fabrication of double pad devices takes place in two steps. First the double pad skin is prepared. Separately, the flexible tendon connection is prepared. After the double pad skin is cured, the two portions are combined to create the final adhesive device.

4.4.2.1 Double Pad Skin

24K unidirectional carbon fiber tape is used for the double pad skin. 5 cm x 15 cm regions are prepared for the elastomer pad at either end of the fabric. A 2.5 cm, 5 cm, or 10 cm region of fabric in the center of the fabric that separates the pads is coated with Bemis adhesive film, and the length of this region is referred to as the pad gap, L_g. The release liner of the adhesive film is left on until after sample fabrication was complete. On polyethylene (PE) coated glass, the double pad skin fabric is placed and securely taped with three pieces of 3M packing tape, over the adhesive film release liner. The uncured elastomer is poured onto the fabric, and smoothed with a glass slide. A thin PE film is

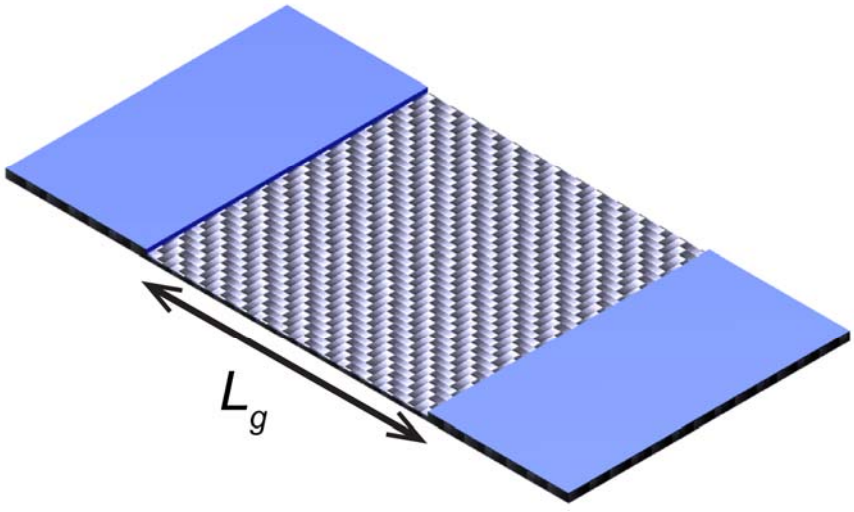

Figure 4.4 - Schematic of the double pad skin. The distance between the pads is an experimental variable, and is referred to as the pad gap length, L_g.

placed on top of the thin layer of uncured polymer. A glass plate is then placed on top of the film, and 25 pounds of force is applied to create a smooth adhesive surface. Samples are cured at room temperature overnight (at least 12 hours), then placed in a 70°C oven for at least 12 hours. After curing a rotary blade cutter is used to cut the samples to the desired size. The release liner is retained. A schematic of the double pad skin is shown in Figure 4.4.

4.4.2.2 Flexible Tendon

Flexible tendons are made consisting of either cotton fabric or Kevlar fabric. The fabricated component consists of two parts, the tendon for applying load, and the flange which connects to the double pad skin. For the cotton fabric, 5 cm, 7.5 cm, or 10 cm wide strips (w_t) of fabric are prepared. Kevlar tape is fixed with w_t = 7.5 cm. Bemis adhesive film is applied to both strips. A line was drawn on the fabric to demarcate the flange region

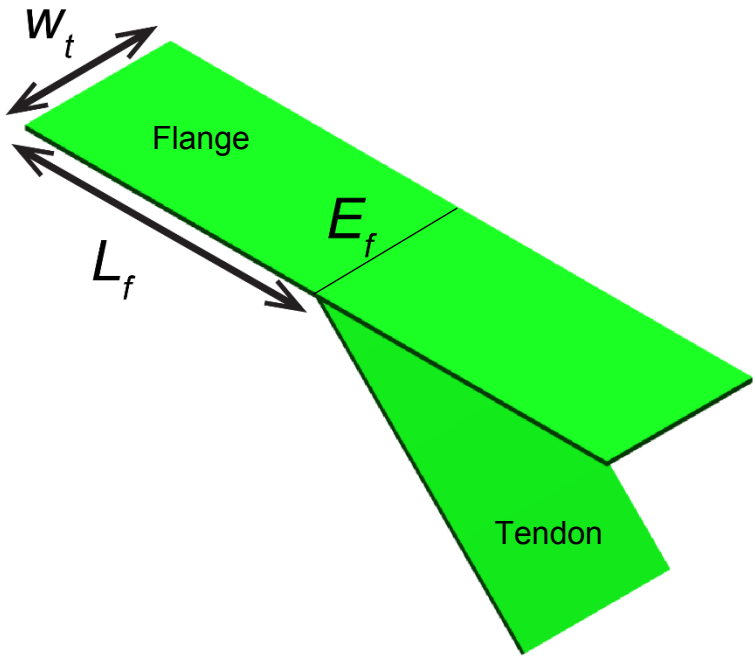

Figure 4.5 - Schematic of the flexible tendon. Experimental variables of the flexible tendon component are the flange length, L_f, the tendon width, w_t, and the tendon modulus, E_f.

(L_f) from the tendon region. The release liner is removed from the tendon portion of the fabric, with the flange region retaining the release liner. The two pieces of fabric are then adhered together with an iron. The resulting structure is shown in Figure 4.5.

4.4.2.3 Component Assembly

After both the double pad skin and flexible tendon components are fabricated, they are then assembled (Figure 4.6). On the back of the double pad skin, nominally in the center of the component, a strip of Bemis adhesive film is applied, with the same dimensions as the flange of the flexible tendon. The release liner from the flange region of the flexible tendon is then removed, and adhered to the double pad skin using an iron to complete the adhesive device. After the device is complete, the release liner between the elastomer pads on the double pad skin is removed.

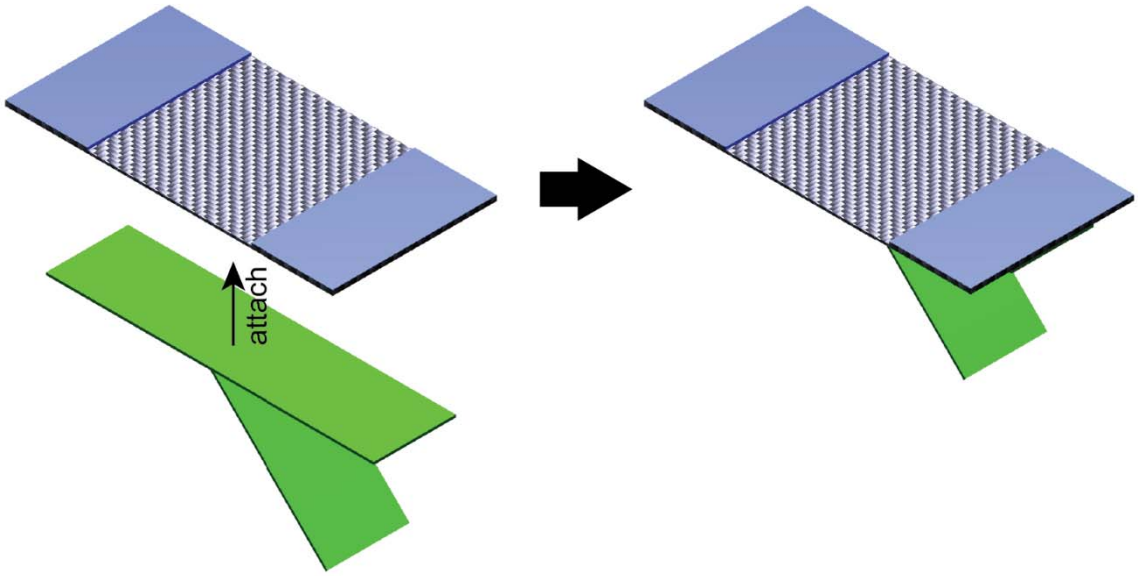

Figure 4.6 – Schematic of the assembly of the device, and the final sample.

4.4.3 Testing

An Instron 5564 tensile tester is utilized for testing. The adhesive is anchored to the base of the tensile tester with a custom builder adhesive anchor, which allows for rotational

freedom in the plane of the adhesive (Figure 4.7). The glass substrate is held in place by a custom built substrate holder, which is tightly attached to the crosshead and displaced at a rate of 10 mm/min, until a maximum force is reached, and the sample detached from the surface. The substrate holder is mounted either normal or parallel to the crosshead displacement direction. The adhesive test setup has a measured compliance of 2.75 x 10^{-7} m/N. Each test is performed at least 5 times, and the first test is excluded to allow for conditioning of the test setup and adhesive pad.

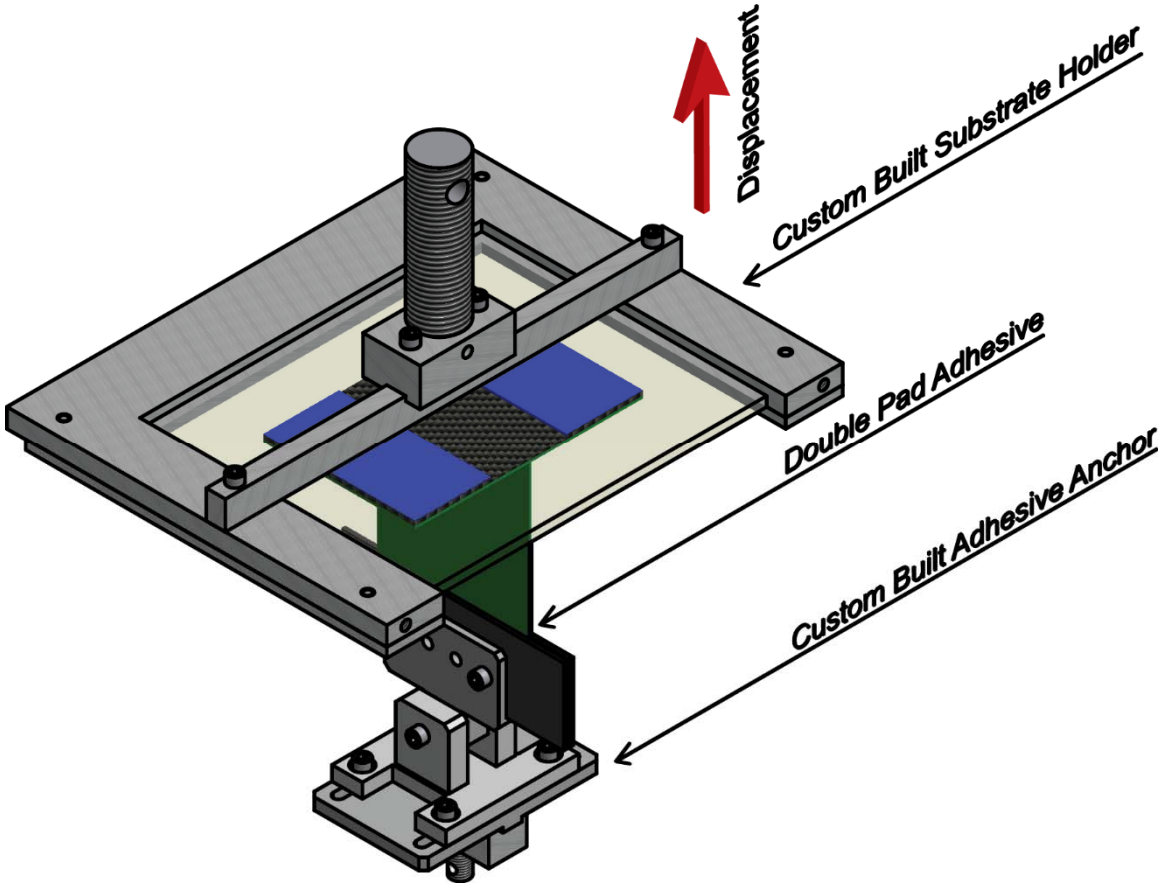

Figure 4.7 - Schematic of the test setup for double pad adhesives.

4.5 Results

4.5.1 Bemis Adhesive Film Tear Strength

The double pad adhesives designed in this chapter are assembled using a Bemis adhesive film. This adhesive allows for rapid conversion of the double pad adhesive skin and flexible tendon into an adhesive device. However the maximum tear strength of the adhesive film will also limit the maximum normal forces supported by the adhesive. If the adhesive strength is greater than the tear strength of the adhesive film, the sample will fail permanently at the adhesive film joint, rather than releasing from the test surface. Figure 4.8 is a plot of tear strength versus displacement for a 180 degree peel test of a 2.5 cm wide carbon fiber fabric and cotton fabric bonded together with Bemis adhesive film. The average tear strength measured is 12.3 N/cm. Because the flexible tendon is adhered on two sides, the average tear strength of the flexible tendon used for the adhesive devices is 24.6 N/cm. This represents the maximum normal adhesive strength the adhesive can undergo before failure of the sample. The tensile tester will be programmed to end the test

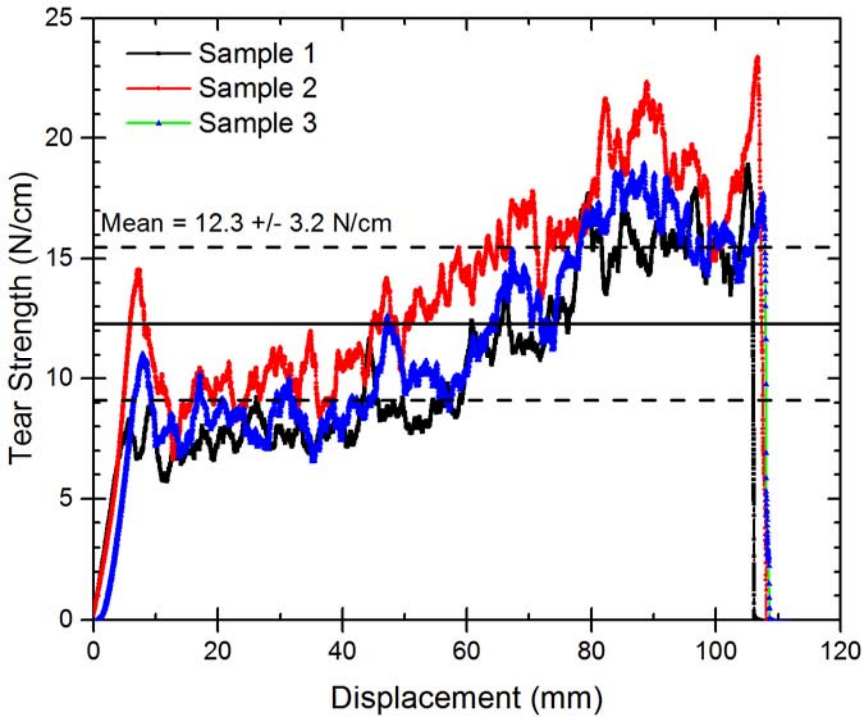

Figure 4.8 - Tear Strength versus displacement, for three samples of unidirectional carbon fiber bonded with Bemis adhesive film to cotton fabric, with a sample width of 2.5 cm.

if this force is reached to protect the sample being tested. Despite this limitation, the Bemis adhesive film is a useful material for quickly fabricating adhesive devices.

4.5.2 Pad Gap Length

Increasing the pad gap length, L_g, is expected to influence normal adhesion strength by decreasing the loading angle of the pads for the same applied load. Since the adhesives created here achieve the highest adhesive strength at zero degree loading angles, it is expected that larger L_g should result in higher normal force capacity. The samples fabricated for this test have a 7.5 cm wide cotton fabric tendon, which can support 185N of load before sample failure. Pad gap lengths of 2.5 cm, 5 cm, and 10 cm are tested. The results for this test are shown in Figure 4.9A. The maximum force is observed with L_g = 5 cm. As expected, the 5 cm pad gap adhesive has higher normal force capacity than the 2.5 cm pad gap adhesive. However the 10 cm pad gap adhesive performed statistically equivalent to the 5 cm pad gap adhesive (P = 0.12). There are two potential explanations to why L_g = 10 cm does not follow the expected trend. First, as the pad gap length increases, the amount of carbon fiber fabric being loaded in extension increases, which results in an increased compliance of the adhesive pad. Also, as the distance between pads increases, it becomes more difficult experimentally to apply the adhesive with no initial angle between the tendon and pads. If the double pad adhesive is not adhered perfectly perpendicular to the flexible tendon (if slack is present in the skin), there will be an initial loading angle before any load is applied. An optimization of these trade-offs is observed at L_g = 5 cm, where compliance is minimized and the pad can easily be applied with no initial peel angle.

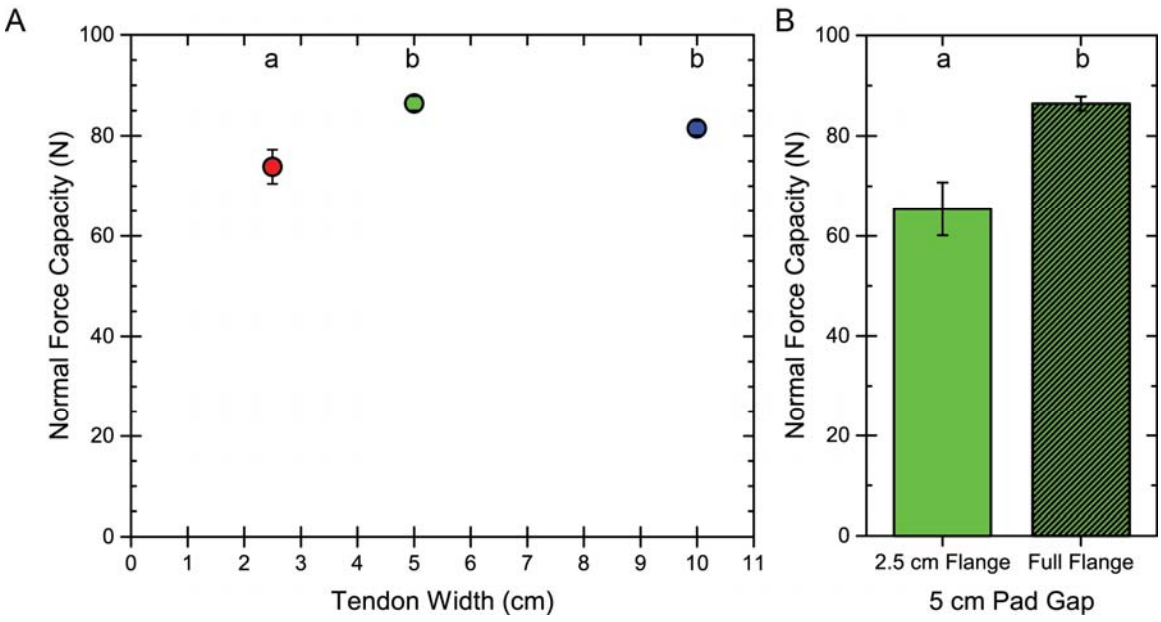

Figure 4.9 - Normal force capacity versus tendon width for double pad adhesives with 7.5 cm wide cotton fiber flexible tendon. (A) Peak is seen at 5 cm. (B) Comparison of the 5 cm pad gap double pad adhesive with flexible tendon flanges of length 2.5 cm and 7.5 cm (full flange). Error bars represent standard deviation. ANOVA testing is used with a post-hoc Tukey test to determine significance, with $P < 0.01$.

It is also possible to vary the length of the flange, L_f, which connects the tendon to the double pad adhesive. The results for adhesives with L_g = 5 cm are shown in Figure 4.9B. A higher normal force capacity is found for the sample with the full flange length, where the flange extends to the edge of the double pad skin. This is understood through Equation 4.7, as additional fabric decreases the compliance of the double pad adhesive, decreasing the loading angle. The remaining tests are performed with optimized adhesives with L_g = 5 cm and full length tendon flanges.

4.5.3 Flexible Tendon Width

In Chapter 2, as tendon width is reduced, adhesive force capacity decreases (Figure 2.14). This variable is again tested to determine if the same results occur when the loading geometry is changed to normal loading. Samples are created with w_t = 5 cm, 7.5 cm, and 10 cm, which have maximum sample loads of 123 N, 185 N, and 246 N, respectively. The

results are shown in Figure 4.10. Similar to Figure 2.14, as tendon width increases, the normal force capacity increases. The load versus displacement curve for the three tendon widths tested is presented in Figure 4.10A. As the fabric width increases, the compliance

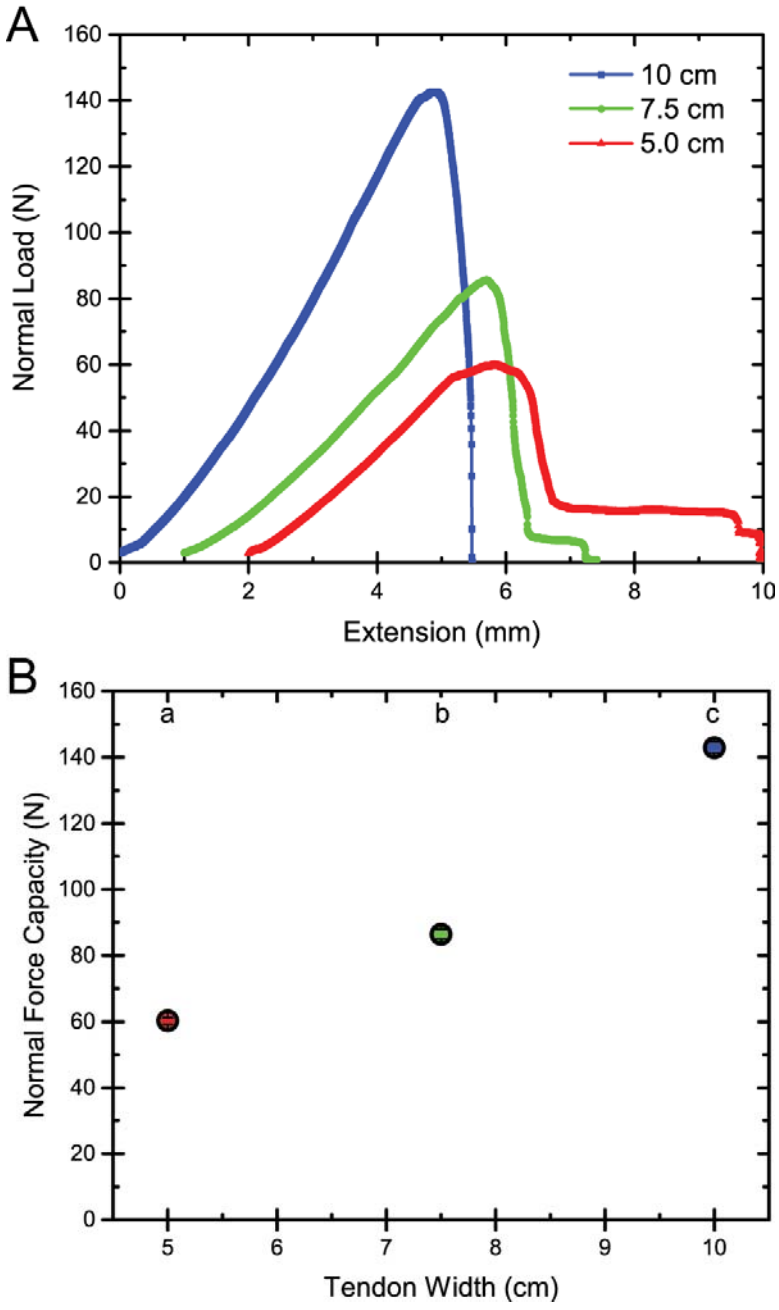

Figure 4.10 – Load versus extension curves for the three tendon widths. (A) A 1 mm horizontal shift is applied to the curves to easily compare loading curves. (B) Normal force capacity as a function of tendon width. Error bars represent standard deviation, and are smaller than the data points. ANOVA testing is used with a post-hoc Tukey test to determine significance, with $P < 0.01$.

of the system decreases. As compliance decreases, the prediction states that force capacity will increase, and a comparison of force capacities is shown in Figure 4.10B. These results are somewhat surprising, because when the tendon width is the same as the pad width peeling often occurs from the edges, and this peeling sometimes initiates failure of the adhesive. In this situation, the decreased compliance and the ability to load the entire pad outweighs any potential early peeling that occurs at the pad edges.

4.5.4 Tendon Material

Increasing the tendon width decreases the compliance as well as increasing the area of the pad that is loaded. The tendon stiffness can also be varied without changing the tendon width, by changing the tendon materials. Two separate flexible tendons are prepared with w_t = 7.5 cm, from cotton fabric and Kevlar fabric. Kevlar is chosen because it has both high modulus and toughness, yet is woven into a plain weave fabric, which

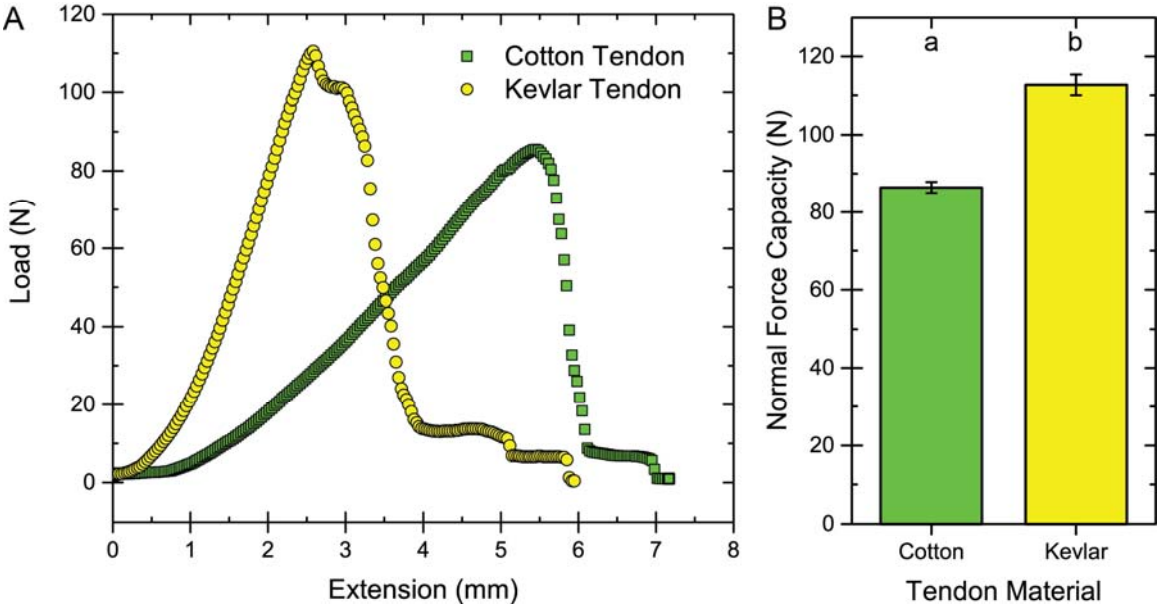

Figure 4.11 –Representative load versus extension curves for double pad adhesives with 7.5 cm wide tendons of cotton or Kevlar. (A) Compliance is greatly decreased for the Kevlar tendon. (B) Normal force capacity results for the two tendon materials tested. Error bars represent standard deviation. ANOVA testing is used with a post-hoc Tukey test to determine significance, with $P < 0.01$.

allows it to maintain flexibility. In Figure 4.11A the load versus displacement curve is shown for double pad adhesives with the different tendon materials. The Kevlar-based tendon has a lower compliance and therefore a higher normal force capacity. The force capacity results for the two tendon materials is seen in Figure 4.11B. Decreasing the compliance of the tendon results in a decreased compliance of the entire adhesive, increasing normal force capacity. Even though the tendon is far from the adhesive interface, the materials chosen play an important role in the normal force capacity.

4.5.5 Shear and Normal Force Capacity Comparison

In the previous sections, the focus is solely on normal force capacity of the double pad adhesives, which is important because some situations require adhesives to be loaded perpendicular to the attachment surface. Another important loading geometry is in shear but with tolerance to potential normal force impulses (such as an accidental bump).

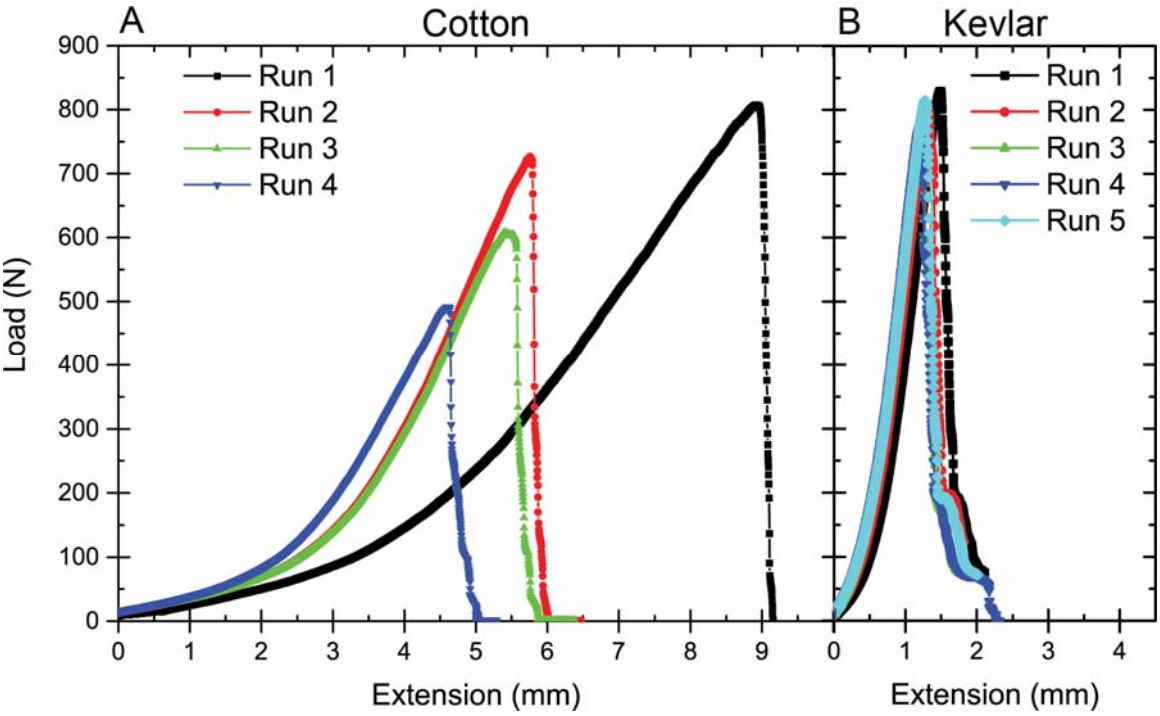

Figure 4.12 – Shear load versus extension curves for double pad adhesives with 7.5 cm wide tendons fabricated from (A) cotton, and (B) Kevlar.

Therefore, shear tests with the double pad adhesives are necessary to compare their performance in both normal and shear loading to the previously developed bottom-loaded adhesive pads.

In a shear loading configuration, the material of the tendon plays an important role. Figure 4.12A and Figure 4.12B show the loading curves of double pad adhesives with cotton and Kevlar tendons, respectively. The scale of the X-axis is fixed. The compliance of the double pad adhesive with cotton fabric tendon is much greater than that of the adhesive with Kevlar fabric tendon. Based on the predictions from Chapter 2, Kevlar-based tendon double pad adhesives are expected to achieve higher force capacity through decreasing the total compliance. The samples are tested multiple times, and for the cotton tendon adhesive, each test in shear results in decreased shear force capacity. After the tests, the cotton samples exhibited noticeable tearing in the tendon. After the fourth run of the adhesive, the tendon completely tore, destroying the sample. Comparatively, run to run deviation is very little in the Kevlar tendon adhesive. The improved mechanical properties of Kevlar make it a preferable material for a double pad adhesive with attached flexible tendon.

The performance of the double pad adhesives is also compared to a bottom-loaded adhesive. A 5 cm x 10 cm (L x w) unidirectional carbon fiber adhesive is fabricated as a control sample, and a 7.5 cm wide cotton fabric tendon is adhered to the back of the adhesive using the Bemis adhesive film. This adhesive is then tested in normal and shear loading configurations. The results are shown in Figure 4.13, with comparisons to the cotton and Kevlar tendon double pad adhesives. For all adhesives the shear force capacity is much higher than the normal force capacity. Normal force capacity increases

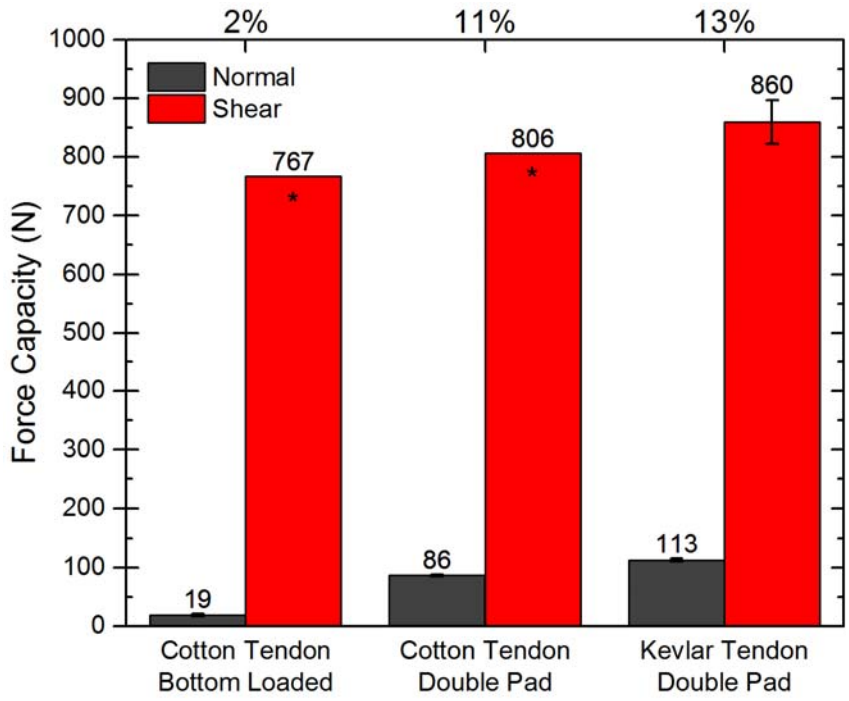

Figure 4.13 – Comparison of the force capacity in both normal and shear. Results shown for the cotton tendon bottom-loaded adhesive, the cotton tendon double pad adhesive, and the Kevlar tendon double pad adhesive. The value listed above the bars represents the mean force capacity for the given test. The values listed above the chart represents the normal loading efficiency, the maximum normal force capacity relative to the shear force capacity. Asterisk represents the sample is damaged after one test, and this force value represents only the first test. Error bars represent standard deviation.

dramatically by switching to a double pad adhesive design. When fabricated with the same tendon, cotton, a greater than fourfold increase in normal force capacity is seen with a double pad adhesive compared to a bottom loaded adhesive. Comparing the cotton tendon bottom loaded pad to the Kevlar tendon double pad, normal force increases by a factor of six. A normal loading efficiency, $F_{c,normal} / F_{c,shear}$, for each adhesive is calculated, and for the Kevlar tendon double pad adhesive, 13% of the maximum shear force capacity is achievable under normal loading conditions, a large increase over the 2% efficiency measured with the cotton fabric bottom loaded adhesive. This demonstrates that double pad adhesives are much more tolerant to normal force perturbations than the previously utilized bottom loaded adhesives.

4.6 Discussion

New adhesives devices are fabricated with the goal of reducing the loading angle on the adhesive pads, to increase normal force capacity. Our hypothesis states that loading angle must be reduced to increase force capacity, and this can be achieved by increasing the separation length between the adhesives pads, by ensuring that no slack exists in the skin when adhered to the surface, and by decreasing the compliance of the system. We saw that as pad gap length increased from 2.5 cm to 5 cm normal force capacity increases. However, when pad gap length was increased to 10 cm, no change in force capacity is observed. We believe this is due to difficulties in applying adhesives with large pad gap lengths to the substrate. When organisms such as geckos and tree frogs adhere to surfaces, they separate their limbs, but also pull their body close to the surface. With large pad gap length adhesives, we are able to increase pad separation, but are not able to effectively ensure that the pad remains close to the surface. Finally, we also see that by decreasing tendon compliance, we increase normal force capacity. Importantly, this also increases the toughness of the adhesive preventing failure of the device, which occurs with the weak cotton fabric adhesives. These results prove that Equation 4.7 provides guidance for creating double pad adhesives to support normal loads.

There are many qualitative fabrication techniques that are important to make high performance double pad adhesives. In the previous chapters, unidirectional carbon fiber is used as the tendon material because it has the highest modulus of any fabric-based material tested. For the double pad adhesives tested here, it is not possible to use this fabric for the attached tendon, because it is not flexible enough to form the 90 degree angle necessary to create the flanges which connect to the skin. A benefit of using woven fabric is the bending

stiffness is much lower than the tensile stiffness.[121] Cotton fabric works very well as a tendon material because the yarns that make up the fabric weave are very thin, which allows the fabric to drape easily. When fabricating the flexible tendon component, this allows the creation of a tight crease at the junction point between the tendon and the flanges that connect to the double pad skin. The Kevlar fabric is much stiffer than cotton fabric, but a crease is still able to be formed. With carbon fiber, attempting to make the crease causes the fabric to tear with only a small load applied. In contrast, the fabric used in the double pad must be very stiff. If a compliant fabric like cotton is used in the double pad skin, when force is applied, the fabric in the gap region of the double pad stretches, and a high peel angle is applied to the pads, which results in low normal force capacity. As a general rule, a very stiff fabric must be used for the double pad skin, and a less stiff fabric must be chosen for the flexible tendon to create high normal force capacity adhesives.

For converting the individual components into an adhesive device, Bemis adhesive film is used. Due to the finite tear strength of this adhesive, we experienced a limited upper bound of normal adhesive strength. This adhesive works well for quickly and simply fabricating adhesives, but it is not the only choice available for making double pad adhesives. For example, the tendon can be physically stitched to the double pad, or mechanical fasteners also can be used, such as rivets. When designing adhesives it is important to take into account the mechanical properties of the entire system, not only the components which contact the surface.

Additionally, the required shear load must be taken into account when choosing tendon materials. In the case of the cotton fabric tendon, the adhesive is so strong in shear that it results in destruction of the tendon at maximum load. For low strength applications

cotton based tendons may be acceptable, but if high loads are desired, a tendon made from a tough engineering plastic such as Kevlar is required to achieve maximum adhesive force capacity.

4.7 Conclusion

In this chapter, we have quantified the adhesive performance of double pad adhesives in both normal and shear loading configurations. We observe that an optimization of pad gap length occurs at 5 cm, which represents a trade-off between low loading angle at the adhesive under load, and an ability to adhere the adhesive to the substrate with minimal slack in the gap region. We saw that increasing tendon width results in higher force capacities due to the ability to load the largest percentage of the pad, and that peel at the edges does not dominate the failure mechanism. The materials chosen for the tendon are very important, because a stiff and tough material allows us to maximize our adhesive strength, and it also prevents fracture of the fabric under high loads. Using these results, we are able to create double pad adhesives with normal adhesive efficiencies of 13% of their shear force capacity. These adhesives represent an effective way to fabricate adhesives with high shear force capacities, while providing tolerance from applied normal forces.

4.8 Acknowledgements

I would like to acknowledge S. Fakhouri for his critical feedback on the work in this chapter. Additionally I would like to thank the Commercial Ventures and Intellectual Property office at UMass Amherst for their help with the invention disclosure and patent application based on this work.

CHAPTER 5

EXTREMELY TOUGH COMPOSITES FROM BIOCOMPATIBLE HYDROGELS AND FABRIC

5.1 Introduction

In most situations the human body is capable of healing when it incurs damage.[122] However, sometimes the damage is too large for healing to happen independently, or the damage occurs to body parts with poor healing capabilities, such as ligaments.[123] To help the body heal, prosthetic materials that mimic the mechanical properties of biological tissue are desired. In the previous chapters, we utilized fabrics for making adhesives capable of draping while maintaining their stiffness. The matrix material of the fabricated composites consisted of elastomers. In this chapter, we show that by strategically combining soft, tough hydrogels with stiff, tough fabrics, water-containing materials with high strength are achieved. Surprisingly, we find that this combination improves the effective tearing energy up to 250,000 J/m^2, much greater than either individual component. Furthermore, these new materials are capable of supporting nearly three times the load of the neat fabric. Even with these improved mechanical properties, the composite materials remain as flexible as silicone rubber. These properties make these new composite materials useful for load-bearing biological prosthetic applications, such as synthetic cartilage or ligaments.

5.2 Background

For over a hundred years, scientists have attempted to develop materials which possess the mechanical properties to heal damaged, soft biological components, yet many of the required characteristics are contradicting; for example, they must be soft and slippery, yet capable of supporting large loads, while containing water.[124] A range of rigid

materials, including metals,[125] stiff fabrics,[126–129] and synthetic polymers,[130–133] have been previously employed for ligament and tendon prosthetics. These materials have not ultimately found widespread use due to poor biocompatibility and fatigue resistance.[128,134,135] In contrast hydrogel materials possess high water content, offering similar characteristics to the biological materials.[123,136–140] However hydrogels are often brittle and lack high ultimate tensile strength required for load bearing applications.[124] To overcome these limitations, double network hydrogels have been developed that retain the benefits of traditional hydrogels (i.e. high water content and low friction), while simultaneously providing improved toughness and tensile strength.[141–146] It was recently discovered that by introducing a secondary polymer system with reversible crosslinks, a gel's toughness is further increased.[147] One approach to take advantage of this mechanism is with polyampholyte gels consisting of both covalent and ionic crosslinks. This leads to soft and wet materials with high toughness, with the added benefit of single-step production.[148,149] While these new materials provide improved mechanical properties over previous hydrogel designs, they are still too soft to support the large loads needed in biological applications, providing an opportunity for the development of new hydrogel composites.

5.3 Approach

The newly designed polyampholyte and fabric composites are compared to two control groups: a traditional polyacrylamide single network hydrogel and fabric composite, as well as a neat fabric without a gel matrix. A variety of tests are performed to characterize the mechanical properties of the polyampholyte hydrogels. First, trouser tear tests are performed to determine the tearing strength and fracture energy of the materials.[144,148,150,151]

Tensile tests are also performed to measure the load at break for the samples, as well as the strain energy density. Finally, three point bend tests are performed to understand the anisotropic mechanical properties, by comparing bending and tensile modulus values.[121]

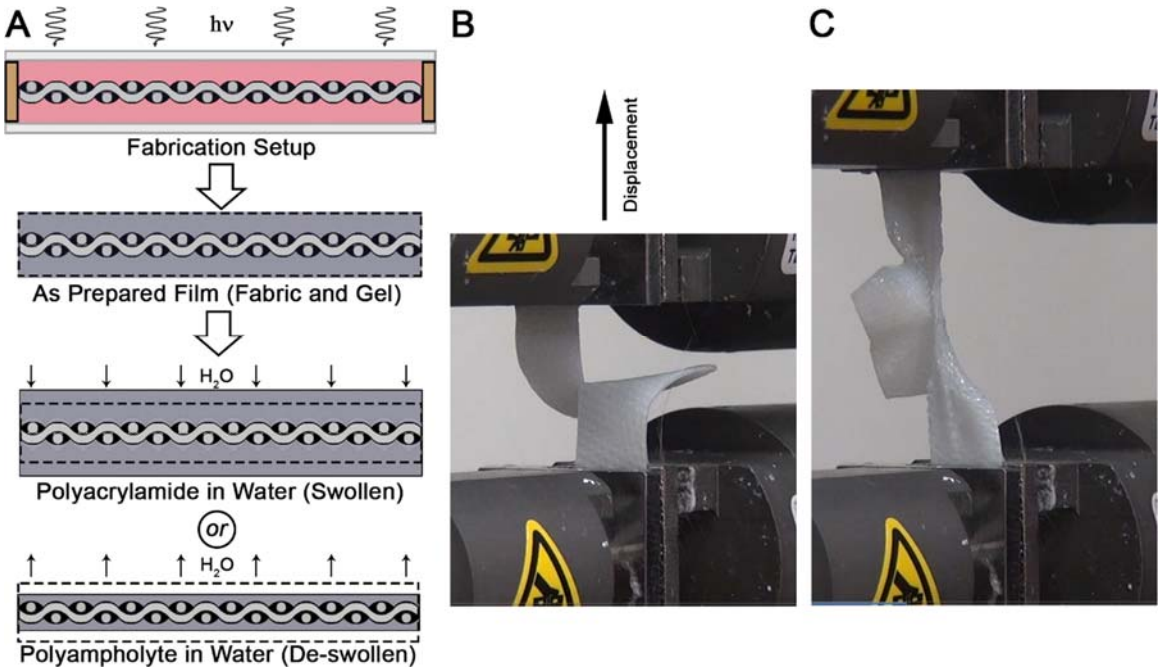

Figure 5.1 - A schematic of the sample preparation for fabricating hydrogel composite samples. (A) Step by step process. (B) A polyampholyte composite sample loaded in the tensile tester about to undergo the tearing test. (C) A polyampholyte sample being loaded during a tearing test.

5.4 Experimental

5.4.1 Polyampholyte Composite Preparation

Polyampholyte composites were prepared at the Laboratory of Soft and Wet Matter at Hokkaido University in Sapporo, Japan, under the guidance of Taolin Sun and Jian Ping Gong. Samples are prepared by placing 300 μm spacers on the fabric (satin weave 8.9 oz., purchased from US Composites), which is inserted between two glass plates (total sample thickness, ~1 mm, figure 5.1A). A 2M solution of dimethylaminoethylacrylate quaternized ammonium and sulfonated polystyrene (1:1 true stoichiometric charge ratio[149]) is chosen as the polyampholyte, and prepared with 0.1 mol% ketoglutaric acid as initiator, 0.1 mol%

methylene bisacrylamide as crosslinker, and an excess of sodium chloride to shield the charged monomers. The solution is prepared and heated until completely dissolved. The solution is then placed into a glove box with the sample mold. The solution is injected into the mold and cured under UV light for 12 hours. After polymerization the gel composites are placed into deionized water for at least four days to allow the gel to reach equilibrium.

5.4.2 Polyacrylamide Composite Preparation

Polyacrylamide composite samples were prepared at the University of Massachusetts Amherst. Samples are prepared by placing 300 μm spacers on the fabric (Satin Weave 8.9 oz., purchased from US Composites), which is inserted between two glass plates (total sample thickness, ~1 mm, figure 5.1A). A 2M solution of acrylamide is prepared in deionized water with 0.1 mol% VA-086 initiator (Wako Pure Chemical Industries, Ltd.) and 1 mol% methylene bisacrylamide as crosslinker. The solution is degassed and injected into the sample mold, then placed into a glove bag filled with nitrogen gas. The sample is cured under UV light (hand lamp) for 20 minutes on each side. After polymerization the gel composite is placed into deionized water for at least four days to allow the gel to reach equilibrium.

5.4.3 Testing

5.4.3.1 Tearing Test

Instron tensile testers are used to test samples. Polyampholyte tear tests were performed at the Laboratory of Soft and Wet Matter at Hokkaido University, and polyacrylamide composite tear tests were performed at the University of Massachusetts Amherst. Samples are prepared approximately 50 mm in length, with widths of 10 mm, 20 mm, and 40 mm. A crack is placed nominally in the center of the sample with a rotary

cutter. One leg is attached to the base, and the other leg is attached to the crosshead, which is displaced at 50 mm/min.

5.4.3.2 Tensile Tests

Tensile tests were performed at the University of Massachusetts Amherst. 10 mm wide samples are prepared, and the length of the sample is recorded as the distance between grips. Due to the aligned fibers in the composite samples, rectangular samples are used rather than dog bone shaped samples. Mechanical grips are used, and the crosshead is displaced at 10 mm/min.

5.4.3.3 Three Point Bend Tests

Three point bend tests were performed at the University of Massachusetts Amherst, with a custom built testing apparatus. Sample width is recorded (approximately 7.5 mm), and length between bottom points is 20 mm. Testing rate is 50 μm/s.

5.5 Results

5.5.1 Tearing Tests

Trouser tearing tests are used to measure the toughness of the samples (Figure 5.1B and Figure 5.1C). In Figure 5.2A tear strength vs displacement for 20 mm wide samples is shown. A 500% increase in maximum tear strength is exhibited by the polyampholyte composite compared to the neat fabric. Interestingly, the tear strength of the polyacrylamide composite is much *less* than the neat fabric. The tearing mechanism can be understood by observation of the sample during testing. For the neat fabric, the fibers in the transverse direction to the applied load quickly escape from the weave as the displacement increases, and the sample fails. In the polyacrylamide composite, the gel fractures first, and then the fibers escape from the weave, similar to the neat fabric sample.

However, the polyampholyte sample appears to fail by a different mechanism. Here, the sample begins to stretch in both the legs and the bulk, and no tearing is observed up to 2 cm of displacement. After tearing begins, the sample continues to stretch as the transverse

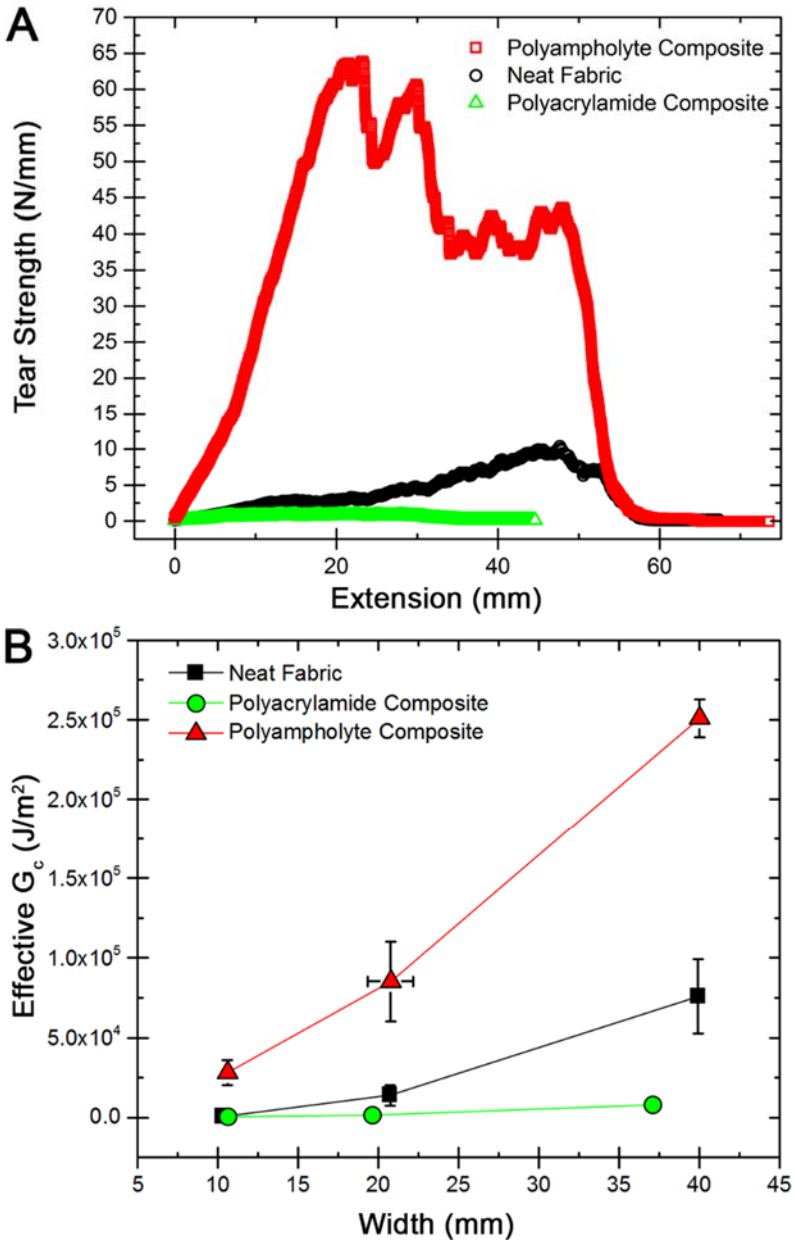

Figure 5.2 - Representative tear strength vs. displacement curves. (A) Results are for neat fabric, polyacrylamide hydrogel composite, and polyampholyte hydrogel composite samples. The polyampholyte exhibits much higher tear strength than the two control groups. (B) Effective G_c vs. thickness for the three test groups. As thickness increases tear strength increases for all samples, due to the fiber pull-out failure mechanism. Measured G_c values are greater than neat fabric for the polyampholyte composite, and less than neat fabric for the polyacrylamide composite. Error bars represent standard deviation, with N > 4

fibers slowly escape from the weave. The maximum tear strength values for the 20 mm wide polyampholyte samples are very high(~65 N/mm); much higher than common elastomers (~0.5 N/mm for a self-healing PDMS material[151]), and approaching high toughness Kevlar/polyurethane blends (~100 N/mm),[152] while still containing 50% water.[149]

Figure 5.2B shows the energy required to tear, or an effective G_c, for composites of varying width. These values are calculated by integrating under the load, F, versus displacement, Δ, curve to determine the energy, and dividing by the projected area of new surface created, $t * L_{bulk}$:

$$G_c = \frac{1}{t * L_{bulk}} \int F d\Delta \tag{5.1}$$

As sample width increases, fracture energy increases. G_c is a material property and generally does not depend on sample size (i.e. width), however due to the composite nature of the material and the failure mechanism, width plays an important role in the fracture toughness of the material system. In these samples, the glass fibers are stiff, and fracture of the fibers is rarely observed during tearing. This is different from previously created fiber reinforced hydrogels, where the fabric fractures first.[153] The main failure mechanism is due to fiber pull out, and subsequent unraveling of the fabric weave within the composite. As sample width increases, fiber pull-out difficulty increases, resulting in increased overall fracture energy.

The G_c values exhibited by the polyampholyte composite are extremely high. For a 40 mm wide sample, a G_c of 250,000 J/m^2 is measured. In comparison, G_c of the neat fabric is 75,000 J/m^2, and G_c of the polyampholyte gel is about 3,000 J/m^2.[148] From general composite theory, we would expect an averaging of mechanical properties, but in this case

the composite greatly exceeds the fracture energy of either neat component. For comparison, the maximum experimental toughness values for an articular cartilage is 1200 J/m^2,[154] showing that the materials created here greatly exceed the toughness of native biological tissues.

5.5.2 Tensile Tests

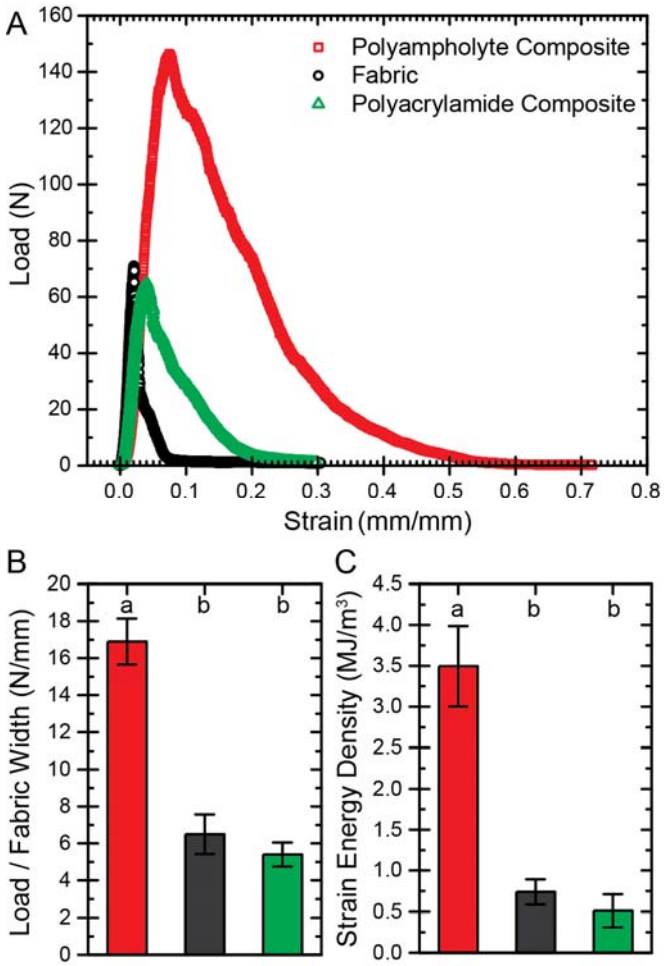

Figure 5.3 - Representative load vs. strain for the three samples tested. (A) Dimensions are t = 0.31 mm w = 10.0 mm and L = 20.5 mm for the neat fabric, t = 0.94 mm, w = 9.2 mm, and L = 14.3 mm for the polyampholyte composite, and t = 1.16 mm, w = 10.0 mm, and L = 21.7 mm for the polyacrylamide composite. Samples are prepared as rectangular strips, and L is the initial distance between the clamps. (B) Load normalized by fabric width, for the three samples tested. The polyampholyte composite supports nearly three times the load per sample with when compared to the neat fabric or the polyacrylamide composite. (C) Strain energy density for the three samples tested. Results agree with the tear strength results. For (B) and (C), ANOVA testing is used with a post-hoc Tukey test to determine significance, with $P < 0.01$. Error bars represent standard deviation, with $N > 5$.

The tensile properties of the polyampholyte composites are improved over the neat fabric and polyacrylamide composites. Representative load versus strain curves for the three sample materials is shown in Figure 5.3A. Loads can be directly compared despite differences in sample thickness, because the maximum load occurs at 0.08 strain, and the load supported by the gel at this strain is extremely low (about 0.075 N, Figure 5.4).[149] The load supported by the polyampholyte composite prior to failure is nearly three times greater than that of the neat fabric (Figure 5.3B). No change is observed between the polyacrylamide composite and the neat fabric. In agreement with the tearing results, the strain energy density of the polyampholyte composite is greater than the neat fabric or polyacrylamide composite (Figure 5.3C), again demonstrating the increased toughness of the prepared polyampholyte composites.

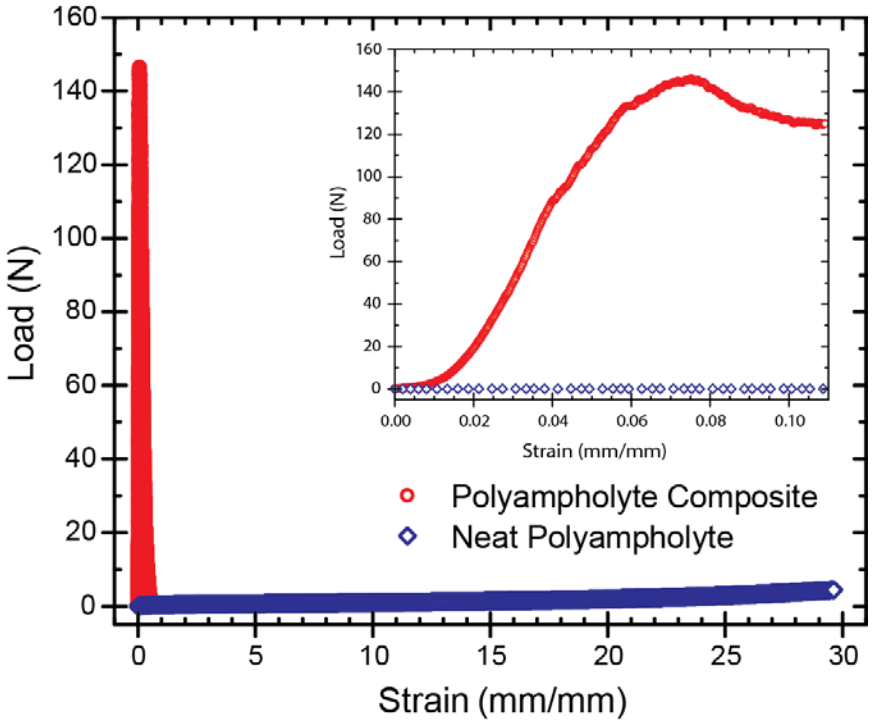

Figure 5.4 – Load versus strain curves for the polyampholyte composite and the neat polyampholyte. The inset plot demonstrates that at the strain where maximum load occurs in the composite, the polyampholyte gel is supporting minimal load.

5.5.3 Bending Tests

Flexibility is an important characteristic for biological prosthetic materials, and bending tests are performed to quantify the flexibility of the fabricated materials. Bending test results are presented in Figure 5.5, with the polyampholyte composite having a bending modulus of 4.7 MPa. The bending modulus is about two orders of magnitude less than the tensile modulus. The composite structures developed here are capable of supporting high loads and are extremely tear resistant, yet are still able to bend easily like a common elastomer, such as Sylgard 184 PDMS.[121]

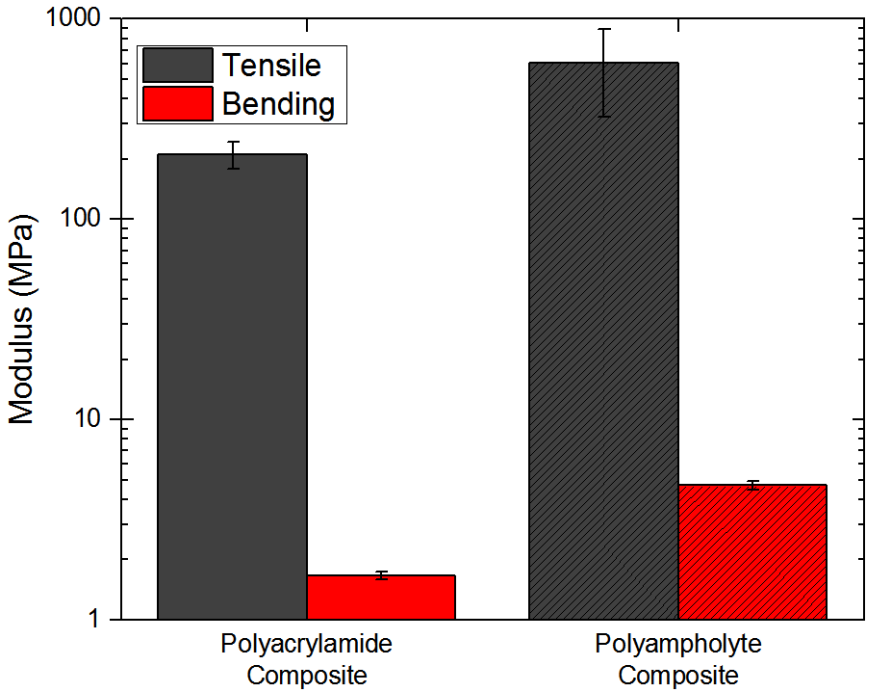

Figure 5.5 - Comparison of tensile and bending moduli for the polyacrylamide and polyampholyte composite.

5.6 Discussion

After polymerization and dialysis of the polyampholyte composite, the sample de-swells. This non-intuitive phenomenon only occurs when the true stoichiometric charge ratio is 1:1, and is the result of salt being flushed from the gel, allowing previously shielded ionic monomers to interact and form a denser polymer network.[148,149] The opposite occurs

in the polyacrylamide composite. When placed into deionized water, additional water is taken in by the system, resulting in a swollen sample. The de-swelling and swelling process influences the tearing strength by changing the density of the weave in the fabric. We propose a mechanism for hydrogel composite toughening based on previously described toughening mechanisms of fabric.[155,156] In a neat fabric tearing test, as the legs displace, the transverse fibers at the crack tip change orientation to align with the loading direction. As these transverse fibers undergo loading, they form a region called the del zone (shown

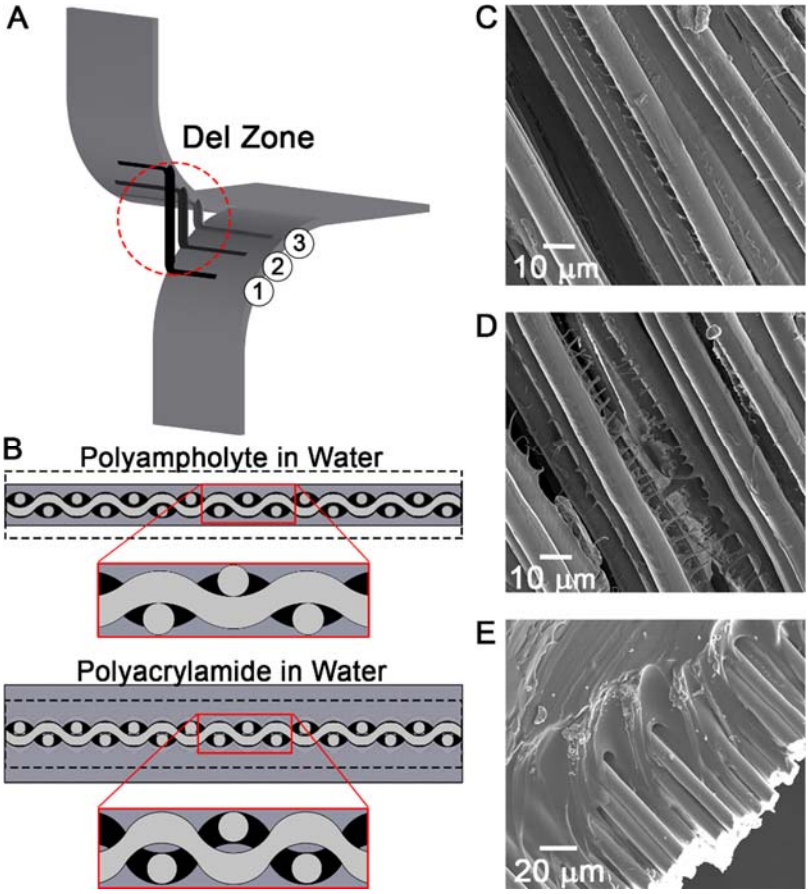

Figure 5.6 –A schematic of the failure mechanism of fabric undergoing tear, emphasizing the del zone. (A) Three fibers are shown, with fiber 1 supporting maximum tension, fiber 2 in the center of the del zone and fiber 3 just entering the del zone. Del zone not drawn to scale for clarity. (B) A schematic representation of the impact of de-swelling and swelling on the fabric. (C) SEM micrographs of fibers covered in the polyampholyte gel, with polyampholyte fibrils between fibers, and (D) cohesive failure of the polyampholyte through a fibrillation process. (E) SEM micrograph of the interface between the polyacrylamide and the glass fibers. Poor adhesion is observed.

in Figure 5.6A). In the del zone, the first fiber is undergoing maximum tension. Each subsequent fiber in the del zone is also undergoing tension, but to a lesser degree, and the bulk is relatively unperturbed. The stretching of the transverse fibers in the del zone pulls in the edges of the fabric as the fibers attempt to pull out of the legs, with friction between the leg fibers and transverse fibers resisting slippage. This leads to twisting of the sample, which is observed during tearing. When the load of the first fiber in the del zone exceeds the maximum tensile strength, the fiber breaks, and the del zone propagates into the bulk of the sample, leaving the second fiber in the del zone as the new first fiber experiencing maximum tension. This process repeats until the entire sample fails.

In the polyampholyte composite, a dramatic increase in toughness is seen due to three events. First, de-swelling results in a tighter fabric weave, increasing the friction on the transverse fibers (Figure 5.6B). This effectively anchors the fibers, making the pull-out failure mechanism more difficult, resulting in higher energy to fracture. Second, in tensile test experiments the polyampholyte composites support higher load per sample width, and therefore the fibers undergoing tension in the del zone can support greater loads before failure. This also increases fracture energy, because a larger del zone can be formed. Finally, fibrillation of the gel between fibers can be seen in Figure 5.6C and Figure 5.6D. De-swelling results in tight bonding between the polyampholyte gel and the fabric, and this dissipative process may increase the fracture toughness of the composite.

In the polyacrylamide composite control sample, the opposite occurs. The swollen gel has a looser fabric weave, decreasing the friction in the legs and allowing the transverse fibers to easily escape from the weave, and therefore decreasing the fracture energy Figure 5.6). Due to the decrease in friction, the transverse fibers have no anchor and cannot utilize

their high stiffness to prevent sample fracture. Furthermore because the polyacrylamide is a brittle gel, it quickly fractures as load is applied to the fabric, resulting in sample failure.

Based on these findings, we propose a general model for creating high toughness composite materials. The system must be composed of two parts, a load bearing primary component, in this case fabric, and a dissipative secondary matrix. The matrix should be able to completely encompass the fabric. A stimulus then must cause a decrease in volume in the matrix, causing a tight weave and increased pressure on the fabric. The pressure applied by the secondary network in this mechanism anchors the transverse fibers in the legs, resisting fiber pull-out and tear. Utilizing a high stiffness fabric allows for high loading without primary network fracture. Additionally, the ability to dissipate energy by the secondary network increases the strength of the del zone which increases toughness. In the system presented here, volume change is implemented by de-swelling of a gel, however this system could be envisioned to work as well by removing volatile solvents from an elastomer polymerized in solution. Furthermore, other fabrics besides glass fabric could be used, and the strength of the fibers in the fabric will influence the tear strength and stiffness of the resulting composite.

Interestingly, the mechanism described is similar to the mechanism proposed for creating high toughness double network hydrogels: the primary network fails, resulting in large dissipation of energy, while the secondary network applies stress, resisting primary network fracture and increasing toughness.[141,146] In the case presented here, the primary network is now *macroscopic*, the fabric weave, rather than a microscopic polymer network. Despite the difference in size scale, the same principles are employed to create extremely tough materials.

5.7 Conclusions

The results shown here demonstrate a simple method to take biocompatible, soft and wet gels, and make them extremely tough, with G_c values as high as 250,000 J/m^2, while capable of supporting high loads. These results will be important in the field of soft biological prosthetics, and more generally for applications such as tear-resistant gloves, bullet-proof vests, or puncture-resistant tires. Importantly, the model presented in this chapter is expected to also work for elastomer-based composites, which opens up a simple, one-step method to make high tear strength materials.

5.8 Acknowledgements

I would like to thank J. P. Gong at Hokkaido University in Sapporo, Japan for providing travel and housing funding, as well as laboratory space for performing the polyampholyte composite experiments. Additional thanks goes to T. Sun, H. Yin, T. Kuriyama, A. Ihsan, and T. Kurikowa, for help with experiments and preparation of the manuscript, and A. W. Hauser for support in proofreading. I would also like to thank the Commercial Ventures and Intellectual Property office at UMass Amherst and the Center for Innovation and Business Promotion at Hokkaido University for their help with the invention disclosure and patent application based on this work.

CHAPTER 6

CONCLUSION AND FUTURE OUTLOOK

6.1 Overview of Results

Biologically inspired adhesives are desirable because they exhibit high adhesive strength, easy releasability, high reusability, and strong anti-fouling properties. Previous attempts to mimic the surface of the gecko toe-pad have resulted in adhesives which achieve high stress, but cannot be scaled to large sizes, and require difficult manufacturing processes. A new technique has recently been developed which mimics the entire foot of the gecko, and is capable of scaling gecko-inspired adhesives to large areas without requiring fibril structures, greatly simplifying fabrication.[74] For high strength reversible adhesives, force capacity scales as:[74–77,119]

$$F_c = \sqrt{2G_c}\sqrt{\frac{A}{C}} \tag{7.1}$$

The work of this thesis utilizes fibril-less gecko-inspired adhesives, and focuses on quantitatively understanding the variables which control force capacity, specifically compliance, C, and area, A. Here we have developed methods to calculate and increase adhesive force capacity for a variety of surfaces and loading configurations, greatly expanding the usefulness of these adhesives. Furthermore, the techniques learned from fabricating these adhesives have proven useful in other areas, resulting in an important advance in the field of ultra-tough hydrogels.

In Chapter 2 we develop an analytical model that is capable of predicting the compliance of fibril-less gecko-inspired adhesives. Combined with the knowledge of Equation 7.1, this model introduces the ability to calculate force capacity by quantifying the role of materials properties and geometry. A general framework is uncovered for

increasing adhesive force capacity, by utilizing high modulus materials, decreasing shape ratio, optimizing tendon length, and increasing tendon width. This understanding allows us to intelligently design adhesives for a given application.

In Chapter 3, we develop gecko-like adhesives for a variety of "real world" surfaces. Previous work focuses on adhering to smooth surfaces, like glass. Under these situations, the true area of contact of the adhesive approaches that of the measured area of the pad. However, when adhering to many other surfaces, such as aluminum or painted drywall, roughness is present and greatly affects the true area of contact. Area, A, also plays an important role in calculating force capacity in Equation 7.1 A model is developed to understand the influence of roughness on adhesive stress capacity, and we see that an optimum elastomer modulus exists for any given surface roughness. Using this knowledge, we create adhesives which adhere strongly to both smooth and rough surfaces, and greatly outperform the adhesive ability of living geckos. The adhesives fabricated in this chapter open up a range of new potential applications, especially including home use.

In Chapter 4, a new adhesive configuration is developed which supports increased loads in high peel angle (normal loading) situations. Utilizing this new method, a six-fold increase in normal force capacity is demonstrated. These adhesives improve the applicability of high strength reusable adhesives, because tolerance to off-angle loads is important to prevent adhesive failure.

Finally, in Chapter 5, we create ultra-tough hydrogel composite materials by incorporating newly developed polyampholyte hydrogels into glass fabric. These composites exhibit extremely high toughness, with G_c values two orders of magnitude greater than the neat polyampholyte hydrogels, and four orders of magnitude greater than

traditional hydrogels such as polyacrylamide. The mechanism which causes this increase in tear strength is explained, and provides a process for creating high toughness composites, regardless of matrix material. These materials possess properties necessary for synthetic ligament prosthetics.

6.2 Future Work

While important steps have been made, as with all scientific research, many interesting, new opportunities were opened through the work performed in this thesis. In this section we introduce some ideas based on observations seen throughout this research.

All of the work on gecko-inspired adhesives has been performed on rigid surfaces. This is important, because the rigid substrate resists the torque that occurs with single lap-shear adhesives.[85,93–95] In many instances, e.g. closures, both materials being adhered are flexible, which allows for rotation to occur. Adhesive devices have been made based on hooks and loops, which is also a bio-inspired device.[7] Using fibril-based adhesives, interlockers have been developed which achieve high strength.[157] Through the work of this thesis we have reinforced that fibrils are not necessary to achieve high strength, reversible adhesives. Future experiments can focus on developing materials which are capable of achieving high loads with smooth overlapping adhesive contacts.

Another area of interest is adhesion to biological tissues.[4,57] Current materials used for bandages and wound closure usually involve thermosetting adhesives such as cyano-acrylates or sticky pressure-sensitive adhesives, which cause pain upon removal. Adhesion to skin is difficult, because biological surfaces are often covered in oils or other particles, and biological tissues are also compliant, which limits adhesive strength.[57] By

understanding the surface properties of skin, materials can be formulated to provide sufficient adhesion for bandages or dermal medications.

A new method for creating extremely tough hydrogel composites is also introduced in this thesis. Here we took advantage of inherent deswelling which occurs in polyampholyte hydrogels to dramatically improve tear strength of fabrics. In traditional single network hydrogels, forced deswelling can occur by introducing a poor solvent for the polymer network. By creating hydrogels which swell in relatively non-polar solvents, such as tetrahydrofuran, then solvent exchanging to water, strong de-swelling should result. Using this technique, it may be possible to create high toughness composite materials from a single network hydrogel matrix.

The mechanism for creating high toughness composites can also be explored using completely dry materials. Double network hydrogels, consisting of two interpenetrating microscopic networks results in high toughness. The composites developed in this thesis consists of one macroscopic fabric network, embedded with a microscopic polymer network. By creating hierarchical fabrics from a high strength fabric, (such as glass fiber fabric or carbon fiber fabric) stitched with a secondary yarn with high toughness (such as nylon or Kevlar) it may be possible to create macro-scale double networks with extremely high toughness. This new material would mimic the mechanisms seen on microscopic length scales in double network hydrogels, but on much larger length scales. This technique could represent a method to create extremely high toughness materials, with already available commodity materials.

6.3 Final Remarks

In this thesis, two areas of active research are covered: gecko-inspired adhesives, and synthetic biocompatible materials. Though these fields are not directly related, we are able to make strong scientific advances by incorporating fabrics, a material which has been used by humans for millennia. An important point learned from this work is that even well-known materials, used in a different way or in a different field, can result in exciting breakthroughs. In conclusion, this thesis demonstrates important scientific achievements by developing a framework for optimizing high strength, reusable adhesives, as well as introducing a first step towards creating extremely tough biocompatible prosthetic materials with fabric and soft materials composites.

BIBLIOGRAPHY

1. Pocius, A. V. *Adhesion and Adhesives Technology*; 2002.

2. Dunn, D. J. *Engineering and Structural Adhesives*; 2004.

3. Creton, C. Pressure-Sensitive Adhesives: An Introductory Course. *MRS bulletin* **2003**, *28*, 434–439.

4. Sarin, A.; Nandkumar, G.; Dakin, G. Tissue Adhesives. In *Materials Science and Technologies: Adhesives: Types, Mechanics, and Applications*; 2011; pp. 137–149.

5. Persson, B. On the Mechanism of Adhesion in Biological Systems. *The Journal of chemical physics* **2003**, *118*, 7614.

6. Autumn, K.; Gravish, N. Gecko Adhesion: Evolutionary Nanotechnology. *Philosophical transactions. Series A, Mathematical, physical, and engineering sciences* **2008**, *366*, 1575–1590.

7. Jenkins, C. H. M. *Bio-Inspired Engineering*; 2011.

8. Feng, L.; Li, S.; Li, Y.; Li, H.; Zhang, L.; Zhai, J.; Song, Y.; Liu, B.; Jiang, L.; Zhu, D. Super-Hydrophobic Surfaces: From Natural to Artificial. *Advanced Materials* **2002**, *14*, 1857–1860.

9. Gao, L.; McCarthy, T. J. "Artificial Lotus Leaf" Prepared Using a 1945 Patent and a Commercial Textile. *Langmuir* **2006**, *22*, 5998–6000.

10. Wong, T.-S.; Kang, S. H.; Tang, S. K. Y.; Smythe, E. J.; Hatton, B. D.; Grinthal, A.; Aizenberg, J. Bioinspired Self-Repairing Slippery Surfaces with Pressure-Stable Omniphobicity. *Nature* **2011**, *477*, 443–447.

11. Mahendra, B. Contributions to the Bionomics, Anatomy, Reproduction and Development of the Indian House-Gecko, Hemidactylus Flaviviridis Ruppel. Part II. the Problem of Locomotion. *Proceedings of the Indian Academy of the Sciences - Section B* **1941**, *13*, 288–306.

12. Irschick, D. J.; Herrel, A.; Vanhooydonck, B. Whole-Organism Studies of Adhesion in Pad-Bearing Lizards: Creative Evolutionary Solutions to Functional Problems. *Journal of Comparative Physiology A* **2006**, *192*, 1169–1177.

13. Gamble, T.; Greenbaum, E.; Jackman, T. R.; Russell, A. P.; Bauer, A. M. Repeated Origin and Loss of Adhesive Toepads in Geckos. *PloS one* **2012**, *7*, e39429.

14. Persson, B. N. J.; Gorb, S. The Effect of Surface Roughness on the Adhesion of Elastic Plates with Application to Biological Systems. *The Journal of Chemical Physics* **2003**, *119*, 11437.

15. Huber, G.; Gorb, S. N.; Hosoda, N.; Spolenak, R.; Arzt, E. Influence of Surface Roughness on Gecko Adhesion. *Acta biomaterialia* **2007**, *3*, 607–610.

16. Wang, K.; He, B.; Shen, R.-J. Influence of Surface Roughness on Wet Adhesion of Biomimetic Adhesive Pads with Planar Microstructures. *Micro & Nano Letters* **2012**, *7*, 1274–1277.

17. Hansen, W. R.; Autumn, K. Evidence for Self-Cleaning in Gecko Setae. *Proceedings of the National Academy of Sciences of the United States of America* **2005**, *102*, 385–389.

18. Federle, W. Why Are so Many Adhesive Pads Hairy? *The Journal of experimental biology* **2006**, *209*, 2611–2621.

19. Youngblood, J. P.; Sottos, N. R. Bioinspired Materials for Self-Cleaning and Self-Healing. *MRS Bulletin* **2008**, *33*, 732–741.

20. Hu, S.; Lopez, S.; Niewiarowski, P. H.; Xia, Z. Dynamic Self-Cleaning in Gecko Setae via Digital Hyperextension. *Journal of the Royal Society, Interface* **2012**, *9*, 2781–2790.

21. Bullock, J. M. R.; Drechsler, P.; Federle, W. Comparison of Smooth and Hairy Attachment Pads in Insects: Friction, Adhesion and Mechanisms for Direction-Dependence. *Journal of Experimental Biology* **2008**, *211*, 3333–3343.

22. Clemente, C. J.; Federle, W. Pushing versus Pulling: Division of Labour between Tarsal Attachment Pads in Cockroaches. *Proceedings of the Royal Society B / Biological Sciences* **2008**, *275*, 1329–1336.

23. Van Casteren, A.; Codd, J. R. Foot Morphology and Substrate Adhesion in the Madagascan Hissing Cockroach, Gromphadorhina Portentosa. *Journal of Insect Science* **2010**, *10*, 1–12.

24. Dirks, J.-H.; Clemente, C. J.; Federle, W. Insect Tricks: Two-Phasic Foot Pad Secretion Prevents Slipping. *Journal of the Royal Society, Interface* **2009**, *7*, 587–593.

25. Labonte, D. Surface Contact and Design of Fibrillar “Friction Pads” in Stick Insects (Carausius Morosus): Mechanisms for Large Friction Coefficients and Negligible Adhesion. *Journal of the Royal Society, Interface* **2014**, *11*.

26. Hanna, G.; Barnes, W. J. Adhesion and Detachment of the Toe Pads of Tree Frogs. *Journal of Experimental …* **1991**, *125*, 103–125.

27. Federle, W.; Barnes, W. J. P.; Baumgartner, W.; Drechsler, P.; Smith, J. M. Wet but Not Slippery: Boundary Friction in Tree Frog Adhesive Toe Pads. *Journal of the Royal Society, Interface / the Royal Society* **2006**, *3*, 689–697.

28. Persson, B. N. J. Wet Adhesion with Application to Tree Frog Adhesive Toe Pads and Tires. *Journal of Physics: Condensed Matter* **2007**, *19*, 376110.

29. Drotlef, D.-M.; Stepien, L.; Kappl, M.; Barnes, W. J. P.; Butt, H.-J.; del Campo, A. Insights into the Adhesive Mechanisms of Tree Frogs Using Artificial Mimics. *Advanced Functional Materials* **2012**, n/a – n/a.

30. Gupta, R.; Fréchette, J. Measurement and Scaling of Hydrodynamic Interactions in the Presence of Draining Channels. *Langmuir* **2012**, *28*, 14703–14712.

31. Endlein, T.; Ji, A.; Samuel, D.; Yao, N.; Wang, Z.; Barnes, W. J. P.; Federle, W.; Kappl, M.; Dai, Z. Sticking like Sticky Tape: Tree Frogs Use Friction Forces to Enhance Attachment on Overhanging Surfaces. *Journal of the Royal Society, Interface* **2013**, *10*.

32. Santos, R.; Gorb, S.; Jamar, V.; Flammang, P. Adhesion of Echinoderm Tube Feet to Rough Surfaces. *The Journal of experimental biology* **2005**, *208*, 2555–2567.

33. Santos, R.; Hennebert, E. The Echinoderm Tube Foot and Its Role in Temporary Underwater Adhesion. *Functional surfaces in …* **2009**.

34. Gasparetto, A.; Seidl, T.; Vidoni, R. A Mechanical Model for the Adhesion of Spiders to Nominally Flat Surfaces. *Journal of Bionic Engineering* **2009**, *6*, 135–142.

35. Wohlfart, E.; Wolff, J.; Arzt, E.; Gorb, S. N. The Whole Is More than the Sum of All Its Parts: Collective Effect of Spider Attachment Organs. *The Journal of Experimental Biology* **2014**, *217*, 222–224.

36. Bullock, J.; Federle, W. Beetle Adhesive Hairs Differ in Stiffness and Stickiness: In Vivo Adhesion Measurements on Individual Setae. *Naturwissenschaften* **2011**, *98*, 381–387.

37. Irschick, D. J.; Austin, C.; Petren, K.; Fisher, R.; Losos, J.; Ellers, O. A Comparative Analysis of Clinging Ability among Pad- bearing Lizards. *Biological Journal of the Linnean Society* **1996**, *59*, 21–35.

38. Autumn, K.; Liang, Y. A.; Hsieh, S. T.; Zesch, W.; Chan, W. P. Adhesive Force of a Single Gecko Foot-Hair. *Nature* **2000**, *405*, 681–685.

39. Autumn, K.; Sitti, M.; Liang, Y.; Peat. Evidence for van Der Waals Adhesion in Gecko Setae. *Proceedings of the National Academy of Sciences of the United States of America* **2002**, *99*, 12252–12256.

40. Tian, Y.; Pesika, N.; Zeng, H.; Rosenberg, K.; Zhao, B.; McGuiggan, P.; Autumn, K.; Israelachvili, J. Adhesion and Friction in Gecko Toe Attachment and Detachment. *Proceedings of the National Academy of Sciences* **2006**, *103*, 19320–19325.

41. Stork, N. Experimental Analysis of Adhesion of Chrysolina Polita (Chrysomelidae: Coleoptera) on a Variety of Surfaces. *The Journal of Experimental Biology* **1980**, *88*, 91–107.

42. Dai, Z.; Gorb, S. N.; Schwarz, U. Roughness-Dependent Friction Force of the Tarsal Claw System in the Beetle Pachnoda Marginata (Coleoptera, Scarabaeidae). *The Journal of experimental biology* **2002**, *205*, 2479–2488.

43. Kesel, A.; Martin, A.; Seidl, T. Adhesion Measurements on the Attachment Devices of the Jumping Spider Evarcha Arcuata. *Journal of Experimental Biology* **2003**, *206*, 2733–2738.

44. Kesel, A. B.; Martin, A.; Seidl, T. Getting a Grip on Spider Attachment: An AFM Approach to Microstructure Adhesion in Arthropods. *Smart Materials and Structures* **2004**, *13*, 512–518.

45. Russell, A. P. A Contribution to the Functional Analysis of the Foot of the Tokay, Gekko Gecko (Reptilia: Gekkonidae). *Journal of Zoology* **1975**, *176*, 437–476.

46. Russell, A. P. Integrative Functional Morphology of the Gekkotan Adhesive System (reptilia: Gekkota). *Integrative and comparative biology* **2002**, *42*, 1154–1163.

47. Autumn, K.; Majidi, C.; Groff, R. Effective Elastic Modulus of Isolated Gecko Setal Arrays. *The Journal of experimental biology* **2006**, *209*, 3558–3568.

48. Boesel, L. F.; Greiner, C.; Arzt, E.; del Campo, A. Gecko-Inspired Surfaces: A Path to Strong and Reversible Dry Adhesives. *Advanced Materials* **2010**, *22*, 2125–2137.

49. Pugno, N. M.; Lepore, E. Observation of Optimal Gecko's Adhesion on Nanorough Surfaces. *Bio Systems* **2008**, *94*, 218–222.

50. Murphy, M. P.; Kim, S.; Sitti, M. Enhanced Adhesion by Gecko-Inspired Hierarchical Fibrillar Adhesives. *ACS applied materials & interfaces* **2009**, *1*, 849–855.

51. Rahmawan, Y.; Kim, T.; Kim, S. J.; Lee, K.-R.; Moon, M.-W.; Suh, K.-Y. Surface Energy Tunable Nanohairy Dry Adhesive by Broad Ion Beam Irradiation. *Soft Matter* **2012**, *8*, 1673.

52. Gillies, A. G.; Fearing, R. S. Shear Adhesion Strength of Thermoplastic Gecko-Inspired Synthetic Adhesive Exceeds Material Limits. *Langmuir* **2011**, *27*, 11278–11281.

53. Kwak, M. K.; Jeong, H. E.; Bae, W. G.; Jung, H. S.; Suh, K. Y. Anisotropic Adhesion Properties of Triangular-Tip-Shaped Micropillars. *Small* **2011**, 2296–2300.

54. Jeong, H. E.; Lee, J.-K.; Kim, H. N.; Moon, S. H.; Suh, K. Y. A Nontransferring Dry Adhesive with Hierarchical Polymer Nanohairs. *Proceedings of the National Academy of Sciences of the United States of America* **2009**, *106*, 5639–5644.

55. Ruffatto, D.; Parness, A.; Spenko, M. Improving Controllable Adhesion on Both Rough and Smooth Surfaces with a Hybrid Electrostatic/gecko-like Adhesive. *Journal of the Royal Society, Interface* **2014**, *11*.

56. Jeong, H. E.; Lee, J.-K.; Kwak, M. K.; Moon, S. H.; Suh, K. Y. Effect of Leaning Angle of Gecko-Inspired Slanted Polymer Nanohairs on Dry Adhesion. *Applied Physics Letters* **2010**, *96*, 043704.

57. Kwak, M. K.; Jeong, H. E.; Suh, K. Y. Rational Design and Enhanced Biocompatibility of a Dry Adhesive Medical Skin Patch. *Advanced Materials* **2011**, *23*, 3949–3953.

58. Ge, L.; Sethi, S.; Ci, L.; Ajayan, P. M.; Dhinojwala, A. Carbon Nanotube-Based Synthetic Gecko Tapes. *Proceedings of the National Academy of Sciences* **2007**, *104*, 10792.

59. Zosel, A. The Effect of Bond Formation on the Tack of Polymers. *Journal of adhesion science and technology* **1997**, 37–41.

60. Creton, C.; Leibler, L. How Does Tack Depend on Time of Contact and Contact Pressure? *Journal of Polymer Science Part B: Polymer Physics* **1996**, *34*, 545–554.

61. Dahlquist, C. A. An Investigation into the Nature of Tack. *Adhesives Age* **1959**, *2*, 25–29.

62. Dahlquist, C. A. Tack. In *Adhesion fundamentals and practice*; 1966; pp. 143–151.

63. Dahlquist, C. A. *Treatise on Adhesion and Adhesives*; Patrick, R. L., Ed.; 2nd ed.; New York, 1969; p. 219.

64. Tordjeman, P.; Papon, E.; Villenave, J.-J. Tack Properties of Pressure-Sensitive Adhesives. *Journal of Polymer Science Part B: Polymer Physics* **2000**, *38*, 1201.

65. Lin, Y.; Hui, C.; Conway, H. A Detailed Elastic Analysis of the Flat Punch (tack) Test for Pressure-Sensitive Adhesives. *Journal of Polymer Science Part B: Polymer Physics* **2000**, 2769–2784.

66. Zosel, A. Adhesive Failure and Deformation Behaviour of Polymers. *The Journal of Adhesion*, 1989, *30*, 135–149.

67. Zosel, A. The Effect of Fibrilation on the Tack of Pressure Sensitive Adhesives. *Journal Of Adhesion* **1998**, *18*, 265–271.

68. Arzt, E.; Gorb, S.; Spolenak, R. From Micro to Nano Contacts in Biological Attachment Devices. *Proceedings of the National Academy of Sciences* **2003**, *100*, 10603–10606.

69. Glassmaker, N. J.; Himeno, T.; Hui, C.-Y.; Kim, J. Design of Biomimetic Fibrillar Interfaces: 1. Making Contact. *Journal of the Royal Society, Interface* **2004**, *1*, 23–33.

70. Glassmaker, N. J.; Jagota, A.; Hui, C. Y.; Noderer, W. L.; Chaudhury, M. K. Biologically Inspired Crack Trapping for Enhanced Adhesion. *Proceedings of the National Academy of Sciences* **2007**, *104*, 10786.

71. Qu, L.; Dai, L.; Stone, M.; Xia, Z.; Wang, Z. L. Carbon Nanotube Arrays with Strong Shear Binding-on and Easy Normal Lifting-Off. *Science* **2008**, *322*, 238–242.

72. Maugis, D.; Barquins, M. Fracture Mechanics and the Adherence of Viscoelastic Bodies. *Journal of Physics D: Applied Physics* **1978**, *11*, 1989–2023.

73. Griffith, A. The Phenomena of Rupture and Flow in Solids. *Philosophical transactions of the royal society of* **1921**, *221*, 163–198.

74. Bartlett, M. D.; Croll, A. B.; King, D. R.; Paret, B. M.; Irschick, D. J.; Crosby, A. J. Looking Beyond Fibrillar Features to Scale Gecko-Like Adhesion. *Advanced Materials* **2012**, *24*, 1078–1083.

75. Bartlett, M. D.; Croll, A. B.; Crosby, A. J. Designing Bio-Inspired Adhesives for Shear Loading: From Simple Structures to Complex Patterns. *Advanced Functional Materials* **2012**, *22*, 4985–4992.

76. Bartlett, M. D.; Crosby, A. J. High Capacity, Easy Release Adhesives From Renewable Materials. *Advanced materials* **2014**.

77. Bartlett, M. D.; Crosby, A. J. Scaling Normal Adhesion Force Capacity with a Generalized Parameter. *Langmuir* **2013**, *29*, 11022–11027.

78. Creton, C.; Gorb, S. Sticky Feet: From Animals to Materials. *MRS Bulletin* **2007**, *32*, 466–472.

79. Jiao, Y.; Gorb, S.; Scherge, M. Adhesion Measured on the Attachment Pads of Tettigonia Viridissima (Orthoptera, Insecta). *The Journal of experimental biology* **2000**, *203*, 1887–1895.

80. Bullock, J. M. R.; Federle, W. Division of Labour and Sex Differences between Fibrillar, Tarsal Adhesive Pads in Beetles: Effective Elastic Modulus and Attachment Performance. *The Journal of experimental biology* **2009**, *212*, 1876–1888.

81. Autumn, K.; Hsieh, S.; Dudek, D.; Chen, J.; Chitaphan, C.; Full, R. J. Dynamics of Geckos Running Vertically. *Journal of Experimental Biology* **2006**, *209*, 260–272.

82. Kaelble, D. H. Theory and Analysis of Peel Adhesion: Bond Stresses and Distributions. *Journal of Rheology* **1960**, *4*, 45.

83. Wright, C. The Effect of Solid-State Reactions upon Solder Lap Shear Strength. *IEEE Transactions on Parts, Hybrids, and Packaging* **1977**, *36*, 202–207.

84. Shen, Y.-L.; Chawla, N.; Ege, E. S.; Deng, X. Deformation Analysis of Lap-Shear Testing of Solder Joints. *Acta Materialia* **2005**, *53*, 2633–2642.

85. Goland, M.; Reissner, E. The Stresses in Cemented Joints. *Journal of Applied Mechanics* **1944**, 17–27.

86. Gent, A. Fracture Mechanics of Adhesive Bonds. *Rubber Chemistry and Technology* **1974**.

87. Kendall, K. Crack Propagation in Lap Shear Joints. *Journal of Physics D: Applied Physics* **1975**, *8*, 512–522.

88. Hart-Smith, L. *Adhesive-Bonded Single-Lap Joints*; 1973.

89. Kafkalidis, M. S.; Thouless, M. D. The Effects of Geometry and Material Properties on the Fracture of Single Lap-Shear Joints. *International Journal of Solids and Structures* **2002**, *39*, 4367–4383.

90. Oplinger, D. W. Effects of Adherend Deflections in Single Lap Joints. *International Journal of Solids and Structures* **1994**, *31*, 2565–2587.

91. Sancaktar, E.; Schenck, S. C.; Padgilwar, S. Material Characterization of Structural Adhesives in the Lap Shear Mode. 1. The Effects of Rate. *Industrial & Engineering Chemistry Product Research and Development* **1984**, *23*, 426–434.

92. Sancaktar, E.; Schenck, S. C. Material Characterization of Structural Adhesives in the Lap Shear Mode. 2. Temperature-Dependent Delayed Failure. *Industrial & Engineering Chemistry Product Research and Development* **1985**, *24*, 257–263.

93. Xiao, X. S.; Foss, P.; others. Stiffness Prediction of the Double Lap Shear Joint. Part1: Analytical Solution. *International journal of adhesion and adhesives* **2004**, *24*, 229–237.

94. Xiao, X. Stiffness Prediction of the Double Lap Shear Joint. Part 2: Finite Element Modeling. *International Journal of Adhesion and Adhesives* **2004**, *24*, 239–246.

95. He, X. A Review of Finite Element Analysis of Adhesively Bonded Joints. *International Journal of Adhesion and Adhesives* **2011**, *31*, 248–264.

96. Bigwood, D. A.; Crocombe, A. D. Elastic Analysis and Engineering Design Formulae for Bonded Joints. *International Journal of Adhesion and Adhesives* **1989**, 230–242.

97. Lakes, R. S.; Drugan, W. J. Dramatically Stiffer Elastic Composite Materials due to a Negative Stiffness Phase? *Journal of the Mechanics and Physics of Solids* **2002**, *50*, 979–1009.

98. Mori, T.; Tanaka, K. Average Stress in Matrix and Average Elastic Energy of Materials with Misfitting Inclusions. *Acta Metallurgica* **1973**, *21*, 571–574.

99. Kendall, K. Thin-Film Peeling-the Elastic Term. *Journal of Physics D: Applied Physics* **1975**, *8*, 1449.

100. Huber, G.; Gorb, S. N.; Spolenak, R.; Arzt, E. Resolving the Nanoscale Adhesion of Individual Gecko Spatulae by Atomic Force Microscopy. *Biology letters* **2005**, *1*, 2–4.

101. Irschick, D. J.; Vanhooydonck, B.; Herrel, A.; Andronescu, A. Effects of Loading and Size on Maximum Power Output and Gait Characteristics in Geckos. *Journal of Experimental Biology* **2003**, *206*, 3923–3934.

102. Aksak, B.; Murphy, M. P.; Sitti, M. Gecko Inspired Micro-Fibrillar Adhesives for Wall Climbing Robots on Micro/nanoscale Rough Surfaces. In *Robotics and Automation, 2008. ICRA 2008. IEEE International Conference on*; IEEE, 2008; pp. 3058–3063.

103. Reddy, S.; Arzt, E.; del Campo, A. Bioinspired Surfaces with Switchable Adhesion. *Advanced Materials* **2007**, *19*, 3833–3837.

104. Lee, H.; Lee, B. P.; Messersmith, P. B. A Reversible Wet/dry Adhesive Inspired by Mussels and Geckos. *Nature* **2007**, *448*, 338–341.

105. Peattie, A. M.; Majidi, C.; Corder, A.; Full, R. J. Ancestrally High Elastic Modulus of Gecko Setal Beta-Keratin. *Journal of the Royal Society, Interface* **2007**, *4*, 1071–1076.

106. Parness, A.; Soto, D.; Esparza, N.; Gravish, N.; Wilkinson, M.; Autumn, K.; Cutkosky, M. A Microfabricated Wedge-Shaped Adhesive Array Displaying Gecko-like Dynamic Adhesion, Directionality and Long Lifetime. *Journal of the Royal Society, Interface* **2009**, *6*, 1223–1232.

107. Yu, J.; Chary, S.; Das, S.; Tamelier, J.; Turner, K. L.; Israelachvili, J. N. Friction and Adhesion of Gecko-Inspired PDMS Flaps on Rough Surfaces. *Langmuir : the ACS journal of surfaces and colloids* **2012**, *28*, 11527–11534.

108. Gillies, A. G.; Henry, A.; Lin, H.; Ren, A.; Shiuan, K.; Fearing, R. S.; Full, R. J. Gecko Toe and Lamellar Shear Adhesion on Macroscopic, Engineered Rough Surfaces. *The Journal of experimental biology* **2014**, *217*, 283–289.

109. Cerda, E.; Mahadevan, L.; Pasini, J. The Elements of Draping. *Proceedings of the National Academy of Sciences of the United States of America* **2004**, *101*, 1806.

110. Fuller, K. N. G.; Tabor, D. The Effect of Surface Roughness on the Adhesion of Elastic Solids. *Proceedings of the Royal Society of London. Series A, Mathematical and Physical Sciences* **1975**, *345*, 327–342.

111. Persson, B. N. J.; Tosatti, E. The Effect of Surface Roughness on the Adhesion of Elastic Solids. *The Journal of Chemical Physics* **2001**, *115*, 5597.

112. Persson, B. N. J.; Albohr, O.; Tartaglino, U.; Volokitin, a I.; Tosatti, E. On the Nature of Surface Roughness with Application to Contact Mechanics, Sealing, Rubber Friction and Adhesion. *Journal of physics. Condensed matter : an Institute of Physics journal* **2005**, *17*, R1–R62.

113. Shull, K. Contact Mechanics and the Adhesion of Soft Solids. *Materials Science and Engineering: R: Reports* **2002**, *36*, 1–45.

114. Davis, C. S.; Martina, D.; Creton, C.; Lindner, A.; Crosby, A. J. Enhanced Adhesion of Elastic Materials to Small-Scale Wrinkles. *Langmuir : the ACS journal of surfaces and colloids* **2012**, *28*, 14899–14908.

115. Johnson, K.; Kendall, K.; Roberts, A. Surface Energy and the Contact of Elastic Solids. *Proceedings of the Royal Society of London. Series A, Mathematical and Physical Sciences* **1971**, *324*, 301–313.

116. Davis, C. S.; Crosby, A. J. Mechanics of Wrinkled Surface Adhesion. *Soft Matter* **2011**, *7*, 5373.

117. Bauer, A. M.; Russell, A. P. Morphology of Gekkonid Cutaneous Sensilla, with Comments on Function and Phylogeny in the Carphodactylini (Reptilia: Gekkonidae). *Canadian Journal of Zoology* **1988**, *66*, 1583–1588.

118. Russell, A. P.; Bauer, A. M. The Morphology of the Digits of the Golden Gecko, Calodactylodes Aureus and Its Implications for the Occupation of Rupicolous Habitats. *Amphibia-Reptilia* **1989**, *10*, 125–140.

119. King, D. R.; Bartlett, M. D.; Gilman, C. A.; Irschick, D. J.; Crosby, A. J. Creating Gecko-Like Adhesives for "Real World" Surfaces. *Advanced Materials* **2014**, *26*, 4345–4351.

120. Vajpayee, S.; Jagota, A.; Hui, C.-Y. Adhesion of a Fibrillar Interface on Wet and Rough Surfaces. *The Journal of Adhesion* **2010**, *86*, 39–61.

121. Pendergraph, S. A.; Bartlett, M. D.; Carter, K. R.; Crosby, A. J. Opportunities with Fabric Composites as Unique Flexible Substrates. *ACS Applied Materials & Interfaces* **2012**, *4*, 6640–6645.

122. Blaiszik, B. J.; Kramer, S. L. B.; Olugebefola, S. C.; Moore, J. S.; Sottos, N. R.; White, S. R. Self-Healing Polymers and Composites. *Annual Review of Materials Research* **2010**, *40*, 179–211.

123. Miller, K.; Hsu, J. E.; Soslowsky, L. J. Materials in Tendon and Ligament Repair. In *Comprehensive Biomaterials*; 2011; pp. 257–279.

124. Gong, J. P. Why Are Double Network Hydrogels so Tough? *Soft Matter* **2010**, *6*, 2583.

125. Corner, E. M. Notes of a Case Illustrative of an Artificial Anterior Crucial Ligament, Demonstrating the Action of That Ligament. *Proceedings of the Royal Society of Medicine* **1914**, *7*, 120–121.

126. Jenkins, D. H. R. The Repair of Cruciate Ligaments with Flexible Carbon Fibre. *Journal of Bone and Joint Surgery* **1978**, *60-B*, 520–522.

127. Mendes, D.; Iusim, M.; Angel, D.; Rotem, A.; Mordehovich, D.; Roffman, M.; Lieberson, S.; Boss, J. Ligament and Tendon Substitution with Composite Carbon Fiber Strands. *Journal of Biomedical Materials Research* **1986**, *20*, 699–708.

128. Amis, A. A.; Kempson, S. A.; Campbell, J. R.; Miller, J. H. Anterior Cruciate Ligament Replacement. *Journal of Bone and Joint Surgery* **1988**, *70-B*, 628–634.

129. Altman, G. H.; Horan, R. L.; Lu, H. H.; Moreau, J.; Martin, I.; Richmond, J. C.; Kaplan, D. L. Silk Matrix for Tissue Engineered Anterior Cruciate Ligaments. *Biomaterials* **2002**, *23*, 4131–4141.

130. Scharling, M. Replacement of the Anterior Cruciate Ligament with a Polyethylene Prosthetic Ligament. *Acta orthopaedica Scandinavica* **1981**, *52*, 575–578.

131. Roth, J.; Kennedy, J.; Lockstadt, H.; McCallum, C.; Cunning, L. Polypropylene Braid Augmented and Nonaugmented Intraarticular Anterior Cruciate Ligament Reconstruction. *The American Journal of Sports Medicine* **1985**, *13*, 321–336.

132. Dürselen, L.; Claes, L.; Ignatius, a; Rübenacker, S. Comparative Animal Study of Three Ligament Prostheses for the Replacement of the Anterior Cruciate and Medial Collateral Ligament. *Biomaterials* **1996**, *17*, 977–982.

133. Mascarenhas, R.; MacDonald, P. Anterior Cruciate Ligament Reconstruction: A Look at Prosthetics-Past, Present and Possible Future. *McGill Journal of Medicine: MJM* **2008**, *11*, 29–37.

134. Jenkins, D. H. R.; McKibbin, B. The Role of Flexible Carbon-Fibre Implants as Tendon and Ligament Substitutes in Clinical Practice. *Journal of Bone and Joint Surgery* **1980**, *62*, 497–499.

135. Moyen, B.; Lerat, J.-L. Artificial Ligaments for Anterior Cruciate Replacement. *The Journal of Bone and Joint Surgery* **1994**, *76*, 173–175.

136. Osada, Y.; Gong, J. P. Soft and Wet Materials: Polymer Gels. *Advanced Materials* **1998**, *10*, 827–837.

137. Tominaga, T.; Takedomi, N.; Biederman, H.; Furukawa, H.; Osada, Y.; Gong, J. P. Effect of Substrate Adhesion and Hydrophobicity on Hydrogel Friction. *Soft Matter* **2008**, *4*, 1033.

138. Gong, J. P. Friction and Lubrication of Hydrogels-Its Richness and Complexity. *Soft Matter* **2006**, *2*, 544.

139. Gong, J. P.; Kurokawa, T.; Narita, T.; Kagata, G.; Osada, Y.; Nishimura, G.; Kinjo, M. Synthesis of Hydrogels with Extremely Low Surface Friction. *Journal of the American Chemical Society* **2001**, *123*, 5582–5583.

140. Cui, J.; Lackey, M. A.; Madkour, A. E.; Saffer, E. M.; Griffin, D. M.; Bhatia, S. R.; Crosby, A. J.; Tew, G. N. Synthetically Simple, Highly Resilient Hydrogels. *Biomacromolecules* **2012**, *13*, 584–588.

141. Gong, J. P.; Katsuyama, Y.; Kurokawa, T.; Osada, Y. Double-Network Hydrogels with Extremely High Mechanical Strength. *Advanced Materials* **2003**, *15*, 1155–1158.

142. Yasuda, K.; Gong, J. P.; Katsuyama, Y.; Nakayama, A.; Tanabe, Y.; Kondo, E.; Ueno, M.; Osada, Y. Biomechanical Properties of High-Toughness Double Network Hydrogels. *Biomaterials* **2005**, *26*, 4468–4475.

143. Brown, H. R. A Model of the Fracture of Double Network Gels. *Macromolecules* **2007**, *40*, 3815–3818.

144. Tanaka, Y.; Kuwabara, R.; Na, Y.-H.; Kurokawa, T.; Gong, J. P.; Osada, Y. Determination of Fracture Energy of High Strength Double Network Hydrogels. *The journal of physical chemistry. B* **2005**, *109*, 11559–11562.

145. DeKosky, B. J.; Dormer, N. H.; Ingavle, G. C.; Roatch, C. H.; Lomakin, J.; Detamore, M. S.; Gehrke, S. H. Hierarchically Designed Agarose and Poly(ethylene Glycol) Interpenetrating Network Hydrogels for Cartilage Tissue Engineering. *Tissue engineering. Part C, Methods* **2010**, *16*, 1533–1542.

146. Myung, D.; Waters, D.; Wiseman, M.; Duhamel, P.-E.; Noolandi, J.; Ta, C. N.; Frank, C. W. Progress in the Development of Interpenetrating Polymer Network Hydrogels. *Polymers for Advanced Technologies* **2008**, *19*, 647–657.

147. Sun, J.-Y.; Zhao, X.; Illeperuma, W. R. K.; Chaudhuri, O.; Oh, K. H.; Mooney, D. J.; Vlassak, J. J.; Suo, Z. Highly Stretchable and Tough Hydrogels. *Nature* **2012**, *489*, 133–136.

148. Sun, T. L.; Kurokawa, T.; Kuroda, S.; Ihsan, A. Bin; Akasaki, T.; Sato, K.; Haque, M. A.; Nakajima, T.; Gong, J. P. Physical Hydrogels Composed of Polyampholytes Demonstrate High Toughness and Viscoelasticity. *Nature materials* **2013**, *12*, 1–6.

149. Ihsan, A. Bin; Sun, T. L.; Kuroda, S.; Haque, M. A.; Kurokawa, T.; Nakajima, T.; Gong, J. P. A Phase Diagram of Neutral Polyampholyte – from Solution to Tough Hydrogel. *Journal of Materials Chemistry B* **2013**, *1*, 4555.

150. Rivlin, R. S.; Thomas, a. G. Rupture of Rubber. I. Characteristic Energy for Tearing. *Journal of Polymer Science* **1953**, *10*, 291–318.

151. Keller, M. W.; White, S. R.; Sottos, N. R. A Self-Healing Poly(Dimethyl Siloxane) Elastomer. *Advanced Functional Materials* **2007**, *17*, 2399–2404.

152. Kutty, S. K. N.; Nando, G. B. Short Kevlar Fiber–thermoplastic Polyurethane Composite. *Journal of Applied Polymer Science* **1991**, *43*, 1913–1923.

153. Lin, S.; Cao, C.; Wang, Q.; Gonzalez, M.; Dolbow, J. E.; Zhao, X. Design of Stiff, Tough and Stretchy Hydrogel Composites via Nanoscale Hybrid Crosslinking and Macroscale Fiber Reinforcement. *Soft matter* **2014**, *10*, 7519–7527.

154. Stok, K.; Oloyede, A. Conceptual Fracture Parameters for Articular Cartilage. *Clinical Biomechanics* **2007**, *22*, 725–735.

155. Scelzo, W. A.; Backer, S.; Boyce, M. C. Mechanistic Role of Yarn and Fabric Structure in Determining Tear Resistance of Woven Cloth: Part I: Understanding Tongue Tear. *Textile Research Journal* **1994**, *64*, 291–304.

156. Scelzo, W. A.; Backer, S.; Boyce, M. C. Mechanistic Role of Yarn and Fabric Structure in Determining Tear Resistance of Woven Cloth Part II: Modeling Tongue Tear. *Textile Research Journal* **1994**, *64*, 321–329.

157. Pang, C.; Kim, T.; Bae, W. G.; Kang, D.; Kim, S. M.; Suh, K. Y. Bioinspired Reversible Interlocker Using Regularly Arrayed High Aspect-Ratio Polymer Fibers. *Advanced Materials* **2011**, 1–5.